Cross-Layer Optimization for Hybrid Wireless-Power Line Sensor Networks

Thesis submitted in accordance with the requirements of
the University of Liverpool for the degree of Doctor in Philosophy

by

Kainan Zhu

May 2019

Declaration

The work in this thesis is based on research carried out at the University of Liverpool. No part of this thesis has been submitted elsewhere for any other degree or qualification and it is all my own work unless referenced to the contrary in the text.

Abstract

Wireless sensor networks (WSNs) have a wide range of applications in the realization of the Internet of Things (IoT). However, WSNs are confronted with dynamic wireless medium, limited bandwidth, limited energy supply (in battery powered WSNs) and the often present blind spot problems. In particular, battery powered WSNs used for the in-door applications, such as impromptu surveillance installation or industrial chemical process monitoring (mains powered WSNs are prohibited due to safety concerns), have stringent energy budgets. Power line communication (PLC) is considered as a promising technology for data transmission that utilises the widespread presence of power line (PL) cables as a communication medium. Owing to this advantage, PLC networking can be considered as a practical supplement to existing in-door WSNs. In this thesis, it is aimed to investigate the performance improvement (*i.e.*, network lifetime) in the hybrid wireless-PL sensor networks for in-door applications through cross-layer design.

In the first contribution, a hybrid sensor network for industrial sensor network applications, which consists of both wireless and PL sensor nodes is proposed. Since the data rate requirement for such applications is typically low, and for the ease of derivation, the power consumption model takes into account the transmission signal power and the power consumption of the power amplifier. To the best of our knowledge, it is the first reported work in the literature that focuses on the cross-layer design of such a heterogeneous network. The hybrid sensor network takes the advantage of the flexibility of WSNs while the PL sensors are deployed to prolong the lifetime of the network. This work studies the joint design of the PHY, MAC and network layers to maximize the hybrid network lifetime, which

is limited by the battery capacity of wireless sensors. Second, closed-form expressions of the globally optimal solution for lifetime maximization of the hybrid sensor network are derived for two different network topologies, namely string topology and linear topology. Such closed-form solutions give insights in factors that are significant to the network lifetime when designing the hybrid sensor network. Third, the impacts of different network configurations such as source rate, sensor node densities, *etc.*, on the hybrid network lifetime are investigated. The impact of different transmission strategies of PL nodes on the effectiveness of the network is studied.

In the second contribution, a hybrid video sensor network (HVSN) which comprises both battery-powered wireless sensor nodes and PL sensor nodes is proposed to maximize the network lifetime. Since HVSN have a high data rate requirement, the power consumption model includes the power consumption due to video encoding, data transmission and reception. To the best of our knowledge, it is the first reported work to investigate video sensor networks with hybrid power sources and hybrid communication schemes. The proposed HVSN utilizes the flexibility of wireless nodes while PL nodes are used to extend the network lifetime. Second, the joint design of video encoding rate, aggregate power consumption, channel access control, along with link rate allocation is studied for maximizing the hybrid network lifetime. The joint design achieves much better performance than separate optimization. Third, a distributed algorithm is proposed for the network lifetime maximization problem. The distributed algorithm divides the computational burden among all nodes with much lower communication overhead. Fourth, the impact of dynamic network change and network scalability is studied. The effectiveness of the proposed algorithm is validated through extensive simulation results.

Acknowledgement

I would like to express my sincerest gratitude to my supervisors, Dr. Xu (Judy) Zhu and Prof. Yi Huang for their invaluable support, patient guidance, and continual encouragement during the period of my study in the University of Liverpool. I would also like to thank Dr. Shusen Yang for his insightful discussion on heterogeneous network and optimization theory. My gratitude also goes to Dr. Jiafeng Zhou and Dr. Ali Al Ataby for their constructive feedback and comments on my research.

I would like to thank the University of Liverpool and the School of Electrical Engineering, Electronics and Computer Science for providing me a studentship as well as the excellent training and facilities.

I would also like to thank my colleagues in the research group: Dr. Linhao Dong, Dr. Yufei Jiang and Dr. Mohammad Heggo for sharing their research experiences, Dr. Chao Zhang and Dr. Jun Yin for their inspiring discussions on power line communications, Dr. Zhongxiang Wei for his encouragement and discussion on energy consumption model, Dr. Yang Li, Mr. Yanghao Wang, Mr. Teng Ma and Mr. Chaowei Liu for providing helpful suggestions in my research. I cherish all the time we had together.

Finally, my gratitude to my parents is beyond words.

This thesis is dedicated to them.

Contents

List of Figures

List of Tables

Abbreviations and Acronyms

ADC	Analog-to-Digital Converter
AM	Amplitude Modulation
ARIB	Association of Radio Industries and Businesses
AWGN	Additive White Gaussian Noise
BAN	Body Area Network
BB	Broadband
BP	Bus topology with conductors placed along the Perimeter
BER	Bit-Error-Rate
bps	bits-per-second
CDMA	Code Division Multiple Access
CENELEC	European Committee for Electrotechnical Standardization
CFR	Code of Federal Regulations
CMOS	Complementary Metal-Oxide Semiconductor
CSMA	Carrier Sensing Multiple Access
CSMA/CA	Carrier Sensing Multiple Access with Collision Avoidance
CTF	Channel Transfer Function

CVS	Compressive Video Sensing
EN	European Norm
EPRI	Electric Power Research Institute
FCC	Federal Communications Commission
FDMA	Frequency Division Multiple Access
FM	Frequency Modulation
FSK	Frequency-shift keying
G.hn	Gigabit home networking
HDTV	High-Definition Television
HV	High-Voltage
HVSN	Hybrid Video Sensor Network
IN	Impulsive Noise
IoT	Internet-of-Things
ISI	inter-symbol interference
ISM	industrial-scientific-medical
ITU	International Telecommunication Union
KKT	Karush-Kuhn-Tucker
LoS	line-of-sight
LV	Low-Voltage
MAC	Medium Access Control
MIMO	Multiple-Input Multiple-Output

MLAS	Minimum Latency aggregation scheduling
MQAM	M-ary Quadrature Amplitude Modulation
MSE	Mean Square Error
MV	Medium-Voltage
NB	Narrow Band
NUM	Network Utility Maximization
OFDM	Orthogonal Frequency Division Multiplexing
OPERA	Open PLC European Research Alliance
P-R-D	Power-Rate-Distortion
PDF	Probability Density Function
PHY	Physical
PL	Power Line
PLC	Power Line Communication
RMS	root mean square
PRIME	Powerline Related Intelligent Metering Evolution
PSD	Power Spectrum Density
QoS	Quality-of-Service
SD	Star structure that satisfies the minimum Distance criteria
SDN	Software-Defined Networking
SDTV	Standard-Definition Television
SNR	signal-to-noise ratio

SP	Star topology with conductors placed along the Perimeter
SSIM	Structure Similarity
TCP	Transmission Control Protocol
TDMA	Time Division Multiple Access
TEM	Transverse Electromagnetic
TL	Transmission Line
WAN	Wide Area Network
WBAN	Wireless Body Area Network
WLAN	Wireless Local Area Network
WSNs	Wireless Sensor Networks
WVSN	Wireless Video Sensor Network
WG	Working Group
UNB	Ultra Narrow Band
VRA	Voltage Ratio Approach

Chapter 1

Introduction

1.1 Background

The Internet of Things (IoT) envisions physical objects of pervasive presence to be equipped with transceivers and micro-controllers for telecommunications [1], and by proper designed protocol stacks, these objects are enabled to share information and cooperate with each other and with the users to achieve common purposes in the foreseeable future [2]. With such a communication paradigm [3], the IoT will boost the development of a wide variety of applications such as home and industrial automation, elderly care, home security surveillance, energy management and smart grids [4–9] that utilise the tremendous amount and diversity of information gathered from these everyday life objects, such as surveillance cameras, home appliances, monitoring sensors, *etc.*, to provide new services to customers [2].

In the realm of IoT, wireless sensor networks (WSNs) are deployed in a plethora of applications due to its advantages such as rapid deployment, low cost and high flexibility [10, 11]. However, WSNs are confronted with dynamic wireless medium, limited bandwidth, limited energy supply (in battery powered WSNs) and the often present blind spot problems [12, 13]. In order to tackle these problems, extensive studies [14–23] have been carried out to investigate the performance improvement (*e.g.* throughput, robustness, energy consumption, network lifetime) on a hybrid network (*i.e.*, mixed wireless and wireline network). The

basic idea of these studies is that by adding a few wireline as the shortcut in the network (termed "small-world network" [19]), the average hop count can be reduced drastically and thus improving the network performance. However, these studies focus on the analysis of the network performance improvement based on a single protocol layer, *e.g.,* physical layer, network layer (details on the network protocol stack will be presented in Chapter 3), in which the resources (*e.g.*, bandwidth, energy) of the hybrid network are not utilised efficiently. For example, in order to improve the quality of service (QoS) of the network, both the channel capacity and the bit error rate (BER) at the physical (PHY) layer and the channel access method at the medium access control (MAC) layer, as well as routing, source rate adaptation, *etc.*, at the upper layers should be jointly considered. Therefore, a cross-layer design of the hybrid network is necessary. In addition, indoor battery powered WSNs are suitable for applications such as chemical and petroleum refining industrial process monitoring (as mains powered WSNs are prohibited due to safety concerns) and impromptu surveillance installation due to the advantages of discreet and unobtrusive installation and removal. Also, indoor battery powered WSNs are immune to the failure of the power distribution system. In such applications, the indoor battery powered WSNs often have stringent energy budgets, how to prolong the network lifetime becomes a challenging problem.

Power line communication (PLC) is considered as a promising technology for data transmission that utilises the widespread presence of power line (PL) cables as a communication medium [24]. This ubiquitous infrastructure enables every line-powered device to become potential target of value-added services [25]. PLC is adopted in advanced energy services such as automatic electricity meter reading, supply management and energy control [26]. Owing to the high data rates that can be supported by PLC (comparable with domestic Ethernet and WiFi), another attractive application of PLC lies in the area of home networking [27–29], in which the advantage of the pervasive presence of PL cables and outlets is fully

capitalised [30]. With the recent advances in PLC technology and regulatory and standardization efforts [31], it is announced by chip manufacturers of PLC devices that millions of these devices are being shipped annually for the application of indoor and smart grid communication and the number is expected to grow in the future [32].

Among all the wired solutions for communication, PLC is the only technology that has a comparable deployment cost with the wireless solution since unlike other wired solutions such as the Ethernet, where the communication medium (Ethernet cables) needs to be installed, PLC uses existing PL cables as the communication medium [33]. Also, the communication through obstacles in PLC is reliable with high transmission rates, which however often degrades the signals in the wireless counterpart [32]. In addition, PLC can be utilised as an economical alternative to complement existing communication networks when ubiquitous coverage is desired. An architecture design of using PLC as a backhaul for WSNs to implement a smart home control network is reported in [34]. Owing to these advantages, PLC networking can be considered as a practical supplement and a strong competitor to existing WSNs.

As both WSNs and PLC are the composing parts of the IoT [3], the integration of existing communication technologies is the trend for future communication networks [15]. This trend of the flourishing of hybrid networks can be forecasted from the recent advances in the development of software-defined networking (SDN) [35–37]. Recent studies in [38–48] have reported the performance improvement in the indoor home networks or smart grids by exploiting the diversity of hybrid wireless and PLC channels. These studies either utilise the hybrid channel in serial or in parallel to improve the network throughput or reliability. Nevertheless, similar to the work in small-world network [14–23], these studies analysed the performance of such a hybrid channel in an information theoretic framework based on a single protocol layer, by which the resources in the hybrid channel are not utilised efficiently.

Network utility maximization (NUM) is used as a modelling tool, to integrate specified objectives, diverse types of constraints, design freedom and stochastic dynamics into a single optimization problem [49]. The basic NUM problem (or the Monotropic Programming) appears in the formulation in [50], and has been studied since the 1960s [51], in which NUM is used as an analytic tool of reverse-engineering transmission control protocol (TCP) congestion control [52]. Recently, it is reported in [49, 53, 54] that different protocol layers can be systematically integrated into a single coherent theory, which provides a general viewpoint to understand the interactions across various layers in the network protocol stack. In such a framework, NUM problem is decomposed into different layers. Each layer iterates on associated subsets of the optimization variables using local information to attain individual optimality [55]. By combining the results from these local algorithms, a global objective can be attained. Therefore, given a network resource allocation problem, a most suitable distributed solution can be obtained by NUM decomposition.

1.2 Research Contributions

The research conducted during this PhD study is aimed to investigate the performance improvement in the hybrid wireless-PL sensor networks for in-door applications through cross-layer design in the framework of NUM. In particular, network lifetime maximization is considered as the main design criteria in this study due to the wide spread applications of battery powered WSNs. Nevertheless, network lifetime is chosen as the network utility function to illustrate the performance improvement of the hybrid network as compared to traditional pure WSNs. The work in this thesis (Chapter 5) can be easily modified to consider other utility functions, such as minimizing total energy consumption. In this PhD research, a joint optimal design of PHY, MAC and network layers to maximize the network lifetime for hybrid wireless-PL sensor networks is investigated, and a cross-layer video encoding, channel access control and like rate allocation scheme

is developed for hybrid wireless-PL video sensor networks.

The main contributions are summarized as follows:

- A hybrid sensor network for industrial sensor network applications (*e.g.,* industrial automation process monitoring), which consists of both wireless and PL sensor nodes is proposed. The next-generation industrial automation system involves three different levels [56]: the field level, where the automation process is monitored and controlled directly by the sensors and actuators, the automation level, where the industrial controllers, such as programmable logic controllers are used to perform the process control decision making, and the management level, where best-effort IP traffic is exchanged. Typically, the devices in the field level are interconnected by an industrial wireless sensor network, while the automation and management levels are connected to wired networks [57]. According to [58], industrial WSNs differ from traditional WSNs mainly in the following aspects. Industrial WSNs are expected to have lower delay and higher QoS requirements than traditional WSNs, such that critical messages can be collected and delivered in a timely manner to handle a process disturbance or emergency. Also, industrial WSNs can be exposed to caustic or corrosive environment, such that attaching the sensor nodes to the mains power is prohibited due to safety concerns. In such environment, industrial wireless sensor nodes are commonly powered by batteries and it is of paramount importance to prolong the operating lifetime of the network. Other aspects of differences between industrial WSNs and traditional WSNs include interoperability, autonomous operation, robustness, and scalability, *etc.* Please refer to [58] for details on these aspects of differences.

  This work is different with existing work in the following aspects. First, to the best of our knowledge, it is the first reported work in the literature that focuses on the cross-layer design of such a heterogeneous network. The hybrid sensor network takes the advantage of the flexibility of WSNs

while the PL sensors are deployed to prolong the lifetime of the network. This work studies the joint design of the PHY, MAC and network layers to maximize the hybrid network lifetime, which is limited by the battery capacity of wireless sensor nodes. Second, closed-form expressions of the globally optimal solution for lifetime maximization of the hybrid sensor network are derived for two different network topologies, namely string topology and linear topology. Such closed-form solutions give insights in factors that are significant to the network lifetime when designing the hybrid sensor network. Third, the impacts of different network configurations such as source rate, sensor node densities, *etc.*, on the hybrid network lifetime are investigated. Finally, the impact of different transmission strategies of PL nodes on the effectiveness of the network is studied.

- A hybrid video sensor network (HVSN) which comprises both battery-powered wireless sensor nodes and PL sensor nodes is proposed to maximize the network lifetime. This work differs with existing work in the following aspects. First, to the best of our knowledge, it is the first reported work to investigate video sensor networks with hybrid power sources and hybrid communication schemes. The proposed HVSN utilizes the flexibility of wireless sensor nodes while PL sensor nodes are used to extend the network lifetime. Second, the joint design of video encoding rate, aggregate power consumption, channel access control, along with link rate allocation is studied for maximizing the hybrid network lifetime. The joint design achieves much better performance than separate optimization. Third, a distributed algorithm is proposed for the network lifetime maximization problem. The distributed algorithm divides the computational burden among all nodes with much lower communication overhead. Fourth, the impact of dynamic network change and network scalability is studied. The effectiveness of the proposed algorithm is validated through extensive simulation results.

1.3 Thesis Organisation

The rest of this thesis is organized as follows. An overview of sensor networks and more detailed background of wireless and PLC communications are provided in Chapter 2. Chapter 3 overviews the network protocol stack and the theory of optimization and decomposition. A joint optimal design of PHY, MAC and network layers to maximize the network lifetime for hybrid wireless-PL sensor networks is presented in Chapter 4. In Chapter 5, a cross-layer video encoding, channel access control and link rate allocation scheme is developed for hybrid wireless-PL video sensor networks. Conclusions and future work are presented in the final chapter.

1.4 Publications

- Kainan Zhu, Xu Zhu, "Cross-layer network lifetime maximization for hybrid sensor networks", in *Proc. IEEE International Conference on Smart Grid Communications (SmartGridComm)*, pp. 404-409, Venice, Italy, Nov. 2014.

- Kainan Zhu, Xu Zhu, Yufei Jiang, and Weiqiang Xu, "Novel hybrid wireless-power line video sensor networks with distributed cross-layer optimization", in *Proc. IEEE International Conference on Systems and Informatics (ICSAI)*, Hangzhou, China, Nov. 2017.

- Kainan Zhu, Xu Zhu, and Yi Huang "Cross-layer network lifetime maximization for hybrid sensor networks based on duality approach", To be submitted to *IEEE Communications Letters*.

- Kainan Zhu, Xu Zhu, Weiqiang Xu and Yi Huang "Distributed algorithms for hybrid wireless-power line video sensor networks", To be submitted to *IEEE Transactions on Circuits and Systems for Video Technology*.

Chapter 2

Overview of Sensor Networks, Wireless Communications and Power Line Communications

In this chapter, the architecture of sensor networks, the background of wireless communications and PLC technology are reviewed. In section 2.1, the basic components, data collection and communication of sensor nodes as well as typical applications of sensor networks are presented. Section 2.2.1 introduces briefly on the history of wireless communications. Section 2.2.2 presents the wireless communication channels, with focus on the large-scale propagation effects, small-scale propagation effects, and the wireless Additive White Gaussian Noise (AWGN) channel. Section 2.3.1 and 2.3.2 shed light on the history, regulation and standards in PLC. The overall PLC network architecture and indoor PLC structure are presented in Section 2.3.3 and 2.3.4, respectively. With a focus on indoor PLC, random PLC topology generator is introduced (Section 2.3.5) along with two PLC channel modelling approaches (Section 2.3.6). Noise modelling is reviewed in Section 2.3.7. Finally, this chapter is summarised in Section 2.4.

2.1 Overview of Sensor Networks

2.1.1 Architecture of Sensor Networks

Sensor nodes are deployed to collect ambient conditions (*e.g.,* temperature, humidity, sound, movement) from the observed phenomenon and then the measure-

ments can be processed and analyzed to reveal some characteristics of interest about the surrounding environment of the sensor nodes [59]. A larger number of the sensor nodes can be networked to perform specific tasks collaboratively and thus forming a sensor network.

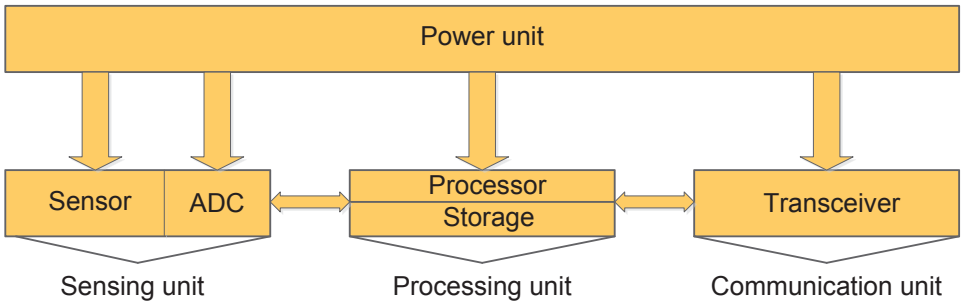

Figure 2.1: Basic components of a sensor node

Typically, a sensor node consists of four basic components [60], namely, a sensing unit, a processing unit, a communication unit and a power unit. As shown in Fig. 2.1, there are two subunits within the sensing unit, which are called the sensor and the analog-to-digital converter (ADC). The sensor collects target information from the observed environment and fed it into the ADC in analog signals. Then the analog signals are converted by the ADC into digital signals and the digital signals are transferred to the processing unit. The processing unit, which generally contains a small storage unit, performs some local information processing, such as data compression, and manages the procedures that allow the sensor node collaborate with the other nodes to carry out assigned sensing tasks [60]. The communication unit connects the node to the sensor network. Finally, the power unit provides energy supply to all the other units. In addition, depending on the specific application, the sensor node may also contain additional units, such as a location finding system to provide knowledge of location and a mobilizer that allows the sensor node to change its location or configuration (*e.g.,* to change antenna's radiation direction to enhance the signal strength) [61].

A sensor network generally contains hundreds or thousands of sensor nodes [59], which are either randomly deployed (*e.g.,* dropped from an airplane in a disaster

area) or the positions of the sensor nodes are predetermined (*e.g.,* fire alarm sensors in a facility). As shown in Fig. 2.2, the sensor nodes are scattered in an area called the sensor field. Each of the sensor nodes is capable of collecting intended data and route data back to the sink node. The sink node may communicate with the task manager node via Internet or mobile network such that the user can have access to the collected information and further data processing and analyzing can be carried out.

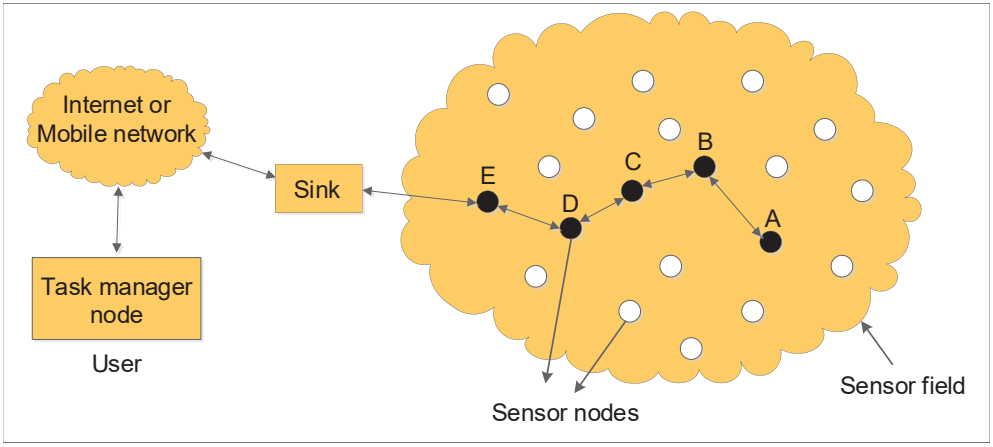

Figure 2.2: Overview of a sensor network

In particular, data collection and communication in sensor nodes can be divided as [62]: *clock-driven*, *event-driven* and *query-driven*. In a *clock-driven* data collection and communication fashion, each sensor node gather and send data at constant periodic intervals. Over time these periodically collected data can be combined to produce temporal and spatial information about the sensor field [62]. An example of such a data gathering and communication scheme is the monitoring of the humidity of soil, where the sensor nodes are buried into the soil and "snapshots" of the humidity is collected and routed to the sink node periodically. The *event-driven* and *query-driven* data collection and communication are triggered by certain events or queries, such as the detection of fire in a warehouse or the user requires the sensor nodes to report their positions. In addition, the communications between sensor nodes to the sink node can be classified into three categories as summarized below [62].

1. **Direct transmission**: In this transmission scheme, each sensor node forwards its locally generated data directly to the sink node and there is no communication between the sensor nodes. The advantage of such a transmission scheme is simple in design. However, for a sensor network that spans a large area, this approach has an inherent scalability problem since it is a many-to-one communication [62], especially when hundreds or thousands of sensor nodes are deployed in the sensor field. Also, the distance of the sink node away from the sensor field is limited since all the sensor nodes should be in reach with the sink directly. In addition, for the sensor nodes that are far away from the sink node, they may consume more energy for transmission than those sensor nodes that are close to the sink. This exposes that the sensor nodes that are far away from the sink node may be drained of energy quickly. Depending on the specific applications, the data rate of each sensor node varies between several kbps to several hundred kbps.
2. **Multi-hop routing**: In such a communication scheme, each sensor node in the sensor filed plays a dual role as data transmitter and data router and may communicate with the sink node in a multi-hop fashion. For example, in Fig. 2.2, sensor node A collects data and forward it to the sink node through the path $A \rightarrow B \rightarrow C \rightarrow D \rightarrow E \rightarrow Sink$. This approach requires collaboration between sensor nodes and it can be designed to realize different objectives, *e.g.,* maximize network throughput or minimize per node energy consumption. One potential drawback of such a routing scheme however is that there may exist some "hot spots" to which many sensor nodes will forward their data. The sensor nodes on "hot spots" may be exhausted of energy rapidly and causes significant topological changes and rerouting of packets and reorganization of the network may be necessary [59]. Generally in this case, depending on the specific applications, the data rate of the sensor nodes that are far from the sink node varies between several kbps to

several hundred kbps. While the sensor nodes that are closer to the sink node perform more duty on relaying and therefore have data rate on the order of several hundred kbps to several Mbps.

3. **Clustering**: In a clustered sensor network, the sensor nodes form clusters dynamically with neighboring sensors. This approach localizes traffic and allows more scalability of the sensor network by selecting a sensor node in each cluster as the cluster head that is responsible for relaying data from each sensor node in the cluster to the sink node. In addition, data fusion and compression may occur in the cluster head due to the fact that data from neighbouring sensors that are close enough may be in high correlation [62]. While due to the nature of the cluster head, it will inevitably consume more energy and run out of power supply than the rest nodes in the cluster. Therefore, some protocol designs (*e.g.,* the Low Energy Adaptive Clustering Hierarchy [63]) have focused on distributed cluster formation and dynamic cluster head selection problem. Depending on the specific applications, the data rate of each sensor node (except the cluster head) varies between several kbps to several hundred kbps, while the sensor nodes performing as the cluster heads have data rate on the order of several hundred kbps to several Mbps.

2.1.2 Applications of Sensor Networks

The networked sensors are widely used and deployed to collect measurements from entities of interest, *e.g.,* they can be distributed on the ground, in the soil, embedded inside building structures, or in human bodies to monitor environmental parameters and detect the occurrence of events [64]. Some applications of sensor networks are listed as follows.

1. **Structural Health Monitoring**: Sensor networks can be deployed to monitor structural parameters such as strain in a large region. Broadly speaking, structural health monitoring [65–68] aims at using sensor networks

to localize damage that is significant enough to influence the properties of the entire structure or large sections of it (*e.g.,* severe damage to an entire cable on a bridge) through structural responses due to external excitations such as heavy winds and passing vehicles. An example of such a sensor network is the deployment of 64 wireless sensor nodes over the main span and a tower of the Golden Gate Bridge to measure ambient structural vibrations [69].

2. **Industrial Process Control**: With the rapid improvement and miniaturization in hardware, low-cost hardware components such as complementary metal-oxide semiconductor (CMOS) cameras and microphones are integrated in wireless sensor nodes and thus enabling the development of wireless multimedia sensor networks [70, 71]. Such networks are able to retrieve visual and audio content, still images and scalar sensor data such as temperature, pressure, location of objects, *etc.* Therefore, wireless multimedia sensor networks are able to simplify and add flexibility to machine vision systems for visual inspections and automated actions in automated manufacturing processes [70].
3. **Homeland Security**: Electrochemical sensor networks can be used to detect weapons of mass destruction such as the bio-weapons equipped by terrorists [64]. Also, sensor networks can be used to monitor and protect critical infrastructures such as railways, airports, utility, and water supplies [72]. For example, sensor networks can be deployed in the airport to monitor the chemistry of the environment such as identifying toxic odours.
4. **Healthcare**: Wireless sensor nodes can be placed inside, on and around the human body to form a body area network (BAN) such that physiological signs and parameters such as blood pressure can be monitored [73]. Unlike conventional wired healthcare system, the wireless body area network (W-BAN) potentially provides ubiquitous real-time monitoring without compromising the convenience of users [64].

2.2 Overview of Wireless Communications

2.2.1 A Very Brief History of Wireless Communications

The very first stage of wireless communications dates back to the Pre-industrial era [74], when signal combinations such as torch signalling, smoke signalling and flag signalling, *etc.*, were designed to enable line-of-sight (LoS) information transmission. An example of such a wireless communication system is the signalling of smoke at beacon towers along the Great Wall to warn of enemy attacks in ancient China.

In 1864, the electromagnetic theory of light was developed by James Clerk Maxwell, who also predicted the existence of radio waves [75]. Later in 1887, Heinrich Hertz proved experimentally the physical existence of these radio waves. Based on the pioneering work of Maxwell and Hertz, the field of radio communications was initiated. The first wireless communication system [74] occurred in 1894, when Oliver Lodge managed to send a radio signal at a distance of 150 *m*. In 1897, the entrepreneur Guglielmo Marconi founded The Wireless Telegraph and Signal Company in the UK, and demonstrated a series of experiments on wireless communications. Years later, Marconi's wireless system became the world's first wireless system that could enable transatlantic communication.

Nowadays, based on various application scenarios, wireless communication systems have been developed into many types, such as cellular telephone systems, wireless local area networks (WLANs), satellite networks and Bluetooth, only to name a few. Detailed descriptions of the aforementioned application scenarios of wireless communication systems can be found in [74].

2.2.2 Wireless Communication Channels

The wireless channel serves as the physical transmission medium between the signal transmitter and receiver. Its characteristics have a dominate impact on the performance of the wireless communication systems, such as the maximum achievable channel capacity and the outage probability. Therefore, it is of paramount

importance to understand the characteristics of wireless channel to enable reliable high-speed communication.

2.2.2.1 Large-Scale Propagation

Large-scale propagation involves variations of the signal strength at the receiver over distance caused by path loss and shadowing. Typically, these variations occur over relatively large distances (100-1000 m in the case of path loss and 10-100 m in the case of shadowing in outdoor scenario and less in indoor scenario), and hence the name "large-scale propagation" [74].

Path Loss

Path loss is the reduction of signal strength owing to the separation of large distance between the transmitter and the receiver. In wireless communications, the transmitter radiates the energy of a signal, which then propagates through a certain medium in the form of electromagnetic waves. If part of the energy can be received at the receiver side, the information carried within the signal can possibly be recovered correctly, and therefore establishing a wireless communication link.

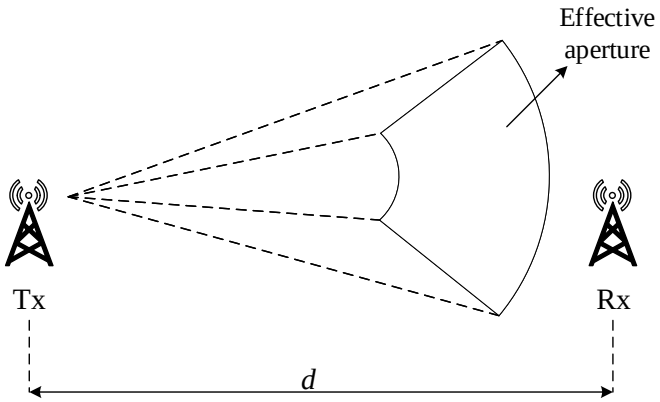

Figure 2.3: Propagation of the electromagnetic wave (d denotes the distance between Tx and Rx)

Assuming the radiation pattern of the antenna is isotropic (*i.e.*, the antenna radiates signal equally in all directions) and the electromagnetic wave propagates in the vacuum environment, then the electromagnetic wave propagates in the pat-

tern of a sphere. The energy conservation law [76] indicates that the total energy of the radiated signal remains constant through any sphere centered at the transmitter. Therefore, in the case of isotropic antenna and free space propagation, the energy at the unit area on the spherical surface centered at the transmitter decreases with the increase of the distance that the electromagnetic wave travels (the area of the spherical surface increases). Denoting the radius of the spherical surface centered at the transmitter as d, and the transmit antenna is isotropic, then the power density, P_{eff}, on the surface can be given as [76]:

$$P_{eff} = \frac{P_t}{4\pi d^2} \tag{2.1}$$

where P_t is the transmit power. In the case that the transmit antenna is not isotropic, the transmit antenna gain G_t in the direction of the receive antenna should be taken into account in the expression of P_{eff} as [76]:

$$P_{eff} = \frac{G_t P_t}{4\pi d^2} \tag{2.2}$$

The effective aperture (shown in Fig. 2.3) is a measure of the effectiveness of an antenna at receiving the power of electromagnetic waves. Mathematically, it can be expressed as [76]:

$$A_{eff} = \frac{\lambda^2}{4\pi} G_r \tag{2.3}$$

where λ is the wavelength of the operation frequency, and G_r is the receive antenna gain. According to the Friis' law [76], the received power P_r can be determined as:

$$P_r = P_{eff} \times A_{eff} = \frac{P_t G_t G_r \lambda^2}{(4\pi)^2 d^2} \tag{2.4}$$

Therefore, the free-space linear path loss (defined as the ratio of the transmit power to the receive power [76]) can be calculated as:

$$PL = \frac{P_t}{P_r} = \frac{(4\pi)^2 d^2}{G_t G_r \lambda^2} \tag{2.5}$$

More generally, the linear path loss can be expressed as:

$$PL = \frac{P_t}{P_r} = \frac{(4\pi)^2 d^n}{G_t G_r \lambda^2} \tag{2.6}$$

where n is the path loss exponent. Typically, the value of the path loss exponent can vary between 1.6 to 6 based on different propagation environments (shown in Table 2.1).

Table 2.1: Path Loss Exponent Values in Different Environment

Environment	Path Loss Exponent n
In building line-of-sight	1.6 to 1.8
Free space	2
Obstructed in factories	2 to 3
Urban area cellular	2.7 to 3.5
Shadowed urban cellular	3 to 5
Obstructed in building	4 to 6

Practically, the path loss often appears in the log form (dB value of the linear path loss). Therefore, (2.6) can be expressed in dB as:

$$PL(dB) = 10\log_{10}\frac{P_t}{P_r} = 10\log_{10}\left[\frac{(4\pi)^2 d^n}{G_t G_r \lambda^2}\right] \tag{2.7}$$

which can also be rewritten as:

$$PL(dB) = C + 10n\log_{10}d \tag{2.8}$$

where $C = 10\log_{10}\left[\frac{(4\pi)^2}{G_t G_r \lambda^2}\right]$. In addition, a simplified path loss model as a function of distance is often used in designing a wireless system, the expression can be given as [74]:

$$P_r = P_t K \left[\frac{d_0}{d}\right]^n \tag{2.9}$$

which can be written in the log form as:

$$P_r(dB) = P_t(dB) + 10\log_{10} K + 10n\log_{10}\left[\frac{d_0}{d}\right] \tag{2.10}$$

where K is a constant that is related to the antenna characteristics and the average channel attenuation, n denotes the path loss exponent, d_0 represents the reference distance for the antenna far field, and d is the distance of interest from the transmitter. Since distance affects the path loss greatly, the path loss plays a major role in designing and analysing a wireless communication system.

Shadowing

A signal may encounter obstacles (such as buildings, trees and walls) in its path of propagation. These obstacles cause effects such as reflection[1], diffraction[2] and scattering[3] to the signal and thus introducing random variations about the path loss. A widely adopted model for such random variations is the log-normal shadowing model, which has been empirically proven to be accurate in both indoor and outdoor radio propagation scenarios [74].

The effect of path loss and shadowing can be captured by a combined model that superimposes these two components. In the combined model, the average path loss is represented by the path loss model and random variations due to shadowing are then added into the model. Specifically, the ratio of the received power to the transmitted power in the log form in the combined model can be expressed as [74]:

$$\frac{P_r}{P_t}(dB) = 10\log_{10} K + 10n\log_{10}\left[\frac{d_0}{d}\right] + X_\sigma \tag{2.11}$$

where X_σ is a Gauss-distributed random variable with a zero mean and variance of σ^2, which is caused by the effect of shadowing.

2.2.2.2 Small-Scale Propagation

Small-scale propagation effect or multipath fading is the rapid fluctuations of the amplitudes, phases, or multipath delays of a wireless signal over a short period of time or distance (on the order of the signal wavelength, and hence the name "small-scale fading"), in which case the large-scale path loss effects could be ignored [74]. Small-scale fading is typically due to multipath propagation, which is often the case in urban environments. In such environments, the presence of buildings, trees, vehicles and pedestrians, *etc.*, around the transmitter and the

[1]Reflection occurs when radio waves encounter a surface with dimensions that are relatively large compared to the wavelength of the signal, *e.g.*, the surface of buildings.

[2]Diffraction occurs when radio waves propagate around the sharp edge of an object that is impenetrable with dimensions larger than the wavelength of the signal, *e.g.*, street corners.

[3]Scattering occurs when radio waves encounter an object with dimensions in the order of the wavelength of the signal or less, *e.g.*, rain drops.

receiver could cause reflection, diffraction, and scattering of the transmitted signal. Consequently, the transmitted signal arrives at the receiver through different paths, and each of the paths generates a unique wave of the transmitted signal with random variations of the amplitude, phase, and delay. Finally, all the waves undergoing different paths are combined at the receiver, and causes distortion and fading to the transmitted signal. In the following, factors and parameters relating to small-scale fading will be introduced.

Root Mean Square Delay Spread

In wireless communications, the transmitted signal undergoes different paths and therefore, arrives at the receiver at different times of arrival. The delay spread is a measure of the difference between the time of arrival of the earliest multipath component and the time of arrival of the latest multipath component. The delay spread can be characterised by the power delay profile, which is the distribution of received signal power as a function of the propagation delays, and can be obtained empirically [74]. Denoting g_i and τ_i as the path gain and delay for the i-th path of a transmitted signal, respectively, then the mean excess delay $\bar{\tau}$, which is the first moment of the power delay profile, can be defined as [77]:

$$\bar{\tau} = \frac{\sum_i g_i^2 \tau_i}{\sum_i g_i^2} \tag{2.12}$$

The root mean square (RMS) delay spread is the square root of the second central moment of the power delay profile [77] and can be determined as:

$$\sigma = \sqrt{\bar{\tau^2} - (\bar{\tau})^2} \tag{2.13}$$

where

$$\bar{\tau^2} = \frac{\sum_i g_i^2 \tau_i^2}{\sum_i g_i^2} \tag{2.14}$$

These delays are measured relative to the first detectable signal arriving at the receiver at $\tau_0 = 0$. If there is only one path, the RMS delay spread would be zero. The RMS delay spread is a representation of the effect of multipath, *i.e.*, a higher RMS delay spread value indicates a larger effect of the multipath.

Coherence Bandwidth

The coherence bandwidth is a statistical measure of the range of frequencies over which the channel can be considered "flat", that is a channel passing all spectral components with approximately equal gain and linear phase. Or coherence bandwidth is the range of frequencies where two frequency components have a strong potential correlation for amplitude [77]. The coherence bandwidth can be derived from the RMS delay spread, while the exact relationship between the coherence bandwidth and the RMS delay spread depends on the definition. If the coherence bandwidth is defined as the bandwidth over which the frequency correlation function is above 0.9, then the coherence bandwidth is approximately [77]:

$$B_c \approx \frac{1}{50\sigma} \tag{2.15}$$

where σ is the RMS delay spread. While in the case that the coherence bandwidth is defined as the bandwidth over which the frequency correlation function is above 0.5, then the coherence bandwidth is approximately [77]:

$$B_c \approx \frac{1}{5\sigma} \tag{2.16}$$

It can be noticed that the coherence bandwidth and the RMS delay spread are inversely related. An increase of the RMS delay spread value will result in a decrease of the coherence bandwidth.

Doppler Spread

Doppler spread, B_d, is a measure of the broadening in spectrum due to the time varying nature of the mobile radio channel. For example, in the case of mobile radio channel, when a pure sinusoidal wave with frequency f_c is transmitted, the received signal spectrum (or the Doppler spectrum[4]) will have components ranging from $f_c - f_d$ to $f_c + f_d$, where f_d denotes the Doppler shift[5]. Specifically, the

[4]Doppler spread can be regarded as the "bandwidth" of the Doppler spectrum.

[5]Doppler shift is caused by the movement of the user (or surrounding physical presences in the environment). The user's velocity will induce a shift in the frequency of the transmitted signal along each signal path.

Doppler shift is a function of the relative velocity of the mobile v, the wavelength of the carrier frequency λ, and the angle between the direction of the mobile user's motion and the direction of the received signal wave θ. Mathematically, the Doppler shift can be expressed as [77]:

$$f_d = \frac{\nu}{\lambda} \cos\theta \tag{2.17}$$

In wireless communications, a transmitted signal may undergo different paths through its way to the receiver, and each path will induce different Doppler shifts. The maximum Doppler shift is achieved when the direction of the mobile user's motion is in accordance with the direction of the received signal wave, with $\theta = 0$ and $f_{max} = \frac{\nu}{\lambda}$. The difference in Doppler shifts between different signal components is referred to as the Doppler spread.

Coherence Time

The coherence time, T_c, is the time duration over which the channel impulse response remains invariant, or the time duration over which two received signals have a strong potential correlation in amplitude [77]. Generally, the coherence time can be employed to characterise the time varying nature of the frequency dispersiveness of the channel in the time domain. The coherence time and Doppler spread are inversely proportional to each other, as given by [77]:

$$T_c \approx \frac{1}{f_{max}} \tag{2.18}$$

where f_{max} is the maximum Doppler shift. In the case that the coherence time is defined as the time over which the time correlation function is above 0.5, then the mathematical expression for coherence time becomes [77]:

$$T_c \approx \frac{9}{16\pi f_{max}} \tag{2.19}$$

The definition of coherence time suggests that two signals arriving with a time separation larger than T_c will be affected differently by the channel.

Types of Small-Scale Fading

With the factors and parameters relating to small-scale fading introduced (*i.e.*, RMS delay spread, coherence bandwidth, Doppler spread, and coherence time), different types of small-scale fading can be categorised based on the thresholds of the relating factors and parameters, together with the characteristics of the transmitted signal, *e.g.*, signal bandwidth and symbol period. Generally, four types of fading effects can be categorised, namely, flat fading, frequency selective fading, fast fading and slow fading [74]. These fading types and the corresponding conditions are shown in Table 2.2. In the following, these types of fading will be explained in detail.

Table 2.2: Small-scale fading types

Flat Fading	Signal Bandwidth $<$ Coherence Bandwidth
Frequency Selective Fading	Signal Bandwidth $>$ Coherence Bandwidth
Fast Fading	Coherence Time $<$ Symbol Duration
Slow Fading	Coherence Time $\gg$ Symbol Duration

- **Flat Fading** - If the symbol period of a transmitted signal, T_s, is larger than the RMS delay spread of a wireless channel, σ, or the bandwidth of the transmitted signal, B_s, is smaller than the channel coherence bandwidth, B_c, then the channel is referred to as a flat fading channel [74]. In a flat fading channel, the channel exhibits approximately the same channel gain and linear phase throughout the transmission bandwidth. The channel gains of a flat fading channel is time-varying according to certain distributions such as Rician fading, Rayleigh fading, and Nakagami fading [77].

- **Frequency Selective Fading** - Contrary to the flat fading channel, if the symbol period of a transmitted signal, T_s, is smaller than the RMS delay spread of a wireless channel, σ, or the bandwidth of the transmitted signal, B_s, is larger than the channel coherence bandwidth, B_c, then the channel

is referred to as a frequency selective fading channel [74]. In a frequency selective fading channel, the previous transmitted symbols can cause interference to the current transmitted symbols, as the waves with long delays of the previous transmitted symbols and the waves with short delays of the current transmitted symbols can arrive at the receiver concurrently. This interference is known as the inter-symbol interference (ISI). In the frequency domain, the ISI is presented by a formation that frequency components of the received signal spectrum have different amplitudes.

- **Fast Fading** - If the symbol period of a transmitted signal, T_s, is larger than the channel coherence time, T_c, or the bandwidth of the transmitted signal, B_s, is smaller than the Doppler spread, B_d, then the channel is referred to as a fast fading channel [74]. In a fast fading channel, the channel changes so rapidly that the signal undergoes different channels within the time duration of one symbol period.

- **Slow Fading** - If the symbol period of a transmitted signal, T_s, is much smaller than the channel coherence time, T_c, or the bandwidth of the transmitted signal, B_s, is much larger than the Doppler spread, B_d, then the channel is referred to as a slow fading channel [74]. In a slow fading channel, the channel remains static over one or several continuous symbol periods.

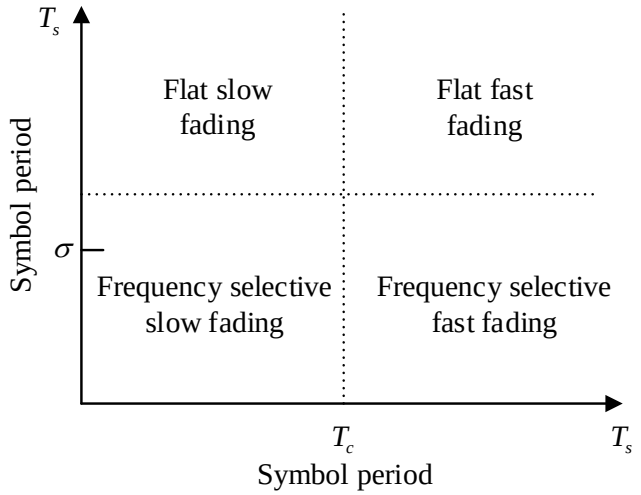

Figure 2.4: Fading types classified by symbol period

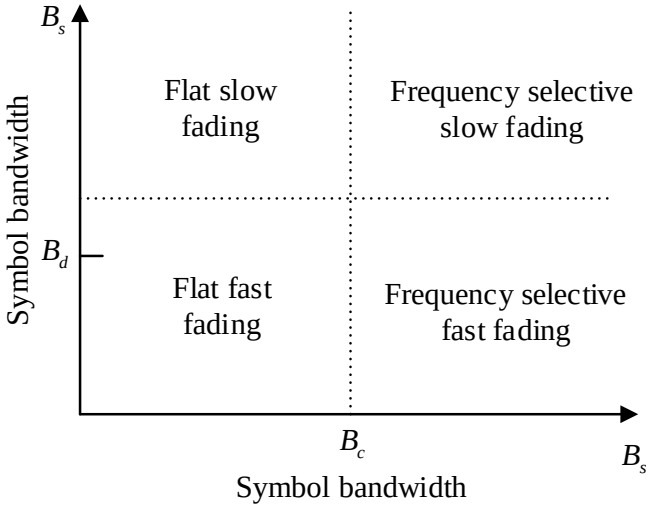

Figure 2.5: Fading types classified by symbol bandwidth

Flat and frequency selective fading determine the frequency diversity of the channel while fast and slow fading determine the time diversity of the channel. Based on the different fading effects, four small-scale fading channels can be categorised, namely, flat fast fading channel, flat slow fading channel, frequency selective fast fading channel, and frequency selective slow fading channel. These four channels are illustrated in Fig. 2.4 and Fig. 2.5 as classified based on the symbol period, T_s, with the RMS delay spread, σ, and the channel coherence time, T_c, as thresholds, and based on the symbol bandwidth, B_s, with the Doppler

spread, B_d, and the channel coherence bandwidth, B_c, as thresholds, respectively.

2.2.2.3 Additive White Gaussian Noise Channel

The wireless communication channel has various channel impairments that could cause errors. Noise, which is an inevitable component in the design and analysis of the performance of a communication system, refers to the undesired signals that would affect the fidelity of the desired signal. In wireless communication systems, there are various types of noise. For example, the thermal noise and the impulse noise. In the case of direct LoS path between the transmitter and the receiver, the additive white Gaussian noise channel can provide a reasonably good model. In the AWGN channel, the noise is always assumed to be white which indicates that all frequency components in the noise exhibit the same power and the transmitted signal is added with a noise component that has a Gaussian distribution with zero-mean. Mathematically, the AWGN channel model can be expressed as [74]:

$$r(t) = s(t) + n(t) \tag{2.20}$$

where $s(t)$ is the transmitted signal, $n(t)$ is the zero-mean white Gaussian noise process with the power spectral density of N_0, $r(t)$ is the received signal, and t denotes the time.

Assuming the AWGN channel has a bandwidth of B, a transmit power of P, then the capacity of this channel, C, can be provided by the Shannon's formula [78]:

$$C = B \log_2(1 + \frac{P}{N_0 B}) \tag{2.21}$$

where N_0 is the power spectral density of the noise.

In this thesis, AWGN channel model is used while there are other channel models such as the Rayleigh fading channel and the Rician fading channel, which are introduced in detail in [74].

2.3 Overview of Power Line Communications

2.3.1 A Brief Historical Evolution

The very early prototype of PLC dates back to 1838 [79], when remote electricity supply metering was proposed aiming to measure the voltage levels of batteries at unmanned sites. Later in 1897 and 1905, the PL signalling electricity meter was patented in the UK and U.S., respectively [80]. Transmitting voice messages over high voltage PL occurred in the 1920s [80], when power companies use PL as a substitute for telephone lines (running parallel to the PL) for the communication between transformer stations. Since the telephone circuits are expensive and telephone lines are fragile to harsh environment (*e.g.*, mountainous terrain, bad weather). In 1950, Ripple Control systems, as recognised as the first PLC systems, were designed and then deployed over medium- and low-voltage electrical networks to enable power companies to deliver electricity alongside with commands such as load control and tariff switching to end-users [81]. Typically, the aforementioned applications of PLC require low data rates and operate in the narrow-band (NB) frequency range of PLC, termed NB PLC, and real-time communication is not required.

With the evolution of technology, the applications in sense of a modern home network include but are not restricted to simultaneous Internet access, shared printers, home control and remote monitoring, only to name a few. In these applications, traditional NB PLC fails to deliver the upsurging data rate requirements. On the other hand, these increasing end-user demands coupled with the deregulated telecommunication market over the past few decades, has prospered the development of what is known as the broadband (BB) PLC. BB PLC operates in high frequency bands and can achieve very high data rates (several Mbps to several hundred Mbps) while at the mean time is able to provide real-time communication, as required in standard-definition television (SDTV) or high-definition television (HDTV).

PLC technologies can be categorized into three classes according to their operational bandwidth [82], namely, ultra narrowband (UNB), NB and BB PLC, which are specified in standards of IEEE 1901.2 and IEEE 1901. Table 2.3 summarizes the corresponding bandwidth, achievable data rates and the modulation types for different PLC technologies.

Table 2.3: Categorization of PLC Technology Based on Operating Bandwidth

PLC classes	UNB	NB	BB
Bandwidth	0.3-3 kHz or 30-300 Hz	3-500 kHz	1.8-250 MHz
Support data rate	around 100 bps	few kbps to 500 kbps	several Mbps to several hundred Mbps
Modulation	CDMA	FSK	OFDM
Communication range	up to 150 km [32]	up to several km	up to several hundred meters

UNB PLC provides a rather modest data rate, near 100 bits-per-second (bps), while it supports a very large operational range (up to 150 km) mainly due to the fact that it has a small path loss effect (around 0.01 dB/km) and it is able to pass through transformers easily [82]. Such a mature PLC technology has been used in field for at least two decades and it has been deployed for various of utilities. NB PLC support higher data rate than UNB PLC at the expense of transmission range. NB PLC can be further divided into low data rate NB PLC and high data rate NB PLC depending on whether single carrier or multiple carriers are used. At last, BB PLC supports data rate up to several hundred Mbps. It is normally limited for the use of home networking due to the fact that it is difficult to pass through transformers and PL signals on different phases may not be able to communicate with each other [82].

2.3.2 Regulation and Standardization Activities

2.3.2.1 Regulation Activities

The superimposing of high-frequency signals on PL causes electromagnetic radiation [83], which is more an issue in BB PLC that operates in high frequency bands. Therefore, regulations are imposed on PLC to limit the strength of the signals coupled into PL. For details of these regulations, refer to [24, 29, 84].

Some regulation bodies of NB PLC include the European Committee for Electrotechnical Standardization (CENELEC) bands, the U.S. Federal Communications Commission (FCC) bands, the Japanese Association of Radio Industries and Businesses (ARIB) bands and the Chinese Electric Power Research Institute (EPRI) bands. In particular, the CENELEC in Europe divides the NB PLC into four frequency bands, where band A (3-95 kHz) is reserved for energy providers, band B (95-125 kHz) is reserved for users, band C (125-140 kHz) is reserved for users as well while it is regulated to carrier-sense multiple-access with collision avoidance (CSMA/CA) mechanism, and band D (140-148.5 kHz) is reserved for users for alarm and security systems [29].

The regulation activities in BB PLC can be found in European Norm (EN) 50561-1 and Code of Federal Regulations, Title 47, Part 15 (47 CFR Part 15) by the U.S. FCC. Particularly, EN 50561-1 applies to indoor PLC within the bandwidth of 1.6-30 MHz. The limits specified in these documents impose power spectral density (PSD) masks of around -55 dBm/Hz for transmission up to 30 MHz at an impedance of 100 Ω, which is compatible with the PSD requirements in the standards ITU-T G. 9964 and IEEE 1901 [32].

2.3.2.2 Industrial and International Standards

Since the formation of the Working Group (WG) in June 2005, IEEE P1901 focuses on indoor and access networks with the frequency band of 2-30 MHz (up to 50 MHz as optional extension) targeting at a transmission data rate of more than 100 Mbps at the PHY layer [32]. The Gigabit Home Networking (G.hn)

standard by International Telecommunication Union (ITU) Telecommunication Standardization Sector applies to PL, phone lines and coaxial cables aiming at a data rate of up to 1 Gbps for indoor networking [32]. In this standard, three bands ranging from 2 MHz to 25, 50, and 100 MHz, are considered for PLC. Other standardization and industry specifications of PLC include HomePlug Power Alliance, Powerline Related Intelligent Metering Evolution (PRIME) and G3-PLC. For details of standards and industry specifications, refer to [24, 29, 32, 84].

2.3.3 PLC Network Architecture

The electricity distribution systems can be categorised into three network levels according to their transmission voltages (shown in Fig. 2.6). Each network level can be used as a communication infrastructure for the realization of PLC networks [85]. Typically, high-voltage (HV) networks (110 - 750 kV) deliver the electricity from power stations to large supply regions through overhead PL cables, which usually range a long distance (on the order of hundreds of km). Medium-voltage (MV) networks (10 - 30 kV) distribute the electricity supply to sub-stations in densely populated area through both overhead and underground PL infrastructures. Low-voltage (LV) networks (220 - 400 V) supply power to end-users through overhead or underground PL networks depending on the deployment environment. In addition, the LV network is composed of two parts: LV access network (outdoor) and indoor network. The indoor network belongs to the end-users while the outdoor part is owned by power companies.

The HV and MV PLC networks can be typically used as a means for smart grid and automatic meter reading. While the indoor PLC network can be used as an infrastructure for indoor automation or indoor multimedia applications. In this thesis, the indoor PLC network is considered since it has a wide spread of applications and is of the interest as a last-mile to the end-users.

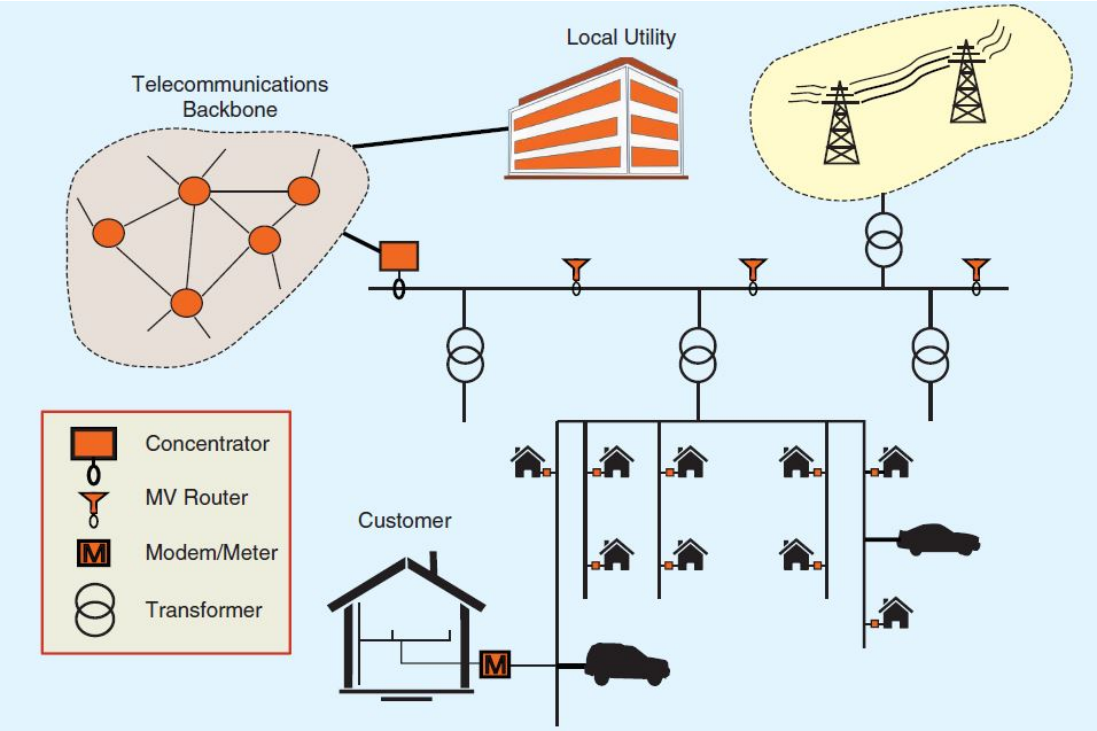

Figure 2.6: Structure of a PLC network [85]

Here, the example of automatic electricity meter readings is described to show the information flow within these network levels. Local usage information is collected by meter that is located in the house of end-user and sent across the LV access network [85]. After data aggregation at an LV router, it reaches an MV router by passing across the transformer. Finally, the MV routers transmit the information to a concentrator that can reach the power supply company through a dedicated communication infrastructure (*e.g.,* Wide area network (WAN)) [85]. Information flow in the opposite direction applies when control data is sent from the power supply company to the end-user.

2.3.4 Indoor PLC structure

Indoor PLC networks take the existing internal PL cables as communication medium, a simplified structure of indoor PLC network is shown in Fig. 2.7. In such a network, different types of home appliances (light bulb, washing machine, microwave oven, *etc.*) are attached to micro-controllers, which collect the infor-

mation, such as energy consumption, of each home appliance. Then through PLC adaptors, home appliances are able to exchange such information through the service panel. The service panel (or gateway), which interconnects all the devices attached to the PLC adaptors, controls the indoor PLC network, and enables inter-device communication. The service panel can be positioned with the Meter (as shown in Fig. 2.6), or in any other places in the indoor PLC network, which can potentially connect to the outdoor network through PLC access system or an access system provided by other communication technology (*e.g.*, Ethernet) [24]. Other applications of indoor PLC include file sharing between laptops (laptops are attached to PLC adaptors), printing (*e.g.*, from computers to printer), *etc.*

Disturbances in the indoor PLC networks can be caused by electricity distribution, operating devices, and the plug in/out of appliances inside the network, along with external interference (*e.g.*, radio station or base station). In addition, the impedance mismatch [24] between different types of loads and PL causes multi-path channel fading, which makes PL a harsh environment for data transmission.

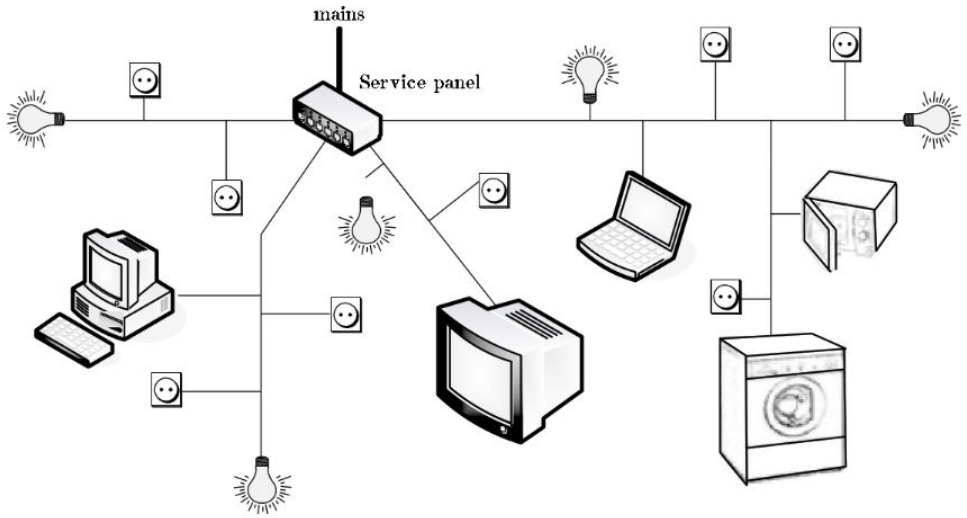

Figure 2.7: Illustration of an indoor PLC network [24]

2.3.5 Random Indoor PLC Topology Generator

Before PLC channel characteristics are presented, it is essential to introduce a random indoor PLC topology generator [86] that can reflect the physical reality. The random topology generator provides an insightful understanding of PLC network dynamics.

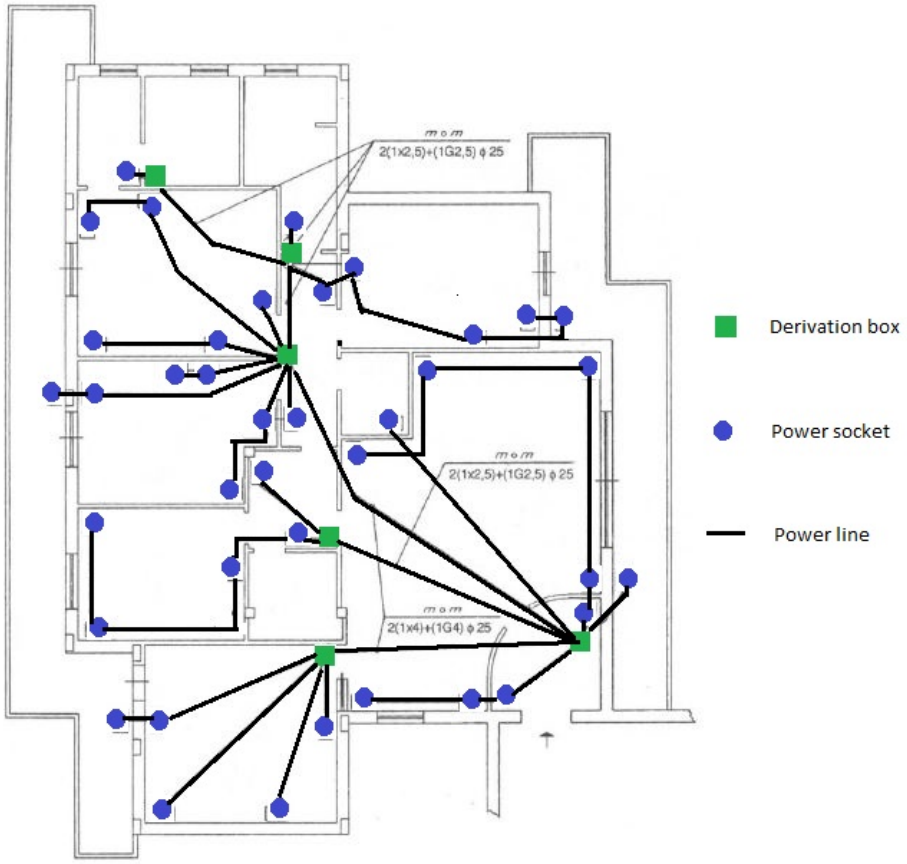

Figure 2.8: An example of detailed indoor PLC structure showing derivation boxes and connections with power sockets [86]

From the analysis of European indoor norms and wiring practices, it is found that an indoor PLC topology can be divided into areas that contain the derivation box and all the power sockets that are connected to it [86], referred to as "clusters" (as shown in Fig. 2.8). A two-level connection structure presents in this network topology. The first connection level exists between the power sockets and the corresponding derivation box and the second connection level is the inter-connection between derivation boxes. The derivation boxes are used as the

coordinator in the associated clusters and typically, for an indoor PLC network to connect with the outdoor network, one of the derivation boxes is assigned as the service panel or gateway (as shown in Fig. 2.7). Generally, as proved by experimental evidence, the clusters have a rectangular shape and are of the same area on average [86]. Therefore, a statistical topology model can be generated based on the concept of clusters.

Considering a certain topology area of A_f and by adopting the concept of clusters, the topology area can be divided into several clusters that are of the same area. If the cluster area is denoted as A_c, it satisfies a uniform distribution over a proper interval, *i.e.*, $A_c \sim \mathcal{U}\ (A_m, A_M)$, where the values of A_m and A_M are obtained from experimental data [86], *i.e.*, the values are obtained from statistical study of numerous real-life scenarios. The number of clusters N_c can be calculated according to:

$$N_c = \left\lceil \frac{A_f}{A_c} \right\rceil \tag{2.22}$$

The symbols $\lceil \cdot \rceil$ represent the ceiling operator.

Given a certain area, and with the concept of clusters, and the number of clusters determined, the random topology can be generated as follows. A boolean matrix of the size $r \times c$ is used to represent the division of the area in rc clusters, where 1 in the matrix represents the presence of the cluster while 0 represents the absence of the cluster area. For the boolean matrix below,

$$M = \begin{bmatrix} 1 & 1 & 1 & 1 \\ 1 & 1 & 0 & 0 \end{bmatrix}$$

it represents the topology layout shown in Fig. 2.9, where each block represents a cluster.

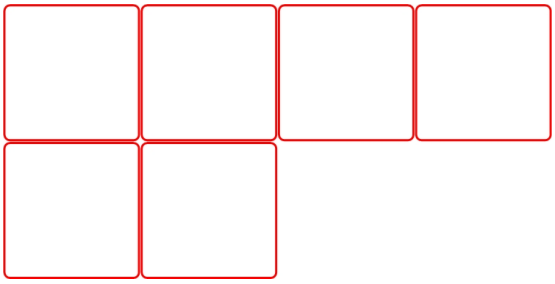

Figure 2.9: An example of cluster arrangement

To increase the randomness of the topology, r is required to obey a uniform distribution that satisfies the condition, $r \sim \mathcal{U}\ (1, N_c)$. Thus the number of column can be find from $c = \lceil N_c/r \rceil$. The above calculation of the number of column may make the overall matrix element number rc larger than the cluster number N_c. Therefore, when the value of rc exceeds the number of clusters, N_c, all the elements in the first r-1 rows and c-1 columns of the matrix are set to 1. Then a set of elements, N_c-(r-1)(c-1), in r-th row and c-th column is randomly chosen and set to 1. Thus the overall elements in the matrix is equal to the number of clusters.

Derivation boxes can be regarded as the "root" of the cluster, as it can be seen as the top node of the tree representation that illustrates the power socket connections inside a cluster [86]. It is assumed that the derivation box is always placed on the top left corner in a cluster. But the position of the derivation box can be shifted from the corner by a bidimensional offset as described in [86]. For a topology representation matrix, one of the derivation box in the clusters is considered as the service panel or gateway of the indoor PLC network [86]. All the derivation boxes in the rest clusters are either directly connected to the gateway or to the nearest derivation box in the direction of the gateway [86]. For the derivation box connections, it is required to satisfy the minimum distance criterion and the root connections cannot be cyclic [86]. Fig. 2.10 shows a possible derivation box connection for the topology layout in Fig. 2.9, where the derivation box located in $M(1, 2)$, *i.e.*, the first row and the second column, is the gateway.

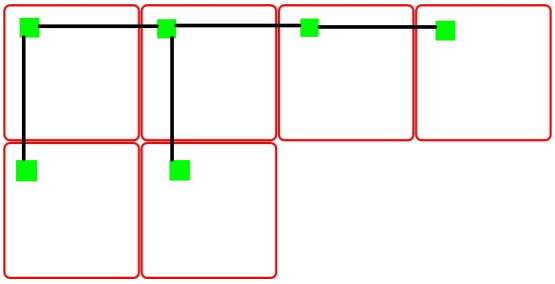

Figure 2.10: An example of connections within derivation boxes (derivation boxes are denoted by the green squares)

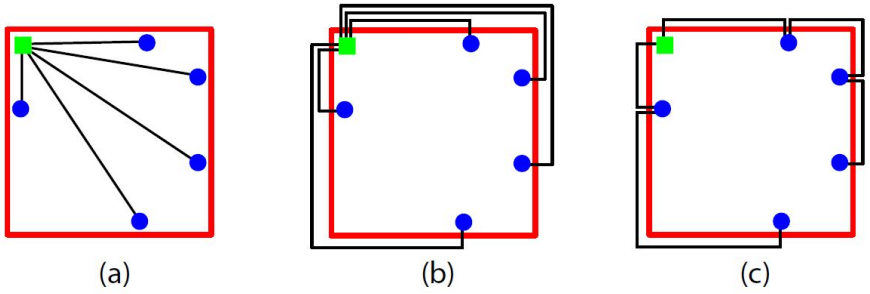

Figure 2.11: Common connection structures between outlets and derivation box (a) type SD (b) type SP and (c) type BP (the blue dots represent power sockets) [86]

The power sockets are situated along the cluster perimeter and the number of power sockets satisfies a Poisson arrival process with a mean of $\Lambda_o A_c$, where Λ_o is the density of power sockets in a cluster [86]. For the connection between the power sockets and the associated derivation box (as shown in Fig. 2.11), there are generally three types, namely type SD (Star structure that satisfies the minimum Distance criteria), type SP (Star topology with conductors placed along the Perimeter) and type BP (Bus topology with conductors placed along the Perimeter). The distance between each power socket to the derivation box follows certain probability density function (PDF) based on cluster side length [86]. Each power socket is then randomly attached with certain load with or without frequency-selective impedance [87]. Fig. 2.12 depicts a randomly generated indoor PLC network topology with the parameters in Table. 2.4.

Table 2.4: Parameters used for random PLC topology generation

Parameter	value	description
$A_f(m^2)$	160	total topology area
$A_c(m^2)$	$\mathcal{U}$(20,50)	cluster area
Λ_0(outlets/m^2)	0.2	outlet density in a cluster

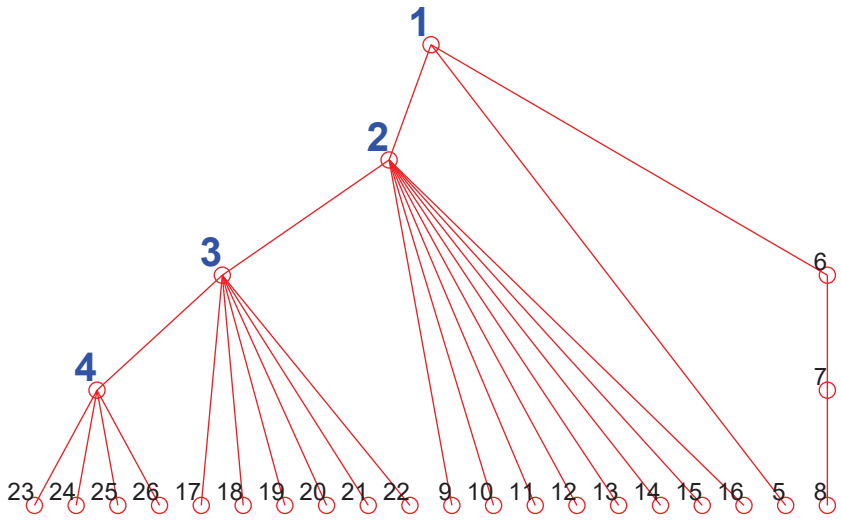

Figure 2.12: Tree plot of a randomly generated indoor PLC network topology with the parameters in Table. 2.4 (circles marked with blue numbers indicate derivation boxes and circles marked with black numbers denote power sockets)

2.3.6 PLC Channel Modelling

Starting from the random indoor PLC topology generator, it is now possible to model the indoor PLC channel. Initially designed for the purpose of electricity distribution, the PL channel is a very harsh medium for data communication. Generally, it suffers from frequency selective fading which is caused by signal reflections due to impedance mismatch between different types of loads and PL cables [24]. Also, it is prone to topology changes caused by factors such as the plug in/out of appliances, which makes the PL channel time-varying. Various sources of noise in PLC further degrade the performance of the PL channel [29]. Therefore, the modelling of PLC channel to explore PLC channel characteristics, which facilitates the development of advanced technology to combat these PLC

channel impairments has become an inevitable necessity.

Research efforts on PLC channel modelling during the recent years have prospered in two directions, the bottom-up approach (or deterministic approach) [30, 86–88] and the top-down approach (or statistical approach) [89–91]. The bottom-up approach exploits the transmission line (TL) theory to compute the channel transfer function (CTF) and henceforth obtaining frequency response of the PL channel. The CTF can be obtained deterministically based on the network topology. While the bottom-up approach captures physical reality, it has a rather high computational complexity. The top-down approach, however, treats the PL channel as a black box and the channel response is obtained by fitting certain statistical data from experiment into the channel parametric function [89]. This approach enables a fast channel simulation while at the cost of lossy link to the physical reality.

2.3.6.1 Bottom-Up Approach

Bottom-up approach is developed based on the TL theory [92], in which complete information of the network topology is required. In order to calculate the CTF between any pairs of power sockets in the PLC network, backbone path (the shortest path between the pair of power sockets) identification and topology remapping is necessary. Fig. 2.13 shows the identification of the backbone path for a randomly generated topology as detailed in Section 2.3.5 to obtain the CTF between node 9 and node 4. Fig. 2.14 depicts the remapped PLC topology along the backbone path.

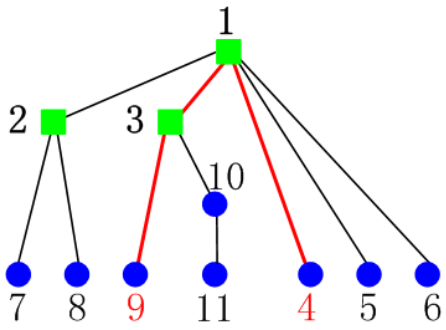

Figure 2.13: Backbone path identification (the path marked by red line is the backbone path)

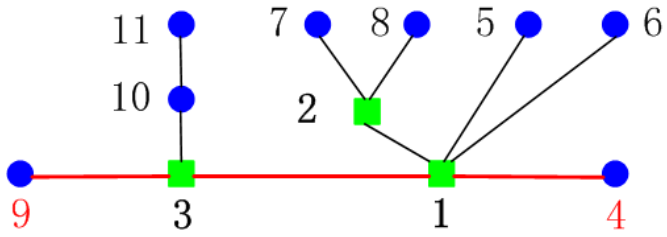

Figure 2.14: Topology remapping along the backbone path

To simplify the calculation of CTF, the impedances that are not on the backbone path are carried back on the backbone path exploiting TL theory (*i.e.*, node 2, 5-8, and 10, 11 in Fig. 2.14). To start with, it is assumed a transverse electromagnetic (TEM) or quasi TEM propagation mode[6] [86]. As shown in Fig. 2.15, for a TL of the length l, characteristic impedance Z_C and propagation constant γ, with an impedance load Z_L, the equivalent impedance Z_R from the line input can be calculated exploiting TL theory [86],

$$Z_R = Z_C \frac{Z_L + Z_C \tanh(\gamma l)}{Z_C + Z_L \tanh(\gamma l)} = Z_C \frac{1 + \rho_L e^{-2\gamma l}}{1 - \rho_L e^{-2\gamma l}} \tag{2.23}$$

where $\rho_L = (Z_L - Z_C)/(Z_L + Z_C)$. The above equation is used recursively for impedance carry-back.

[6] In the Transverse Electric (TE) mode, the electric vector (E) is always perpendicular to the direction of propagation, while there is only a magnetic field along the direction of propagation. In the Transverse Magnetic (TM) mode, the magnetic vector (H) is always perpendicular to the direction of propagation, while there is only an electric field along the direction of propagation. In the TEM mode, both the electric vector (E) and the magnetic vector (H) are perpendicular to the direction of propagation.

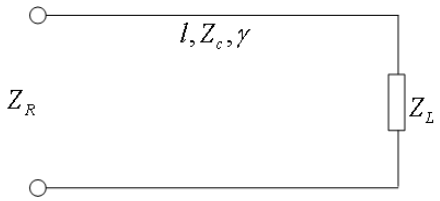

Figure 2.15: Illustration of a section of transmission line terminated with load

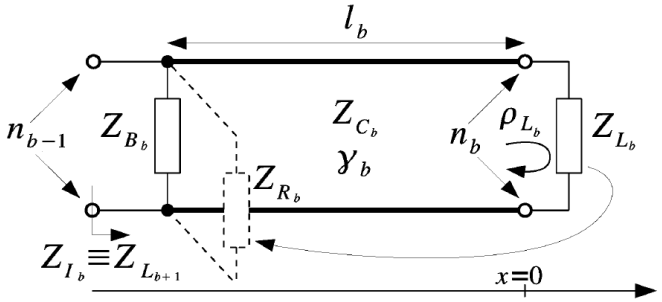

Figure 2.16: Elements in backbone portion [86]

To calculate the CTF, considering a backbone portion (shown in Fig. 2.16) that consists an output node (towards the receiver terminal) and an input node (towards the transmitter terminal), if the characteristic impedance of a transmission line segment is denoted as Z_{C_b}, the propagation coefficient is denoted as γ_b, the length of the associated backbone line unit is l_b and the load at the output node is Z_{L_b}, then the load reflection coefficient for the backbone portion is calculated as [86]

$$\rho_{L_b} = \frac{Z_{L_b} - Z_{C_b}}{Z_{L_b} + Z_{C_b}} \tag{2.24}$$

Then, based on the voltage ratio approach (VRA) [86], the CTF for a backbone portion can be obtained by

$$H_b = \frac{V_b}{V_{b-1}} = \frac{1 + \rho_{L_b}}{e^{\gamma_b l_b} + \rho_{L_b} e^{-\gamma_b l_b}} \tag{2.25}$$

where V_{b-1} and V_b are the voltage at the input node and output node, respectively. If the backbone is divided into $N + 1$ units, and denoting f as the operating frequency, the total CTF can be computed as [86]

$$H(f) = \prod_{b=1}^{N+1} H_b(f) \tag{2.26}$$

where the characteristic impedance of the transmission line segment, Z_{C_b}, and the propagation coefficient, γ_b, are frequency dependent.

Other than VRA, ABCD matrix method [93] can also be used to calculate the CTF.

2.3.6.2 Top-Down Approach

The bottom-up approach is able to obtain deterministic CTF with the requirement of global information of all elements in the PLC network (*e.g.*, PL cable types, PL cable lengths, load impedances). Especially, when a large scale of PLC network is considered, it would incur tremendous computational complexity, not to mention the required global information is usually difficult, if not impossible, to obtain [89]. In light of the drawbacks of bottom-up approach, top-down approach is advocated by a lot of studies [89–91] due to much reduced complexity. Top-down approach treats the PL channel as a black box [89], of which the general statistics of CTF is studied based on extensive experimental measurements. By analysing the measurement results, general channel parametric function is derived to obtain CTF by data fitting, which requires very few relevant parameters (or statistical data) of the PLC network.

A widely adopted top-down approach to model the CTF is reported in [89], in which the effects of multipath propagation, cable length, multipath delay, and frequency selective attenuation are jointly considered. In this model [89], the frequency response of CTF is given by

$$H(f) = \sum_{i=1}^{N} g_i \cdot e^{-(a_0 + a_1 \cdot f^k) \cdot d_i} \cdot e^{-j2\pi f (d_i / v_p)} \tag{2.27}$$

where N is the number of paths, g_i is a weighting factor that is related to the reflection and transmission factors along a propagation path. a_0 and a_1 are attenuation parameters, while k is the exponent of the attenuation factor with typical values between 0.5 and 1. These three parameters are typically derived from measurement statistics of the CTF. d_i and f indicate the length of path i and the frequency, respectively. The second term, $e^{-(a_0 + a_1 \cdot f^k) \cdot d_i}$, as a whole accounts

for the attenuation on the ith path, which becomes more severe with the increase of d_i and f. v_p represents the propagation speed and $\frac{d_i}{v_p}$ indicates the delay τ_i on the ith path. The last portion of this model, $\sum_{i=1}^{N} e^{-j2\pi f(d_i/v_p)}$, accounts for the multipath delay.

In the PL signal propagation, it does not only occur along a direct line-of-sight (LoS) path between the transmitter and the receiver, but additional paths (signal reflections) should also be taken into account, which results in a multipath signal propagation scenario. For example, in the network topology shown in Fig. 2.17, considering point A as the transmitter and C as the receiver, then the signal propagation paths due to multiple reflections could be: $A \rightarrow B \rightarrow C$, $A \rightarrow B \rightarrow D \rightarrow B \rightarrow C$, $A \rightarrow B \rightarrow D \rightarrow B \rightarrow D \rightarrow B \rightarrow C$, and so on. The signal propagation undergoing different paths would arrive at the receiver at different times, and hence causes multipath delay.

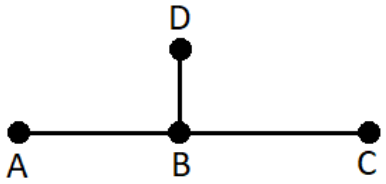

Figure 2.17: PLC multipath signal propagation

The top-down model allows fast CTF generation with statistical data fitting. However, extensive experimental measurements are required to determine the parameters (*e.g.*, a_0, a_1 and k). In [94], the Open PLC European Research Alliance (OPERA) classed 9 reference channels as representatives of real PL channels for LV/MV network. Later in [95], 9 sets of parameters are reported corresponding to the 9 reference channels in [94], which allows the fast statistical generation of 9 class CTF.

2.3.7 PLC Noise Modelling

Unlike other communication systems, PLC channel experiences various types of noise from various sources. Generally, noise in PLC can be broadly classified in-

to two categorises [96]: background noise and impulsive noise (IN). Background noise can be considered as stationary since it varies slowly for a relatively long period of time [96]. Based on the origin, occupant spectrum, duration and intensity, background noise can be further classified into coloured background noise and NB noise, while IN can be categorised into periodic IN asynchronous to the mains frequency, periodic IN synchronous to the mains frequency, and asynchronous IN. A detailed classification of noise in PL channel is shown in Fig. 2.19 and detailed descriptions are provided below.

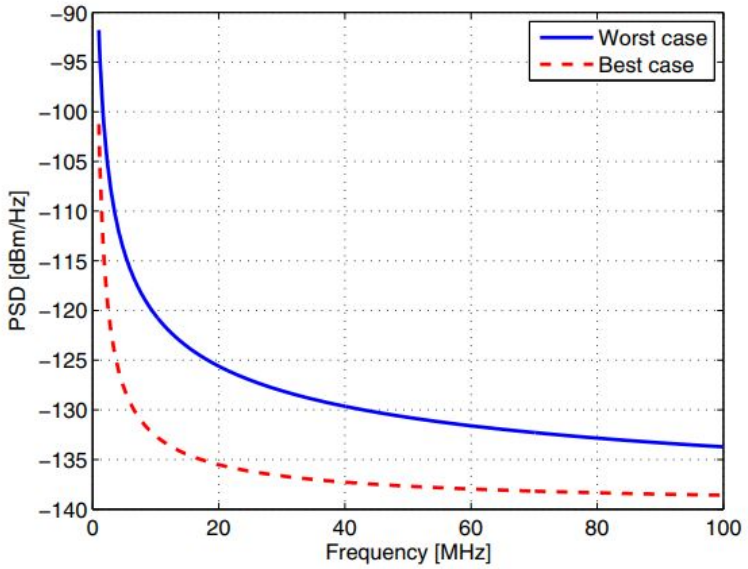

Figure 2.18: Coloured background noise by the model in eq. 2.28

- Coloured background noise: This type of noise is caused by electric devices. Generally, it has a smooth and relatively low PSD. Owing to numerous sources of noise occupied in the low frequency spectrum, the PSD of this type of noise exhibits a decreasing trend with the increase of frequency, as shown in Fig.2.18, and hence the name coloured (coloured noise has different signal power at different frequencies). Also, since this type of noise is stationary for a relatively long period of time, hence it is called background noise.

- NB noise: NB noise is introduced by external broadcasters, *i.e.*, AM, FM

and amateur radio. It typically has the form of sinusoidal.

- Periodic IN asynchronous to the mains frequency: This type of noise originates from the switching of power supplies with a repetition rate of 50 to 200 kHz.

- Periodic IN synchronous to the mains frequency: This type of noise is mainly induced by light dimmers and typically has a repetition rate of 50 to 100 Hz.

- Asynchronous IN: This is caused by switching transients of load or lights in the PLC network. The impulse spans a large frequency band and causes the occurrence of burst error due to its high amplitudes.

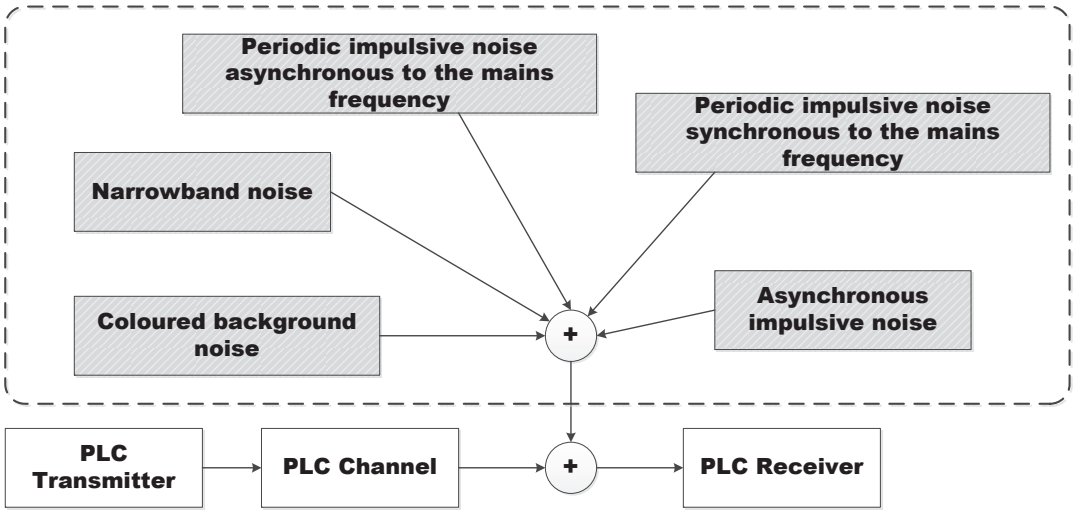

Figure 2.19: Noise classification of PLC networks

The closed-form expression of typical PL noise models facilitate the development and design of advanced PLC systems. In the following, some well-known noise models in PLC are introduced.

2.3.7.1 Coloured Background Noise Model

A widely accepted model for coloured background noise is presented in [97], where three parameters are required for data fitting and the noise is treated as Gaussian

with PSD,

$$P(f) = a + b \cdot |f|^c \qquad [\frac{dBm}{Hz}] \tag{2.28}$$

where a, b and c are parameters obtained from measurements and f is the frequency in MHz.

The OPERA consortium suggested a model for coloured background noise in [94] as

$$P(f) = P_\infty + P_0 \cdot e^{-f/f_0} \qquad [\frac{dBm}{Hz}] \tag{2.29}$$

where P_∞ is the PSD as $f \to \infty$, P_0 is the difference between P_∞ and the maximum PSD. f_0 indicates the decaying exponential rate.

2.3.7.2 Impulsive Noise Model

IN exists for short time intervals in the PL channel, but is the main cause of errors in PLC due to its high PSD. Some well-known IN models in PL are the Bernoulli-Gaussian model [96], the Middleton's class A model [98] and the cyclostationary Gaussian model [99].

The Bernoulli-Gaussian model [96] is based on Gaussian mixture distribution with two terms, in which one term is used for IN and the other for background noise. Mathematically, the PDF in this model at a certain time instant can be expressed as [96]

$$p_\eta(\nu) = (1-p) \cdot \mathcal{N}(0, \sigma_b^2) + p \cdot \mathcal{N}(0, \sigma_b^2 + \sigma_i^2) \tag{2.30}$$

where p is the probability that the impulsive noise occurs, which follows Bernoulli random process, σ_b^2 and σ_i^2 are the variances for background noise and IN, respectively.

The Middleton's class A model [98] is an infinite Gaussian mixture model. The PDF of this model is given by [98]

$$p_\eta(\nu) = \sum_{k=0}^{\infty} \frac{e^{-A} \cdot A^k}{k!} \cdot \frac{1}{\sqrt{2\pi\sigma_k^2}} \cdot \exp(-\frac{v^2}{2\sigma_k^2}) \tag{2.31}$$

with

$$\sigma_k^2 = (1 + \frac{1}{\Gamma}) \cdot (\frac{(k/A) + \Gamma}{1 + \Gamma}) \cdot \sigma_b^2 \tag{2.32}$$

where $\frac{1}{\sqrt{2\pi\sigma_k^2}} \cdot \exp(-\frac{v^2}{2\sigma_k^2})$ is a Gaussian distribution with zero mean and variance σ_k^2, *i.e.*, $\mathcal{N}(0, \sigma_k^2)$. $\frac{e^{-A} \cdot A^k}{k!}$ is the Poisson distributed probability for the kth IN term, which reflects the occurrence of IN. The parameter A is called impulsive index and Γ is the background-to-impulsive noise ratio, and σ_b^2 is the variance of background noise. Typically, the first three terms are sufficient (*i.e.*, $k = 0, 1, 2$) to approximate the Middleton's class A model. In this case, the PDF is very similar to the Bernoulli-Gaussian model [96].

The periodic IN synchronous to the mains frequency can be represented by the cyclostationary Gaussian model [99]. This type of noise changes periodically with the frequency the same as or twice the mains frequency [24]. Therefore, it can be modelled as a sum of sinusoidal wave of different amplitudes and frequencies [99]. The periodic IN can be modelled with zero mean and time-varying variance Gaussian process, in which the amplitude PDF is expressed as

$$p_\eta(\nu(iT_s)) = \frac{1}{\sqrt{2\pi\sigma^2(iT_s)}} \cdot \exp(-\frac{v^2(iT_s)}{2\sigma^2(iT_s)}) \tag{2.33}$$

where T_s is the sampling period, $\sigma^2(iT_s)$ is the instantaneous variance of the noise that is synchronous to the mains frequency owing to different phases of AC voltage, and is given by

$$\sigma^2(t) = \sum_{l=0}^{L-1} A_l \left|\sin(\frac{2\pi t}{T_0} + \theta_l)\right|^{n_l} \tag{2.34}$$

where T_0 is the mains cycle duration, A_l, θ_l, n_l denotes the characteristics of the noise.

To summarise, noise in PLC exhibits the coloured nature, and is the superposition of noise sources from the classifications in Fig. 2.19. Also, the power of numerous noise sources are situated in the low frequency spectrum and hence the background noise and the periodic IN dominate the noise in NB PLC. In BB PLC, the aperiodic IN is considered as the dominant term [100]. The background noise in BB PLC has low and constant PSD, and can be considered as AWGN, and since the periodic IN has relatively low amplitude, it has a low impact on noise power in BB PLC [96].

2.4 Summary

In this chapter, the general overview of sensor networks, wireless communications and PLC were provided. The basic components, data collection and communication of sensor nodes were outlined along with some applications of sensor networks. A brief history of wireless communications is provided together with the introduction of wireless channel characteristics (large-scale and small-scale propagation effects) and the wireless AWGN channel. Also, background and the general architecture of PLC network were discussed. With a focus on indoor PLC structure, random PLC topology generator was introduced together with the bottom-up and top-down channel modelling approaches. Finally, noise classification and some well-known PLC noise models were presented. With the characteristics of WSNs and PLC network, it is a natural process to utilise both technologies to supplement each other.

Although random topology change, the time-varying and frequency-selective fading nature, and the complex noise scenarios of PLC make PL a harsh medium for data communication, some advanced PLC technologies such as PLC topology inference [101–104], orthogonal frequency division multiplexing (OFDM) PLC [105–107], and PLC noise detection and mitigation [85, 108–110] have been developed to combat the channel impairments of PLC.

Chapter 3

Overview of Network Protocol Stack and Optimization Theory

This chapter presents the foundations of the research topics covered in this thesis. In Section 3.1, the network protocol stack is discussed. The general optimization theory is presented in Section 3.2. Finally, Section 3.3 summarises this chapter.

3.1 Overview of Network Protocol Stack

This section outlines the structure in the network protocol stack and the corresponding functionalities in each layer. Then the drawbacks of traditional layered design is discussed. Finally, the architecture of cross-layer design and the main challenges are presented.

The network protocol stack can be divided into the PHY layer, data link layer, network layer, transport layer and the application layer as shown in Fig. 3.1 with the illustration of some main functionalities in each layer. More details of each layer are provided below.

1. The PHY layer concerns with establishing a reliable communication link through robust modulation, transmission and data receiving techniques. The design factors corresponding to the PHY layer include carrier frequency selection and generation, power control, modulation, coding, equalization, (multiple-input multiple-output) MIMO, signal detection and data encryption [60].

2. The data link layer deals with data stream multiplexing, detection of data frame and medium access (or the MAC layer, which is embedded in the data link layer) and error control [60]. In particular, the MAC layer manages the mechanism of channel access for multiple users (or devices). Depending on the channel access scheme, users/devices can access the channel in a deterministic or a random manner. In the deterministic channel access method, based on the channelization mechanism, the entire spectrum is divided into channels by time, frequency or code, and each user/device is assigned with dedicated channels, termed time division multiple access (TDMA), frequency division multiple access (FDMA), and code division multiple access (CDMA), respectively. In a random channel access fashion, each active user/device (by active, it means the user/device has data to transmit) can access the channel dynamically. Some well-known mechanisms are Aloha, carrier sensing multiple access (CSMA), and CSMA/CA.

3. The network layer connects the users/devices in the network by establishing end-to-end links. Typical functions in this layer are neighbour discovery and routing. In particular, in applications where users/devices always have data to transmit, two effective routing strategies are the centralised and the distributed routing [74]. In the centralised routing, each user/device determines its local channel conditions and network topology and transfers such information to a centralised panel. The panel then decides and broadcasts the routing tables for all users/devices based on the global information of the network. While this routing strategy provides the most effective solution, it is vulnerable to rapid changes in channel conditions and network topology. Also, this strategy incurs heavy communication overhead. In the distributed routing, each user/device exchange its local information to its neighbouring users/devices. Each user/device determines the routes based on its local information, which saves much communication overhead and can respond to topology changes rapidly.

4. The transport layer manages retransmissions, error recovery and flow control and is especially needed when the network has an urge to be accessed by external networks [60].

5. The application layer generates and processes the data in the network with main functions of source coding and source decoding.

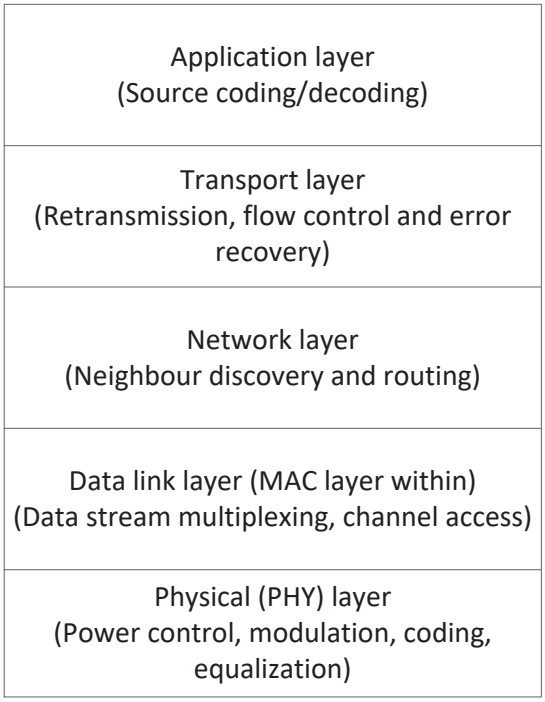

Figure 3.1: Network protocol stack with illustration of main functionalities in each layer

A through discussion of network layers and the corresponding functionalities can be found in [60, 70, 74, 111–113]. The network protocol stack depicted in Fig. 3.1 was initially proposed for computer networking [111], with which the modularity simplifies and facilitates the development of the protocols in the Internet. In this architecture, each layer is developed individually with static established interfaces only with neighbouring layers, and neglecting specific network constraints and requirements of different applications. The overall system flexibility, therefore, is compromised in this architecture since the interfaces are predefined and each layer is concealed from non-neighbouring layers [112].

The fundamental reasons for the layered design of the protocol stack to provide adequate performance in computer networking are [74]: the dynamics in each layer are limited since the communication medium (e.g., Ethernet cables) has little channel impairment, and the performance in each layer can be over-designed to combat the dynamics from neighbouring layers as the system resources (*e.g.*, power and bandwidth) are relatively unrestricted. However, in wireless network or PLC network, the communication channel is prone to the environment and experiences various channel impairments such as time-varying channel condition, and frequency selective fading. Also, in these networks, the available resources (*e.g.*, power and bandwidth) are usually limited (*e.g.*, due to PLC regulations as discussed in Chapter 2). Consequently, to overcome the dynamics by over-designing the layers is unacceptable in these networks. Therefore, the overall wireless/PLC network design focused on isolated elements of the layered structure would lead to poor performance, especially under stringent resource constraints or performance requirements (*e.g.*, energy consumption, delay). To overcome these challenges, a cross-layer protocol design that takes the resource constraints, application requirements into account, with interdependencies between different layers is favoured.

Contrary to the layered design of the protocol stack, a cross-layer design improves the overall network performance by jointly optimizing multiple layers in the protocol stack with application specific resource constraints and requirements in an integrated and hierarchical framework [74]. Such a design mechanism allows information exchange between different neighbouring or non-neighbouring layers (as shown in Fig. 3.2), and adds on the adaptivity at each layer of the protocol stack [74]. For example, to minimize the total energy consumption of a sensor network, the application layer of each node should adapt its source rate by source coding to ensure the minimum QoS requirements (*e.g.*, distortion). This information can be used by the power management plane to monitor the encoding power and the network layer to establish routes for each node. The adaptivity at

both the application layer and the network layer should be informed to the PHY layer and the MAC layer to determine the power control and channel access for each link. Such information can then be used in the power management plane to monitor the transmission and data reception power, and be fed back to the application layer to compensate for the channel diversity. The major challenges in the cross-layer design are to integrate the resource constraints and application specific requirements into protocol designs at each layer, and to determine the information to be exchanged across different protocol layers as well as the mechanism of each layer to adapt to such information [74].

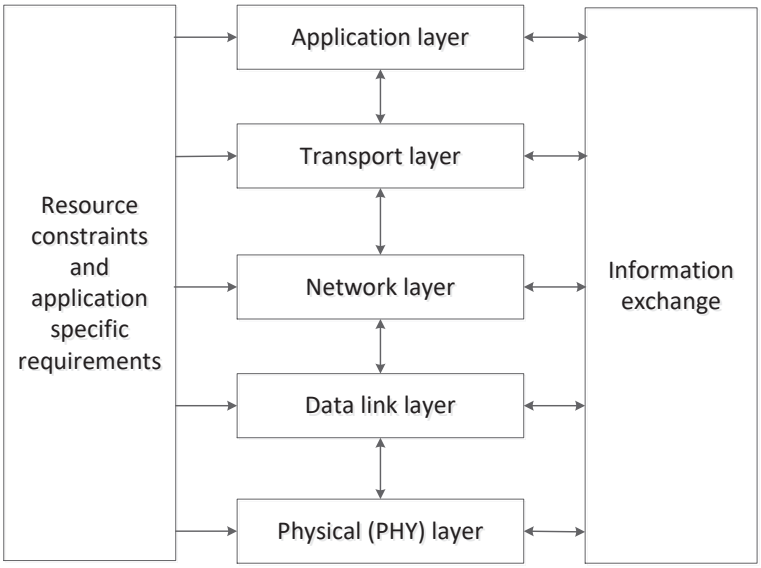

Figure 3.2: Cross-layer design architecture

3.2 Overview of Optimization Theory

In section 3.1, the major challenges in the cross-layer design are discussed, which are detailed as follows:

1. How the resource constraints and application originating requirements can be integrated into the protocol designs at each layer?

2. What kind of information should be exchanged across each protocol layer?

3. How each layer should adapt to the exchanged information?

Recent development in NUM has reported that different protocol layers can be systematically integrated into a single coherent theory, which provides a general viewpoint to understand the interactions across various layers in the network protocol stack [49, 53, 54]. In such a framework, NUM is used as a modelling tool, to integrate specified objectives, diverse types of constraints, design freedom and stochastic dynamics into a single optimization problem [49], which is then decomposed into different layers. Each layer iterate on associated subsets of the optimization variables using local information to attain individual optimality [55]. By combining the results from these local layers, a global objective can be attained. Therefore, NUM provides a coherent approach to solve the challenges in the cross-layer design. In the following, the general optimization theory, as the foundation of NUM is outlined, including the basics of convexity, Lagrange duality, optimality conditions, different decomposition techniques and distributed solutions. Detailed descriptions concerning these subjects can be found in [49, 52–54, 114].

3.2.1 Convexity

A set S is said to be convex if the line segment between any two points in S lies in S. Mathematically, for any points $x_1, x_2 \in S$ and any θ with $0 \leq \theta \leq 1$, the set S is convex if [114],

$$\theta x_1 + (1 - \theta)x_2 \in S \tag{3.1}$$

Fig. 3.3 depicts the idea of convex and non-convex sets with simple illustrations.

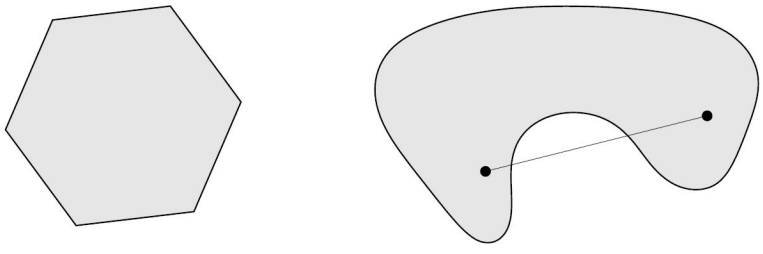

Figure 3.3: Simple illustrations of convex (left) and non-convex (right) sets [114]

A function f: $\mathbb{R}^n \rightarrow \mathbb{R}$ (n indicates the number of elements and $\mathbb{R}$ is used to

indicate the set of real numbers) is convex if the domain (denoted as **dom**) of f is a convex set and if for all $x, y \in \mathbf{dom} f$, and θ with $0 \leq \theta \leq 1$, the following inequality holds [114]:

$$f(\theta x + (1-\theta)y) \leq \theta f(x) + (1-\theta) f(y) \tag{3.2}$$

Roughly, the above inequality indicates that the line segment between $(x, f(x))$ and $(y, f(y))$ lies above the graph of f, as shown in Fig. 3.4. A function f is said to be concave if $-f$ is convex.

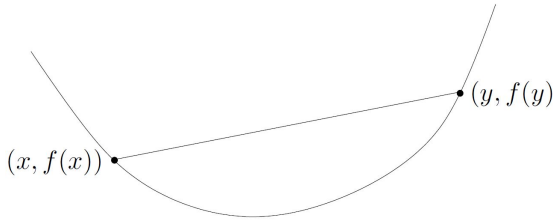

Figure 3.4: Illustration of a convex function. The line segment between any two points on f lies above the graph [114].

Generally, a problem to find x that minimizes $f_0(x)$ among all x that satisfy the conditions $f_i(x) \leq 0, i = 1, ..., m$, and $h_i(x) = 0, i = 1, ..., p$, can be formulated into an optimization problem as:

$$\begin{aligned} \min_{x} \quad & f_0(x) \\ s.t. \quad & f_i(x) \leq 0 \qquad 1 \leq i \leq m \\ & h_i(x) = 0 \qquad 1 \leq i \leq p \end{aligned} \tag{3.3}$$

where $x \in \mathbb{R}^n$ is the optimization variable, f_0 ($\mathbb{R}^n \to \mathbb{R}$) is the objective function, $f_1, ..., f_m$ ($\mathbb{R}^n \to \mathbb{R}$) are the m inequality constraint functions, and $h_1, ..., h_p$ ($\mathbb{R}^n \to \mathbb{R}$) are the p equality constraint functions. The optimization problem in (3.3) is a convex optimization problem if the objective (f_0) and inequality constraint functions ($f_i, i = 1, ..., m$) are convex and the equality constraint functions ($h_i, i = 1, ..., p$) are linear (or affine, in general). A point $x \in \mathbf{dom} f_0, f_i, h_i$ (the domain of the optimization problem) is said to be feasible if all the inequality and equality constraints are satisfied ($f_i(x) \leq 0$, and $h_i(x) = 0$). The optimization problem

in (3.3) is feasible if there exists at least one feasible point of x. The optimal solution of the problem is denoted as x^*, at which the optimal value f^* can be obtained, *i.e.*, $f^* = f_0(x^*)$.

A convex optimization problem is much easier to solve than a non-convex one. A local optimum solution (optimal feasible point in a local domain of the problem) is also globally optimal (optimal feasible point in the whole domain of the problem) in convex optimization problems [114].

3.2.2 Lagrange Duality and Optimality Conditions

The theory of Lagrange duality can transform the original optimization problem (or primal problem) in (3.3) into a dual maximization problem, which facilitates the decomposition. The basic idea of Lagrange duality is to integrate the constraint functions into the objective function with a weighted sum. The Lagrangian associated with problem (3.3) is defined as [114]:

$$L(x, \lambda, \nu) = f_0(x) + \sum_{i=1}^{m} \lambda_i f_i(x) + \sum_{i=1}^{p} \nu_i h_i(x) \tag{3.4}$$

where λ_i and ν_i are the Lagrange multipliers corresponding to the ith inequality constraint, $f_i(x) \leq 0$ and to the ith equality constraint, $h_i(x) = 0$, respectively. The optimization variable x is the primal variable and the Lagrange multiplier vectors λ and ν are called the dual variables. $f_0(x)$ is the primal objective, and the dual objective $g(\lambda, \nu)$ is defined as the minimum value of the Lagrangian over x. Mathematically,

$$g(\lambda, \nu) = \inf_{x} L(x, \lambda, \nu) \tag{3.5}$$

$g(\lambda, \nu)$ is concave regardless of the convexity of the original problem [114]. The dual objective $g(\lambda, \nu)$ takes the infimum regarding to all x (could be an infeasible point). The dual variables λ and ν are dual feasible if $\lambda \geq 0$.

For any feasible x, λ and ν, the primal and dual objectives satisfy $f_0(x) \geq g(\lambda, \nu)$ [114]. Therefore, a lower bound on the optimal value f^* of problem (3.3)

can be obtained by maximizing the dual function, as

$$\begin{aligned} \max_{\lambda,\nu} \quad & g(\lambda,\nu) \\ s.t. \quad & \lambda \geq 0 \end{aligned} \tag{3.6}$$

which is always a convex optimization problem whether or not the primal problem is convex.

The duality gap is defined as the difference between the optimal primal objective f^* and the optimal dual objective g^*, of which $f^* - g^* \geq 0$ always holds since g^* is a lower bound on f^* (weak duality). Given the original problem is a convex optimization problem, strong duality (*i.e.*, the duality gap is 0, $f^* = g^*$) usually (not always) holds. One simple constraint qualification for strong duality is Slater's condition [114].

Assuming strong duality holds, let x^* denotes the primal optimal and (λ^*, ν^*) indicates the dual optimal point, it can be derived that

$$f_0(x^*) = g(\lambda^*, \nu^*) \tag{3.7}$$

$$= \inf_x \left(f_0(x) + \sum_{i=1}^{m} \lambda_i^* f_i(x) + \sum_{i=1}^{p} \nu_i^* h_i(x) \right) \tag{3.8}$$

$$\leq f_0(x^*) + \sum_{i=1}^{m} \lambda_i^* f_i(x^*) + \sum_{i=1}^{p} \nu_i^* h_i(x^*) \tag{3.9}$$

$$\leq f_0(x^*) \tag{3.10}$$

The equality (3.7) indicates that strong duality holds, (3.8) is obtained from the definition of the dual function. (3.9) holds since the infimum of the Lagrangian over x should not exceed its value at $x = x^*$. (3.10) follows since $\lambda^* \geq 0$, $f_i(x^*) \leq 0$, $i = 1, ..., m$ and $h_i(x^*) = 0$, $i = 1, ..., p$. It is obvious that the inequalities (3.9) and (3.10) should hold with equality and

$$\sum_{i=1}^{m} \lambda_i^* f_i(x^*) = 0 \tag{3.11}$$

$$\lambda_i^* f_i(x^*) = 0 \tag{3.12}$$

in which (3.12) is known as the complementary slackness condition [114].

Further, since x^* minimizes the Lagrangian $L(x, \lambda^*, \nu^*)$ over x, it follows that the gradient of the Lagrangian should be 0 at x^*. Mathematically, it holds that

$$\nabla f_0(x^*) + \sum_{i=1}^{m} \lambda_i^* \nabla f_i(x^*) + \sum_{i=1}^{p} \nu_i^* \nabla h_i(x^*) = 0$$

Therefore, it concludes that

$$\begin{aligned} f_i(x^*) &\leq 0, & i = 1, ..., m \\ h_i(x^*) &= 0, & i = 1, ..., p \\ \lambda_i^* &\geq 0, & i = 1, ..., m \\ \lambda_i^* f_i(x^*) &= 0, & i = 1, ..., m \\ \nabla f_0(x^*) + \sum_{i=1}^{m} \lambda_i^* \nabla f_i(x^*) + \sum_{i=1}^{p} \nu_i^* \nabla h_i(x^*) &= 0, \end{aligned} \tag{3.13}$$

which are known as the Karush-Kuhn-Tucker (KKT) conditions [114]. For any optimization problem (convex or non-convex) with differentiable objective and constraint functions for which strong duality holds, the necessary condition for any pair of primal and dual points to be optimal is to satisfy the KKT conditions [114]. In particular, if the primal optimization problem is convex, the KKT conditions are also sufficient for the points to be primal and dual optimal.

3.2.3 Decomposition Theory

Basically, decomposition is to divide the original optimization problem into distributively solvable subproblems that are controlled by a high-level master problem through certain types of messaging [49, 52–54]. Typically, there are two types of decomposition techniques, namely, dual decomposition and primal decomposition. Dual decomposition deals with decomposing the Lagrangian dual problem, while primal decomposition concerns with decomposing the original primal problem [49, 53]. In the dual decomposition technique, the master problem decides the prices for the resources to each subproblem, which then acquires certain amount of resources depending on the price. In the primal decomposition technique, the master problem assigns some amount of the available resources directly to each subproblem.

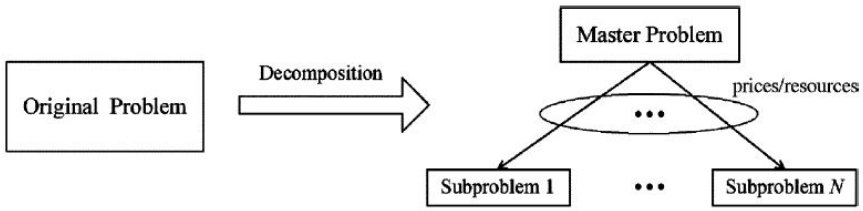

Figure 3.5: Illustration of optimization problem decomposition [52]

3.2.3.1 Dual Decomposition

The dual decomposition suits in the occasions when the problem has a coupling constraint, and when it is relaxed, the optimization problem is able to be decoupled into several subproblems. For instance, consider an optimization problem [52]

$$\begin{aligned} \max_{x_i} \quad & \sum_i f_i(x_i) \\ s.t. \quad & x_i \in \mathcal{X}_i, \quad \forall i \\ & \sum_i h_i(x_i) \leq c \end{aligned} \tag{3.14}$$

For example, the above optimization problem applies to a communication network that has a fixed capacity on each link, and a certain number of nodes, each transmitting at a source rate, which is to be optimized. Each node has a specified path which includes a fixed set of links. The objective function in this case could be to maximize the total utility, $\sum_i f_i(x_i)$, say the network throughput. The constraint $x_i \in \mathcal{X}_i$ means that the source rate for each node should satisfy a pre-defined range. The inequality constraint $\sum_i h_i(x_i) \leq c$ indicates that the total data rate on each link originating from all the nodes should not exceed the maximum capacity of the link.

Obviously, if the inequality constraint were absent, the original problem could decouple. Therefore, the optimization problem can be relaxed by forming the Lagrangian with respect to the coupling constraint in (3.14) as

$$\max_{x_i} \quad \sum_i f_i(x_i) - \lambda^T \left(\sum_i h_i(x_i) - c \right)$$

$$s.t. \qquad x_i \in \mathcal{X}_i, \quad \forall i \tag{3.15}$$

where λ is the Lagrange multipliers. The original problem is now divided into two levels of optimization. At the lower level, there are the subproblems (Lagrangians), one for each i, as

$$\begin{aligned} \max_{x_i} \quad & f_i(x_i) - \lambda^T h_i(x_i) \\ s.t. \quad & x_i \in \mathcal{X}_i, \quad \forall i \end{aligned} \tag{3.16}$$

The master dual problem at the higher level updates the dual variable λ by solving the dual problem, as

$$\begin{aligned} \min_{\lambda} \quad & g(\lambda) = \sum_i g_i(\lambda) + \lambda^T c \\ s.t. \quad & \lambda \geq 0 \end{aligned} \tag{3.17}$$

in which $g_i(\lambda)$ is the dual function obtained as the maximum value of the Lagrangian solved in (3.16) for a certain λ. This decomposition technique actually solves the dual problem instead of the original primal optimization problem.

3.2.3.2 Primal Decomposition

The primal decomposition suits in the occasions when the problem has a coupling variable such that, when it is fixed to certain value, the remaining optimization problem can be decoupled into several subproblems. For instance, consider an optimization problem [52]

$$\begin{aligned} \max_{y,x_i} \quad & \sum_i f_i(x_i) \\ s.t. \quad & x_i \in \mathcal{X}_i, \quad \forall i \\ & A_i x_i \leq y \\ & y \in \mathcal{Y} \end{aligned} \tag{3.18}$$

Obviously, if the variable y were fixed to certain value, the original optimization problem could decouple. Therefore, it is easier to solve the problem in (3.18)

by separating it into two levels of optimization. At the lower level, there are the subproblems, one for each i, in which the original optimization problem decouples with a fixed value of y, as

$$\begin{aligned} \max_{x_i} \quad & f_i(x_i) \\ s.t. \quad & x_i \in \mathcal{X}_i, \quad \forall i \\ & A_i x_i \leq y \end{aligned} \tag{3.19}$$

While the master problem at the higher level updates the coupling variable y by solving the problem, as

$$\begin{aligned} \max_{y} \quad & \sum_i f_i^*(y) \\ s.t. \quad & y \in \mathcal{Y} \end{aligned} \tag{3.20}$$

where $f_i^*(y)$ is the optimal objective value obtained from problem (3.19) for a fixed value of y.

3.2.3.3 Hierarchical Decomposition

For a complex optimization problem, the use of dual and primal decomposition alone would fail to deliver a simple and manageable solution. However, such complex optimization problems can be divided into smaller and smaller subproblems by using the dual and primal decomposition techniques recursively (as depicted in Fig. 3.6).

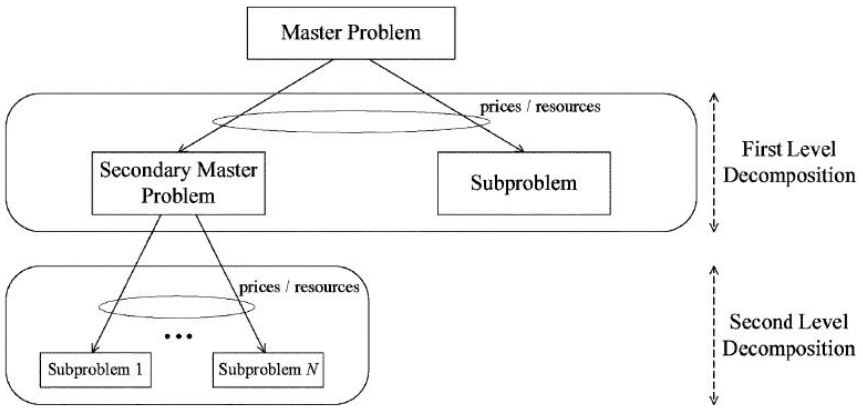

Figure 3.6: Illustration of hierarchical decomposition [52]

For instance, consider a problem that has both a coupling constraint and a coupling variable [52]

$$\begin{aligned} \max_{y,x_i} \quad & \sum_i f_i(x_i, y) \\ s.t. \quad & x_i \in \mathcal{X}_i, \quad \forall i \\ & \sum_i h_i(x_i) \leq c \\ & A_i x_i \leq y \\ & y \in \mathcal{Y} \end{aligned} \tag{3.21}$$

A possible solution to solve the above optimization problem is by first taking a primal decomposition with respect to the coupling variable y, followed by taking a dual decomposition with respect to the coupling constraint $\sum_i h_i(x_i) \leq c$. Therefore, this leads to a two-level optimization decomposition: a master primal problem, a secondary master dual problem, and the subproblems.

If multiple levels of decomposition are applied to an optimization problem, and in each level some iterative algorithms are used to find the solution, the convergence and stability are guaranteed if the lower level master problem can be solved on a faster time scale than the higher level master problem. In this case, at each iteration of a master problem, convergence of the algorithms applied to all the problems at a lower level has already been achieved [115]. It is worth noting as reported in [55] that in principle, the algorithm at the lower level subproblem should run till convergence before the higher level master problem could be updated, while in practice, the algorithms at both levels can run simultaneously.

3.2.4 Gradient and Subgradient Algorithms

With the original optimization problem being decoupled into subproblems, efficient algorithms can be used to obtain the solutions. Depending on whether the resulting problem is differentiable or not, gradient and subgradient algorithms provide a simple and straight-forward way to find a solution owing to their advantages such as simplicity, and little requirements of memory usage [52, 114].

For a concave maximization (or convex minimization) problem over a convex set in its general form:

$$\begin{aligned} \max_{x} \quad & f_0(x) \\ s.t. \quad & x \in \mathcal{X} \end{aligned} \tag{3.22}$$

Both the gradient and subgradient projection approaches generate a sequence of feasible points $\{x(t)\}$ as [52],

$$x(t+1) = [x(t) + \alpha(t)s(t)]_{\mathcal{X}} \tag{3.23}$$

where $s(t)$ is a gradient or subgradient of the objective function f_0 calculated at the point $x(t)$ depending on whether f_0 is differentiable or non-differentiable. $\alpha(t)$ is a positive step-size and $[\cdot]_{\mathcal{X}}$ indicates the projection onto the feasible set $\mathcal{X}$. Different choices of the step-size impact on the convergence of the gradient and subgradient algorithms. For instance, it is reported in [116] that a diminishing step-size rule with $\alpha(t) = \frac{1+m}{t+m}$ can guarantee the algorithms to converge to the optimal value, where m is a fixed non-negative number. The widely used constant step-size $\alpha(t) = \alpha$ in distributed algorithms can guarantee the gradient algorithm to converge to the optimal value with a sufficiently small step-size [117], while gives a best value to converge to some range of the optimal value in the subgradient algorithm [116].

3.2.5 Time Scale and Order of Updates

The update of different variables in the optimization problem differs in timescale and order. For instance, the variables can have full convergence and thus be optimized in one-shot, or can be optimized iteratively with the gradient or subgradient algorithm. Also, there are generally two types of algorithms concerning the order of updates. In the nonlinear Gauss-Seidel algorithm, one set of variables are iteratively optimized in a circular fashion while the rest variables are kept fixed [115]. In the nonlinear Jacobi algorithm, one set of variables are iteratively optimized in a parallel fashion while the rest variables are kept fixed [115].

Mathematically, for the Gauss-Seidel algorithm, variable x is updated as

$$x_i(t+1) = \arg\min_{x_i \in \mathcal{X}_i} f\big(x_1(t+1), ..., x_{i-1}(t+1), x_i, x_{i+1}(t), ..., x_n(t)\big) \tag{3.24}$$

and for the Jacobi algorithm, variable x is updated as

$$x_i(t+1) = \arg\min_{x_i \in \mathcal{X}_i} f\big(x_1(t), ..., x_{i-1}(t), x_i, x_{i+1}(t), ..., x_n(t)\big) \tag{3.25}$$

The combinations of all these possibilities lead to various algorithms that have different characteristics in terms of convergence properties, amount of message exchange. Therefore, it is necessary to design an algorithm with specific application requirements.

3.3 Summary

In this chapter, the background of network protocol stack and optimization theory have been reviewed, which provide the foundations of the research topics covered in this thesis. The general structure in the network protocol stack and the corresponding functionalities in each layer have been presented, followed by a discussion on the drawbacks of traditional layered design as well as the architecture of cross-layer design and the main challenges. To address these design challenges, the optimization theory and decomposition theory have been introduced, covering topics of convexity, Lagrange duality, optimality conditions, different decomposition techniques and distributed solutions.

Chapter 4

Cross-Layer Network Lifetime Maximization for Hybrid Sensor Networks

In this chapter, a hybrid sensor network, which consists of both wireless sensor nodes and PL sensor nodes is proposed for industrial sensor network applications. In particular, the network lifetime is chosen as the main design criteria to demonstrate the performance improvement of such a hybrid sensor network as compared to the traditional pure WSNs. This study can also be applied to other applications of the sensor network with stringent energy budgets, such as structural health monitoring, where building stress and motion sensors are inserted into the concrete before it is poured [74].

The next-generation industrial automation system involves three different levels [56]: the field level, where the automation process is monitored and controlled directly by the sensors and actuators, the automation level, where the industrial controllers, such as programmable logic controllers are used to perform the process control decision making, and the management level, where best-effort IP traffic is exchanged. Typically, the devices in the field level are interconnected by an industrial wireless sensor network, while the automation and management levels are connected to wired networks [57].

In such networks, the wireless sensors in the automation level are required to constantly monitor and sample the process, and to send critical messages such

as the measurement and actuation signals to the automation and management levels within a given time. Such that a process disturbance or emergency can be handled in a timely manner, or actuators may misbehave and potentially cause material or physical damage or even hazardous consequences. An example of such a network is the chemical and petroleum refining industry [118] where wireless sensors are scatted in the chemical reaction pool or refineries to monitor the process. For the wired network in the automation and management level, the cost of installing wires for communication within refineries is very high due to safety requirements [119]. One potential candidate for the implementation of the wired network in industrial applications is the PLC, which has the advantage of the ubiquitous infrastructure of PL cables. Also, in situations where wired communication infrastructure is a problem (*e.g.*, installing new communication systems in old facilities), PLC is an attractive solution that provides a much lower installation time and costs [120].

In this chapter, a hybrid sensor network for industrial automation system, which consists of both wireless and PL sensor nodes is proposed. This work is different in the following aspects. First, to the best of our knowledge, it is the first reported work in the literature that focuses on the cross-layer design of such a heterogeneous network. The hybrid sensor network takes the advantage of the flexibility of WSNs while the PL sensors are deployed to prolong the lifetime of the network. This work studies the joint design of the PHY, MAC and network layers to maximize the hybrid network lifetime, which is limited by the battery capacity of wireless sensors. Second, closed-form expressions of the globally optimal solution for lifetime maximization of the hybrid sensor network are derived for two different network topologies, namely string topology and linear topology. Such closed-form solutions give insights in factors that are significant to the network lifetime when designing the hybrid sensor network. Third, the impacts of different network configurations such as source rate, sensor node densities, *etc.*, on the hybrid network lifetime are investigated. Finally, the impact of different

transmission strategies of PL nodes on the effectiveness of the network is studied.

The rest of this chapter is organized as follows. Related work is presented in section 4.1. Section 4.2 describes the system model. Section 4.3 formulates the optimization problem. In section 4.4, analytical expressions for the hybrid network lifetime are derived for two topologies. Section 4.5 analyzes the numerical results. This chapter is summarised in section 4.6.

4.1 Related Work

The ubiquitous deployment of WSNs is limited by the energy supply of wireless sensor nodes since energy is a scarce resource. This arouses tremendous upsurge of research interest on prolonging the network lifetime of WSNs through different approaches. Network lifetime has various definitions in the research community. For example, in [121–124], the network lifetime is defined as the the time duration till the first node in the network being drained out of energy (as adopted in this thesis, since each sensor collects critical information in the network). Network lifetime is defined as the time duration till some target area is uncovered by any sensor node in [125, 126]. In [127], it is defined as the time duration till the first occasion that data collection fails. For a detailed survey on the definition of network lifetime, please refer to [128].

There are various techniques to save the energy consumption and to maximize the network lifetime in WSNs (the definition of network lifetime in each work may be different though). In [129], the authors focused on the placement issues of wireless sensor nodes to increase the power efficiency. In [130], a data compression algorithm is proposed to reduce the amount of data to be transmitted for each sensor node and thus reducing the energy consumption. In the work of [131] and [132], the authors considered the routing problems to reduce energy consumption for wireless sensor nodes. A sensor node control approach that schedules the nodes' sleep/wakeup activities is studied in [133–136]. Among these aforementioned approaches, cross-layer design of the sensor network is an

active research area [137].

Early studies of cross-layer design of WSNs have been focused on minimizing the total energy consumption. For example, in [138], the authors investigated the energy consumption minimization problem for an interference-free TDMA based WSN through joint design of the PHY, MAC, and routing layers. By solving the approximated convex optimization problems, the results reveal that the minimum energy transmission scheme is a combination of multi-hop and single-hop transmissions. In [139], the energy consumption minimization problem is extended to a clustered WSNs where slot reuse and packet retransmission are considered to increase the network throughput.

However, it is pointed out that [140] the minimization of energy consumption may lead to some nodes being drained of energy rather rapidly. Therefore, the spatial information collected from the particular sensor node may be lost and this influences the following data analysis. Hence, instead of minimizing energy consumption of the sensor nodes, the authors in [140] attempted to maximize the network lifetime of the sensor network, which is defined as the first sensor node in the network being exhausted of energy. In [141], the joint design of the PHY, MAC and the network layer is considered together with the transmission success probability to maximize the network lifetime. More recently, the authors in [142] considered the problem of network lifetime maximization with MAC-aware routing that is capable of multichannel access. In [143], contention and sleep control probabilities of each node are integrated into the network lifetime maximization problem. A joint design on the PHY, MAC and network layers to maximize the network lifetime considering spatially periodic time sharing scheme is proposed in [122] for a string topology. It is later extended to a fully-connected WSN with random topology by introducing the concept of route lifetime for each node in [124].

The aforementioned work has considered different approaches to either minimize the energy consumption of sensor nodes or to maximize the network lifetime

in a pure WSN. In this chapter, a hybrid sensor network is proposed. With the integration of both wireless sensor nodes and the PL nodes, the hybrid sensor network is expected to prolong network lifetime significantly.

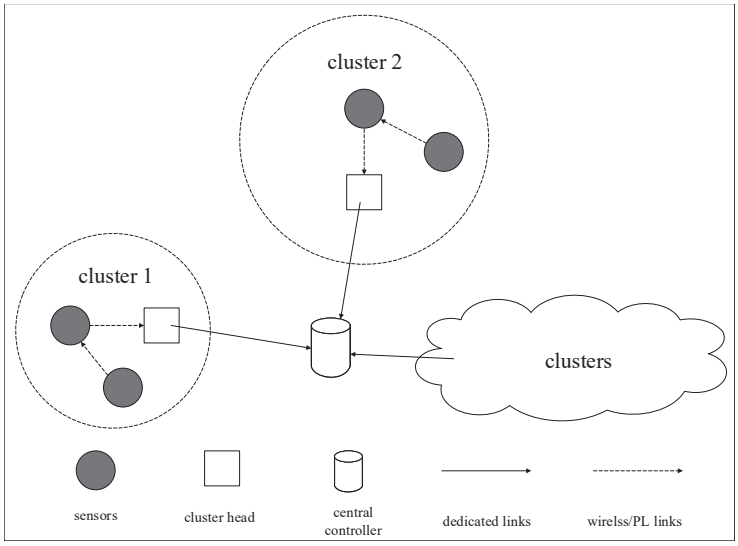

Figure 4.1: A clustered sensor network

4.2 System Model

A cluster based sensor network for industrial automation system divides the industrial area into multiple clusters and the operation within each cluster is independent. As shown in Fig. 4.1, each cluster covers a certain region and contains the sensors and a cluster head (or wired access point [118]), where critical messages such as the measurement and actuation information, is collected by sensors and is forwarded to the cluster head. The cluster heads will forward the data to the central controller by dedicated links (such as Ethernet) for further analysis.

A hybrid sensor network that includes both the wireless nodes and PL nodes (shown in Fig. 4.2) is considered, which could be viewed as the sensor network in one of the clusters. The wireless nodes can be used to collect critical messages such as the measurement and actuation information. For example, the wireless nodes can be scatted in the chemical reaction pool to monitor the process constantly. The PL nodes can be installed on the overhead power sockets on the ceiling and

be used as complements of wireless nodes to collect critical information and relay data through the PL nodes (or be used as the wired network in the automation and management levels as introduced in the beginning of this chapter), such that the network lifetime can be prolonged.

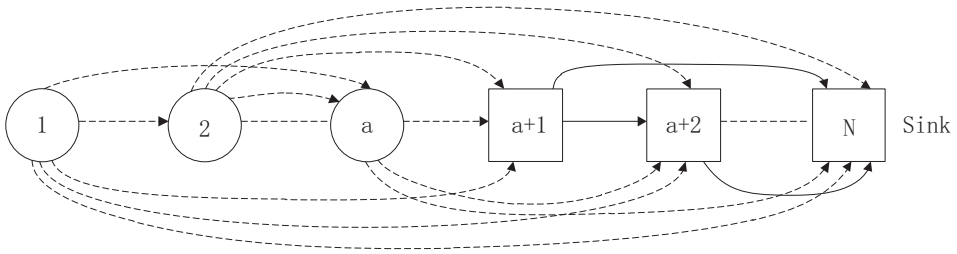

Figure 4.2: Topology of the hybrid sensor network, which could be viewed as the sensor network in one of the clusters (The circles denote wireless nodes, the squares are PL nodes, dashed arrows represent wireless links and the solid arrows are PL links, the Sink node is also a PL node)

It is assumed that the N sensor nodes in the hybrid sensor network are positioned in a line such that two neighbouring nodes has a separation of d, and the first a nodes are wireless nodes, followed by $(N-a)$ PL nodes, as shown in Fig. 4.2. The N-th node is considered as the Sink (or cluster head, also a PL node), to which all the other nodes in the cluster will forward their collected data. It is also assumed that all the PL nodes are equipped with antennas to receive wireless signals from the wireless nodes (the received signals are down converted to baseband by a low pass filter, modulated by the PL carrier frequency, and then forwarded to the adjacent PL node. A prototype of such a platform can be found in [144]), such that the following transmission links exist.

- Wireless node $\rightarrow$ wireless node (through wireless link)
- Wireless node $\rightarrow$ PL node (through wireless link)
- PL node $\rightarrow$ PL node (through PL link)

Notations: The wireless nodes set is denoted by $\mathbb{W} = \{1, ..., a\}$ and the PL nodes set is denoted by $\mathbb{P} = \{a+1, ..., N\}$. L_w is defined as the number of

wireless links and L_p is the number of PL links. $\mathcal{L}_w$ and $\mathcal{L}_p$ are used to label all the wireless and PL links, such that $\mathcal{L}_w = \{1, ..., L_w\}$ and $\mathcal{L}_p = \{1, ..., L_p\}$. $l_w \in \mathcal{L}_w$ is the index used to denote the l-th wireless link and $l_p \in \mathcal{L}_p$ is used to represent the l-th PL link. $\mathcal{L} = \mathcal{L}_w \bigcup \mathcal{L}_p$ denotes all the links in the hybrid sensor network and $l \in \mathcal{L}$ indicates the l-th link, which is from a transmitter node i to a receiver node j and is denoted by (i, j). Finally, $\mathcal{O}(i)$ and $\mathcal{I}(i)$ represent the set of outgoing and incoming links at node i, respectively. x and $x^{'}$ are used to denote variables and parameters related to wireless and PL links, respectively.

4.2.1 Physical Layer

The path loss for the l-th wireless link, G_{l_w}, is assumed to be given by $G_{l_w} = G_0/d_{l_w}^m$, where G_0 is the path loss at $d = 1$ m, d_{l_w} is the transmission distance for link l_w, and m is the path loss exponent with typical value $2 \leq m \leq 6$. The noise is assumed to be AWGN with single-sided power spectral density N_0. Let p_{l_w} denote the transmission power over the link l_w, then the signal-to-noise ratio (SNR) is,

$$\gamma_{l_w} = \frac{p_{l_w} G_{l_w}}{N_0 B} \tag{4.1}$$

where B is the transmission bandwidth for wireless links.

For PL nodes, NB PLC in band B (95-125 kHz), which is specified by CENELEC is considered [145]. A deterministic propagation model is assumed for the PL channel, such that the power gain for PL link is given by

$$G_{l_p} = 10^{-a(f) \cdot d_{l_p}} \tag{4.2}$$

where f is the frequency, $a(f)$ varies between 0.004 m^{-1} (best case) and 0.01 m^{-1} (worst case), and d_{l_p} is the transmission distance for link l_p [146]. As in [145], the single sided noise power spectral density is assumed to be $N_0^{'}$. Let p_{l_p} denote the transmission power, then the SNR over link l_p is given by,

$$\gamma_{l_p} = \frac{p_{l_p} G_{l_p}}{N_0^{'} B^{'}} \tag{4.3}$$

where $B^{'}$ is the transmission bandwidth for PL links.

Therefore, for a general transmission link l, it follows that

$$\gamma_l = \begin{cases} \gamma_{l_w} & : \quad l \in \mathcal{L}_w \\ \gamma_{l_p} & : \quad l \in \mathcal{L}_p \end{cases} \tag{4.4}$$

M-ary Quadrature Amplitude Modulation (MQAM) is assumed to be used in the sensor network. The data rate over link l is expressed as [138],

$$r_l = B_l \log_2(1 + K\gamma_l) \tag{4.5}$$

where B_l is the transmission bandwidth for link l and $K = -1.5/\ln(5BER)$ is the maximum possible coding gain with target bit error rate (BER), BER, for modulation schemes such as MQAM [147]. This data rate is upper bounded by the maximum allowable transmission power, p_{max}, for wireless links and the PSD mask, $\bar{p}$, for PL links. The maximum data rate can be achieved for wireless and PL links (*i.e.,* C_{l_w} and C_{l_p}) can be obtained by substituting p_{max} and $\bar{p}$ into (4.4) and (4.5), respectively. Therefore, the maximum transmission rate constraint is

$$r_l \leq C_l \tag{4.6}$$

where

$$C_l = \begin{cases} C_{l_w} & : \quad l \in \mathcal{L}_w \\ C_{l_p} & : \quad l \in \mathcal{L}_p \end{cases} \tag{4.7}$$

4.2.2 MAC Layer

The TDMA approach is considered as the MAC scheme for both transmission mediums due to interference free and energy saving advantages. In a slotted synchronous TDMA MAC scheme, each frame of length T is divided into multiple slots of length Δ. It is assumed that only one wireless/ PL link is allowed to transmit in each time slot in the wireless/ PL medium. Also, note that wireless links and PL links follow TDMA approach separately. Therefore, within each TDMA frame of length T, if link l is allocated n_l slots, it transmits for time

$$t_l = n_l \Delta \tag{4.8}$$

Note that the transmission can occur in the wireless link and PL link simultaneously and the interference between wireless links and PL links is neglected (*e.g.,* due to the coupling circuit in the PL nodes) since they operate in two different frequency bands. Therefore, it follows that

$$\begin{cases} \sum_{l\in\mathcal{L}_w} t_l & \leq & T \\ \sum_{l\in\mathcal{L}_p} t_l & \leq & T \end{cases} \tag{4.9}$$

This means the transmission in either wireless or PL links should be completed within time period T.

4.2.3 Traffic Flow

A single commodity flow [138] is assumed in this work where each node collect energy management information such as temperature, humidity that needs to be forwarded to a single Sink node. Assuming each node (except the Sink node) collects data at the same rate of R, then the Sink node (N-th node) will have data rate

$$R_N = -\sum_{i=1}^{N-1} R_i \tag{4.10}$$

where the negative sign indicates that the Sink node only has incoming traffic. If data is transmitted over link l with a data rate of r_l for time t_l, then the amount of data transmitted over link l in period T is

$$W_l = r_l t_l \tag{4.11}$$

In particular, the flow conservation constraints should be satisfied at the end of every time period T, *i.e.,* the difference between the outgoing data and incoming data is equal to the data collected locally of each node i,

$$\sum_{l\in\mathcal{O}(i)} W_l - \sum_{l\in\mathcal{I}(i)} W_l = R_i T \tag{4.12}$$

4.3 Problem Formulation

In order to investigate the hybrid network lifetime, which is defined as the time duration till the first wireless node being drained of energy, it is assumed that the

PL nodes are powered by PL and thus have unlimited power supply, while the wireless nodes are powered by non-rechargeable batteries (wireless nodes are likely to be placed where mains power can not be attached, for example the wireless nodes scatted in the chemical reaction pool and can not be attached to the mains power due to safety concerns). Therefore, this work only focuses on the energy consumption model for the wireless nodes. Also, only the energy consumption for transmission is considered to illustrate the main ideas (as widely adopted in for example [122, 124, 140]). Therefore, if the transmission power over wireless link l_w is p_{l_w}, the power consumption at the transceiver circuit of wireless transmitter node i of link l_w is given by

$$P_{transceiver} = (1 + \alpha)p_{l_w} \tag{4.13}$$

where α is the inefficiency of the power amplifier and is taken to be a constant [148].

The actual power consumption of the sensor should take into account the power consumption for the active mode, the sleep mode, and the transient mode [149]. The active mode power includes the transmission signal power and the circuit power consumption. For the ease of derivation, and as widely adopted in [122, 124, 140], only the power consumption of transmission signal power and the power consumption of the power amplifier is considered. In the sleep mode the power consumption is dominated by the leakage current of the switching transistors. Since for analog circuits the leakage power consumption is usually much smaller than the power consumption in the active mode, leakage power is neglected in the total energy consumption. Also, since the duration of the transient mode is much smaller as compared to the slot time, the power consumption for the transient mode is relatively small and not considered in this chapter. Some notations of the parameters used in the problem formulation are summarised in Table 4.1.

From the wireless communication model, the power consumption required to

support the data rate, $\frac{W_{l_w}}{t_{l_w}}$, over link l_w is given by

$$p_{l_w} = \frac{N_0 B}{K G_{l_w}} (2^{\frac{W_{l_w}}{B t_{l_w}}} - 1) \tag{4.14}$$

This is derived as follows. By substituting eq. (4.1) into eq. (4.5), it has

$$r_{l_w} = B \log_2(1 + K \frac{p_{l_w} G_{l_w}}{N_0 B}) \tag{4.15}$$

Note that r_{l_w} here is the data rate on the wireless link (notation l_w instead of l), and can be represented by $\frac{W_{l_w}}{t_{l_w}}$, therefore, it has

$$\frac{W_{l_w}}{t_{l_w}} = B \log_2(1 + K \frac{p_{l_w} G_{l_w}}{N_0 B}) \tag{4.16}$$

or

$$2^{\frac{W_{l_w}}{B t_{l_w}}} = 1 + K \frac{p_{l_w} G_{l_w}}{N_0 B} \tag{4.17}$$

From the above equation, eq. (4.14) can be obtained.

Therefore, assuming the initial battery energy is E_c, the lifetime of wireless node i is defined as,

$$T_i = \frac{E_c}{\Sigma_{l_w \in \mathcal{O}(i)} p_{l_w} (1 + \alpha) \frac{t_{l_w}}{T}} \tag{4.18}$$

where $i \in \mathbb{W}$. Then the network lifetime can be represented as,

$$T_{net} = \min_{i \in \mathbb{W}} T_i \tag{4.19}$$

Table 4.1: Parameters used in problem formulation

T_{net}	Network lifetime
q	The inverse of T_{net}
E_c	Initial energy
R_i	Data arrival rate for the $i-th$ node
T	Time frame
Δ	Time slot duration
a	Number of the wireless sensor node
N	Number of the total sensor node
α	Power inefficiency
$p_{i,j}$	Transmission power over wireless link $i \rightarrow j$
$W_{i,j}, W'_{i,j}$	Data transmitted over wireless, PL link $i \rightarrow j$ in period T
$t_{i,j}, t'_{i,j}$	Transmission time allocated to wireless, PL link $i \rightarrow j$ in period T
$C_{i,j}, C'_{i,j}$	Maximum transmission data rate over wireless, PL link $i \rightarrow j$

The objective is to maximize the hybrid network lifetime. Note that the original objective function T_{net} is not convex, it however can be transformed into a convex function by taking an inverse of the network lifetime, $1/T_{net}$.

Lemma 4.3.1. *The objective function after transformation,* $1/T_{net}$ *is jointly convex over* W_l *and* t_l*.*

Proof. From the definition of network lifetime, it follows that

$$\begin{aligned}\frac{1}{T_{net}} &= \max_{i\in\mathbb{W}} \frac{1}{T_i} \\ &= \max_{i\in\mathbb{W}} \frac{\Sigma_{l_w\in\mathcal{O}(i)} p_{l_w}(1+\alpha)\frac{t_{l_w}}{T}}{E_c} \\ &= \max_{i\in\mathbb{W}} \frac{\Sigma_{l_w\in\mathcal{O}(i)} \frac{N_0 B}{KG_{l_w}}(2^{\frac{W_{l_w}}{Bt_{l_w}}}-1)(1+\alpha)\frac{t_{l_w}}{T}}{E_c}\end{aligned}$$

To prove $1/T_{net}$ is jointly convex over W_l and t_l, the first step is to prove $\Sigma_{l_w\in\mathcal{O}(i)} \frac{N_0 B}{KG_{l_w}}(2^{\frac{W_{l_w}}{Bt_{l_w}}}-1)(1+\alpha)\frac{t_{l_w}}{T}$ is jointly convex over W_l and t_l. Note that this expression can be decomposed into $\frac{N_0 B}{KG_{l_w}}(2^{\frac{W_{l_w}}{Bt_{l_w}}}-1)(1+\alpha)\frac{t_{l_w}}{T}$.

Define,

$$f(t_{l_w}, W_{l_w}) = \frac{N_0 B}{KG_{l_w}}(2^{\frac{W_{l_w}}{Bt_{l_w}}}-1)(1+\alpha)\frac{t_{l_w}}{T}$$

and by denoting

$$\beta_{l_w} = \frac{N_0 B}{KG_{l_w}}(1+\alpha)$$

$f(t, W)$ becomes

$$f(t, W) = \beta(2^{\frac{W}{t}}-1)\frac{t}{T}$$

where the subscripts in $f(t, W)$ are ignored for the ease of notation, and B is integrated into t since it is a constant.

The Hessian matrix [114] of $f(t, W)$ can be calculated as

$$\mathbf{H}(f) = \begin{bmatrix} \frac{\partial^2 f}{\partial t^2} & \frac{\partial^2 f}{\partial t\cdot\partial W} \\ \frac{\partial^2 f}{\partial W\cdot\partial t} & \frac{\partial^2 f}{\partial W^2} \end{bmatrix} = \frac{1}{\ln 2}\begin{bmatrix} \frac{\beta}{T}\cdot e^{\frac{W}{t}}\cdot\frac{W^2}{t^3} & -\frac{\beta}{T}\cdot e^{\frac{W}{t}}\cdot\frac{W}{t^2} \\ -\frac{\beta}{T}\cdot e^{\frac{W}{t}}\cdot\frac{W}{t^2} & \frac{\beta}{T}\cdot e^{\frac{W}{t}}\cdot\frac{1}{t} \end{bmatrix}$$

According to Schur's complement condition [114], for a matrix in the form of $\begin{bmatrix} a & b \\ b & c \end{bmatrix}$ with $a > 0$, it is positive semi-definite as long as the following holds

$$b^2 = ac$$

It is obvious that the Hessian matrix $\mathbf{H}(f)$ satisfies the Schur's complement condition. Therefore, $\mathbf{H}(f)$ is positive semi-definite, and thus $f(t, W)$ is jointly convex over t and W when they take real values [114]. Since the summation of convex functions are also convex, and taking the maximum of a convex function does not change its convexity [114], it follows that $1/T_{net}$ is jointly convex over W_l and t_l.

This completes the prove. □

Therefore, the network lifetime maximization problem can be formulated as a mixed integer convex optimization problem [114]:

$$\begin{array}{rrcll} & & \min & 1/T_{net} & \\ s.t. & T_{net} & \leq & E_c/\Sigma_{l\in\mathcal{O}(i)} p_l(1+\alpha)\frac{t_l}{T} & (i\in\mathbb{W}) \\ & C_l{\cdot}t_l & \geq & W_l & \\ & W_l & \geq & 0 & \\ & t_l & \in & \{0, \Delta, 2\Delta, ...\} & \end{array} \tag{4.20}$$

along with (4.9) and (4.12).

The variables to determine are T_{net}, W_l and t_l. The first inequality in (4.20) means that the energy consumption for each wireless node should not exceed the battery capacity for the whole network lifetime. The second inequality is the maximum transmission power constraint for all links. Constraint (4.9) ensures that the data relaying in either wireless or PL link is finished within time period T. Equality (4.12) is the flow conservation constraints for all nodes. For the above problem formulation, if the integer constraints are relaxed on t_l, the optimization problem would be a convex problem.

4.4 Optimization Approach

In this section, the KKT conditions are used to derive analytical expressions for the hybrid network lifetime from the relaxed problem for two topologies, which

provide upper bounds on the network lifetime for the optimization problem in (4.20). The Lagrangian of the optimization problem in (4.20) is:

$$\begin{aligned}\mathbf{L}(q,\mathbf{t},\mathbf{W},\boldsymbol{\lambda},\boldsymbol{\mu},\varphi,\varphi^{'},\boldsymbol{\nu}) =& q+\sum_{i\in\mathbb{W}}\lambda_i\cdot\Big[\sum_{l\in\mathcal{O}(i)}\beta_{l_w}\cdot(2^{\frac{W_{l_w}}{B\cdot t_{l_w}}}-1)\cdot t_{l_w}-E_c\cdot q\cdot T\Big]\\ &+\sum_{l\in\mathcal{L}}\mu_l\cdot(W_l-C_l\cdot t_l)\\ &+\varphi\cdot(\sum_{l\in l_w}t_l-T)+\varphi^{'}\cdot(\sum_{l\in l_p}t_l-T)\\ &+\sum_{i\in\mathbb{W}\bigcup\mathbb{P}}\nu_i\cdot(\sum_{l\in\mathcal{O}(i)}W_l-\sum_{l\in\mathcal{I}(i)}W_l-R_iT) \qquad (4.21)\end{aligned}$$

where $q=1/T_{net}$ and $\beta_l=\frac{BN_0(1+\alpha)}{G_lK}$. $\boldsymbol{\lambda}$ and $\boldsymbol{\mu}$ are the Lagrange multipliers associated with the first and the second inequality constraints in (4.20), respectively. φ and $\varphi^{'}$ are the Lagrange multipliers associated with (4.9) for the wireless and PL links, respectively. $\boldsymbol{\nu}$ is the Lagrange multiplier with respect to (4.12).

The KKT conditions [114] are

$$1-E_cT(\lambda_1+\lambda_2+\cdots+\lambda_a)= 0 \qquad (4.22)$$

$$\frac{\beta_{1,2}}{B}\cdot 2^{\frac{W_{1,2}}{Bt_{1,2}}}\cdot\lambda_1+\mu_{1,2}+\nu_1-\nu_2= 0 \qquad (4.23)$$

$$\cdots$$

$$\frac{\beta_{1,a+1}}{B}\cdot 2^{\frac{W_{1,a+1}}{Bt_{1,a+1}}}\cdot\lambda_1+\mu_{1,a+1}+\nu_1-\nu_{a+1}= 0 \qquad (4.24)$$

$$\cdots$$

$$\frac{\beta_{a,a+1}}{B}\cdot 2^{\frac{W_{a,a+1}}{Bt_{a,a+1}}}\cdot\lambda_a+\mu_{a,a+1}+\nu_a-\nu_{a+1}= 0 \qquad (4.25)$$

$$\beta_{1,2}[(1-\frac{W_{1,2}}{Bt_{1,2}})\cdot 2^{\frac{W_{1,2}}{Bt_{1,2}}}-1]\cdot\lambda_1-C_{1,2}\cdot\mu_{1,2}+\varphi= 0 \qquad (4.26)$$

$$\cdots$$

$$\beta_{a,a+1}[(1-\frac{W_{a,a+1}}{Bt_{a,a+1}})\cdot 2^{\frac{W_{a,a+1}}{Bt_{a,a+1}}}-1]\cdot\lambda_a-C_{a,a+1}\cdot\mu_{a,a+1}+\varphi= 0 \qquad (4.27)$$

$$\mu_{a+1,a+2}+\nu_{a+1}-\nu_{a+2}= 0 \qquad (4.28)$$

$$\mu_{N-1,N}+\nu_{N-1}-\nu_N= 0 \qquad (4.29)$$

$$-C^{'}_{a+1,a+2}\cdot\mu_{a+1,a+2}+\varphi^{'}= 0 \qquad (4.30)$$

$$\cdots$$

$$-C^{'}_{N-1,N}\cdot\mu_{N-1,N}+\varphi^{'}= 0 \qquad (4.31)$$

In particular, the complementary slackness conditions are

$$\lambda_1 \cdot [\beta_{1,2} \cdot (2^{\frac{W_{1,2}}{Bt_{1,2}}} - 1) \cdot t_{1,2} + ... + \beta_{1,a+1} \cdot (2^{\frac{W_{1,a+1}}{Bt_{1,a+1}}} - 1) \cdot t_{1,a+1} - E_c \cdot q \cdot T] = 0 \tag{4.32}$$

$$\cdots$$

$$\lambda_a \cdot [\beta_{a,a+1} \cdot (2^{\frac{W_{a,a+1}}{Bt_{a,a+1}}} - 1) \cdot t_{a,a+1} - E_c \cdot q \cdot T] = 0 \tag{4.33}$$

$$\mu_{1,2} \cdot (W_{1,2} - C_{1,2} \cdot t_{1,2}) = 0 \tag{4.34}$$

$$\cdots$$

$$\mu_{a,a+1} \cdot (W_{a,a+1} - C_{a,a+1} \cdot t_{a,a+1}) = 0 \tag{4.35}$$

$$\cdots$$

$$\mu_{N-1,N} \cdot (W_{N-1,N} - C_{N-1,N} \cdot t_{N-1,N}) = 0 \tag{4.36}$$

$$\varphi \cdot [(t_{1,2} + t_{1,a+1} + \cdots + t_{a,a+1}) - T] = 0 \tag{4.37}$$

$$\varphi^{'} \cdot [(t_{a+1,a+2} + t_{a+1,N} + \cdots + t_{N-1,N})] = 0 \tag{4.38}$$

$$\boldsymbol{\lambda}, \boldsymbol{\mu}, \varphi, \varphi^{'}, \boldsymbol{\nu} \geq 0 \tag{4.39}$$

4.4.1 String Topology

In a string topology, only one wireless node generates data (*i.e.*, node 1 in Fig. 4.2). All the other nodes act as relays for that node. To obtain the analytical expression for the hybrid network lifetime in a string topology, the following lemma is first proved.

Lemma 4.4.1. *Given $W_{1,2}, t_{1,2} \geq 0$, the following expression holds:*

$$\beta_{1,2}[(1 - \frac{W_{1,2}}{Bt_{1,2}}) \cdot 2^{\frac{W_{1,2}}{Bt_{1,2}}} - 1] \leq 0$$

Proof. Since $\beta_{l,2} = \frac{BN_0(1+\alpha)}{G_{l,2}K} \geq 0$, define $x = \frac{W_{1,2}}{B \cdot W_{1,2}}$, it is equivalent to prove

$$f(x) = (1 - x) \cdot 2^x - 1 \leq 0$$

The derivation of $f(x)$ with respect to x can be calculated as

$$\frac{df(x)}{dx} = 2^x \cdot [(1-x)\ln 2 - 1]$$

Since $x = \frac{W_{1,2}}{B \cdot W_{1,2}} \geq 0$, it follows that $\frac{df(x)}{dx} < 0$. This indicates that $f(x)$ is monotonically decreasing in the region of $x \geq 0$. Also, since $f(0) = 0$, it follows that $f(x) \leq 0$.

This completes the prove. □

Lemma 4.4.2. $\varphi \neq 0$ *always holds.*

Proof. It is first assumed that $\varphi = 0$. According to (4.26), it can be derived that

$$\beta_{1,2}[(1 - \frac{W_{1,2}}{Bt_{1,2}}) \cdot 2^{\frac{W_{1,2}}{Bt_{1,2}}} - 1] \cdot \lambda_1 = C_{1,2} \cdot \mu_{1,2}$$

From lemma (4.4.1), $\beta_{1,2}[(1 - \frac{W_{1,2}}{Bt_{1,2}}) \cdot 2^{\frac{W_{1,2}}{Bt_{1,2}}} - 1] \leq 0$, and $C_{1,2} > 0$. Therefore, λ_1 and $\mu_{1,2}$ must have different signs (this implies that $\lambda_1 \geq 0, \mu_{1,2} \leq 0$ or $\lambda_1 \leq 0, \mu_{1,2} \geq 0$). However, from (4.39), $\lambda_1 \geq 0$ and $\mu_{1,2} \geq 0$. This contradicts with the assumption of $\varphi = 0$. Therefore, it concludes that $\varphi \neq 0$ always holds.

This completes the prove. □

From lemma (4.4.2) and equation (4.37), it can be derived that

$$T = \sum_{l \in \mathcal{L}_w} t_l$$

Therefore, let

$$t_{1,2} = t_{2,3} = ... = t_{a,a+1} = \frac{T}{a} \tag{4.40}$$

$$W_{1,2} = W_{2,3} = ... = W_{a,a+1} = RT \tag{4.41}$$

It can be proved that the values in (4.40) and (4.41) satisfy the KKT conditions, and since it is a convex optimization problem, KKT conditions are both sufficient and necessary for the values in (4.40) and (4.41) to be optimal. The expression in (4.32) simplifies to

$$\lambda_1 \cdot [\beta_{1,2} \cdot (2^{\frac{W_{1,2}}{Bt_{1,2}}} - 1) \cdot t_{1,2} - E_c \cdot q \cdot T] = 0 \tag{4.42}$$

Hence by combining (4.40), (4.41) and (4.42), it can be obtained that

$$q = \frac{\beta_{1,2} \cdot (2^{\frac{W_{1,2}}{Bt_{1,2}}} - 1) \cdot t_{1,2}}{E_c \cdot T} = \frac{\beta_{1,2} \cdot (2^{\frac{aR}{B}} - 1)}{E_c \cdot a} \tag{4.43}$$

Therefore, the closed-form expression for the hybrid network lifetime in a string topology becomes

$$T_{net} = \frac{1}{q} = \frac{E_c \cdot a}{\beta_{1,2} \cdot (2^{\frac{aR}{B}} - 1)} \tag{4.44}$$

In eq. (4.44), since $\beta_{1,2}$ is a constant, it is clear that the network lifetime of the hybrid network in the string topology is only related to the initial battery capacity, E_c, the number of battery powered wireless nodes a, and the data arrival rate R. Further, the increase of the initial battery capacity will cause the network lifetime to increase linearly, while the increase of the number of battery powered wireless nodes and the data arrival rate will result in the network lifetime to decrease exponentially. Further, as indicated by eq. (4.40), it is obvious that the optimal routing strategy for the sensor network in the string topology would be in a multihop fashion, but not a one-hop routing strategy. This derived closed-form expression provides intuitive guideline for the design of sensor network based industrial automation system.

4.4.2 Linear Topology

Unlike the string topology, in the linear topology, all the wireless sensor nodes collect data. In the network configuration shown in Fig. 4.2, the network lifetime will be maximized if all the wireless nodes relay their data to the first PL node (the $(a+1)$-th node), since the transmission distance is shortest compared to other PL nodes. Therefore, in order to simplify the derivation, four terms (*i.e.,* $W_{i,i+1}$, $W_{i,a+1}$, $W'_{i,i+1}$ and $W'_{i,N}$) are considered for optimization. This means, all the wireless nodes only relay data to the next wireless node or to the first PL node and the PL nodes relay data to the next PL node or to the Sink node directly.

Assuming that all the wireless links use the same constellation size in MQAM. Then it follows that,

$$\frac{W_{1,2}}{t_{1,2}} = \frac{W_{1,a+1}}{t_{1,a+1}} = \frac{W_{2,3}}{t_{2,3}} = \frac{W_{2,a+1}}{t_{2,a+1}} = \cdots = \frac{W_{a,a+1}}{t_{a,a+1}} \tag{4.45}$$

Note that in an optimal optimization scheme, all the wireless nodes should be drained of energy at the same time. Therefore, it can be obtained from (4.32) and (4.33) that,

$$\beta_{1,2}(2^{\frac{W_{1,2}}{Bt_{1,2}}} - 1)\cdot t_{1,2} + \beta_{1,a+1}(2^{\frac{W_{1,a+1}}{Bt_{1,a+1}}} - 1)\cdot t_{1,a+1} = \cdots = \beta_{a,a+1}(2^{\frac{W_{a,a+1}}{Bt_{a,a+1}}} - 1)\cdot t_{a,a+1} \tag{4.46}$$

Substituting (4.45) into (4.46), and by further derivation, yields

$$\begin{aligned} W_{1,2} + a^m W_{1,a+1} &= W_{2,3} + (a-1)^m W_{2,a+1} = \cdots \\ &= W_{a-1,a} + 2^m W_{a-1,a+1} = W_{a,a+1} \end{aligned} \tag{4.47}$$

Now from the flow conservation constraint (4.12), it follows that

$$W_{a,a+1} - W_{a-1,a} = RT \tag{4.48}$$

From (4.47), it has

$$W_{a-1,a} + 2^m W_{a-1,a+1} = W_{a,a+1} \tag{4.49}$$

Solving (4.48) and (4.49), gives,

$$W_{a-1,a+1} = \frac{RT}{2^m} \tag{4.50}$$

Combining (4.12) and (4.47), and by repeating the process above, all the values of $W_{i,j}$ can be determined. Now with the values of $W_{i,j}$, the values of $t_{i,j}$ can be obtained from (4.45).

The optimal values of $W_{i,j}$, and $t_{i,j}$ are summarised as follows.

$$W_{i,a+1} = \begin{cases} \frac{RT+[(a-i)^m-1]W_{i+1,a+1}}{(a+1-i)^m} & : \quad 1 \leq i \leq a-2 \\ \frac{RT}{2^m} & : \quad i = a-1 \end{cases} \tag{4.51}$$

$$W_{i,i+1} = \begin{cases} iRT - \sum_{j=1}^{i} W_{j,a+1} & : \quad 1 \leq i \leq a-1 \\ aRT - \sum_{j=1}^{a-1} W_{j,a+1} & : \quad i = a \end{cases} \tag{4.52}$$

$$\begin{cases} t_{i,a+1} &= \frac{W_{i,a+1}}{W_M+W_N} \cdot T \\ t_{i,i+1} &= \frac{W_{i,i+1}}{W_M+W_N} \cdot T \end{cases} \tag{4.53}$$

where $W_M = \sum_{i=1}^{a-1} W_{i,a+1}$ is the total amount of data transmitted from each wireless node (except the a-th node) to the 1-st PL node and $W_N = \sum_{i=1}^{a} W_{i,i+1}$ is the total amount of data transmitted from each wireless node to the next node.

Since the PL nodes have unlimited power supply, it is assumed that all the PL nodes will relay their data to the next PL node (the effectiveness of this transmission strategy will be examined in section 4.5) and all PL nodes transmit at the maximum power, therefore, $W'_{i,j}$ and $t'_{i,j}$ can be calculated as,

$$\begin{cases} W'_{i,i+1} &= iRT \quad : \quad a+1 \leq i \leq N-1 \\ t'_{i,i+1} &= \frac{W'_{i,i+1}}{C'_{i,i+1}} \quad : \quad a+1 \leq i \leq N-1 \end{cases} \tag{4.54}$$

From (4.33), and the results of $W_{a,a+1}$ and $t_{a,a+1}$, the closed-form expression for the hybrid network lifetime maximization can be derived as:

$$T_{net} = \frac{E_c(W_M + W_N)}{\beta_{a,a+1}(aRT - W_M)(2^{\frac{W_M+W_N}{BT}} - 1)} \tag{4.55}$$

Equation (4.55) provides the globally optimal value for hybrid network lifetime maximization. Since the integer constraints on t_l are relaxed, therefore, the closed-form expression of network lifetime maximization in (4.55) provides an upper bound to the network lifetime of the hybrid sensor network.

In eq. (4.55), since $\beta_{a,a+1}$ is a constant, it is clear that the network lifetime of the hybrid network in the linear topology is only related to the initial battery capacity, E_c, the number of battery powered wireless nodes a, and the data arrival rate R. While the closed-form expression in the linear topology is complication, it facilities to sensor network system design by fast parameter fitting to investigate the relationship between the network lifetime and the related system parameters. Also, unlike in the string topology, where the optimal routing strategy is single-path multihop routing, the optimal routing strategy in the linear topology is multi-path multihop routing.

4.5 Numerical Results and Analysis

In this section, numerical results obtained from the proposed approach are used to demonstrate the effectiveness of the proposed hybrid sensor network. The parameters used are summarised in Table 4.2. The radio frequency operates in the 2.4 GHz in the industrial-scientific-medical (ISM) band, with a reference path loss at $d = 1m$ of 40 dB. The initial energy of the wireless node is 5000 J, which is typical for the capacity of an AAA alkaline long-life battery [122]. The maximum transmit power of the wireless node is 10 mW, as specified in the standard in [150], and is used as in the literature in [151].

Table 4.2: Parameters Used For Simulation

Symbol	Value	Description
f_c	2.4 GHz	Radio frquency
E_c	5000 J [122]	Initial energy of wireless node
p_{max}	10 mW [138]	Maximum Tx power of wireless node
N_0	-105 dBm/Hz	Noise PSD level of wireless link
B	10 kHz	Bandwidth of wireless link
d	1.5 m	Distance between adjacent nodes
T	1 s	Time frame
Δ	0.001T	Time slot duration
G_0	40 dB	Path loss at $d = 1$m
m	3.5	Path loss exponent
α	1.9	Power inefficiency
BER	10^{-3}	Target BER
$f_c^{'}$	110 kHz	Carrier frequency of PL link
$B^{'}$	30 kHz	Bandwidth of PL link
$N_0^{'}$	-80 dBm/Hz	Noise PSD level of PL link
$\bar{p}$	-25 dBm/Hz	PSD mask

4.5.1 String Topology

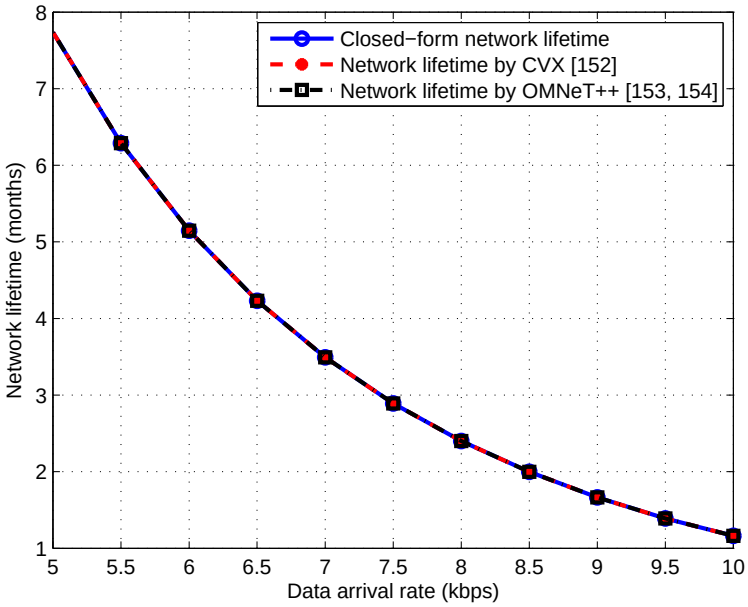

Figure 4.3: Comparison of network lifetime in string topology with CVX [152] and OMNeT++ [153, 154]

In this subsection, the effectiveness of the hybrid sensor network in a string topology is examined. To setup the simulation, the default separation between adjacent nodes is set to 1.5 m. The total number of sensor nodes is 10 with 5 PL nodes. In order to show the accuracy of the derived closed-form expression, the results obtained from (4.44) are compared to the results obtained by the CVX optimisation tool [152] and the results obtained by an event simulation framework built in OMNeT++ [153, 154]. As shown in Fig. 4.3, the network lifetime obtained from the closed-form expression matches exactly with the results obtained by CVX and OMNeT++.

The point of this comparison is that in order to derive the close-form expression, the number of time slots that each link occupies is relaxed to a positive real number in the derivation (as in eq. 4.40), which should be a positive integer. Therefore, the accuracy of the derived closed-form expression should be tested. While in the CVX optimisation tool [152] and the OMNeT++ [153, 154],

the number of time slots is strictly restricted to a positive integer. Therefore, by comparing the results obtained from the derived closed-form expression and the results obtained from the CVX optimisation tool and the OMNeT++, it can examine the accuracy of the derived closed-form expression. In the case of string topology, the optimal solution for time slot allocation is that each wireless link should occupy the same amount of time slots, as derived mathematically. In the simulation, there are 5 wireless nodes and 5 wireless links (each wireless node only transmit to the next node in the string topology), which shares evenly of the 1000 time slots (time frame divided by the time slot duration). Therefore, each wireless link occupies 200 time slots, which is exactly an integer. Therefore, the result matches exactly with the results obtained by CVX and OMNeT++.

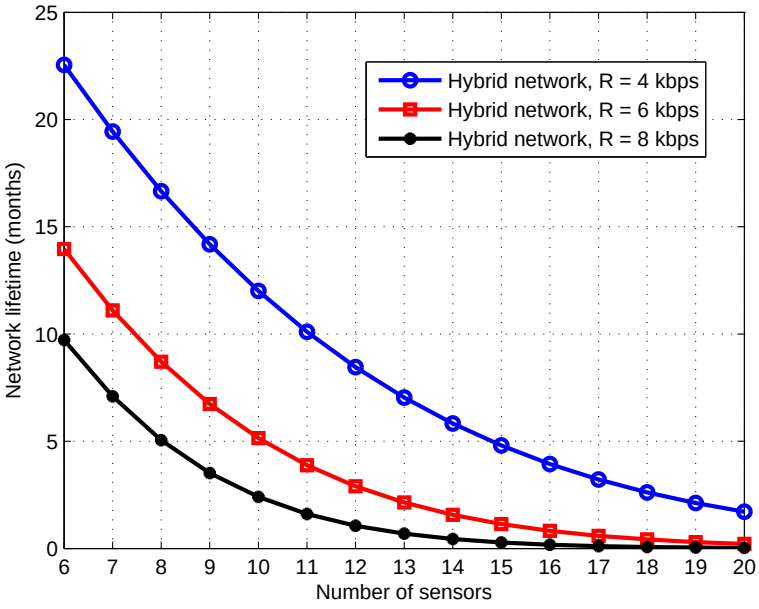

Figure 4.4: Network lifetime vs. the total number of sensor nodes in string topology under different data arrival rates (with 5 PL nodes for the hybrid network)

Fig. 4.4 shows the impact of the total number of sensors on the network lifetime of the hybrid sensor network (the separation between adjacent nodes is set to 1.5 m). The number of PL nodes in the hybrid sensor network is fixed to 5. Actually the number of PL nodes is not quite strict as long as the data rate in the

PL channel can support the data rate requirement of the sensor network, or by increasing the number of PL nodes, the intermediate PL nodes may act as relays, thus improving the throughput of the PL channel. For example, in the industrial automation system, the PL nodes can act as the nodes in the automation and management levels. Or PL nodes can act as relay nodes, where the wireless signal may not penetrate.

It can be observed that when the total number of sensors increases, the network lifetime of the hybrid network drops rapidly. This is due to the fact that with the increase of the wireless nodes in the network, as each wireless node is allocated the same portion of the total time period T. Thus each node is allocated less transmission time. Since the amount of data to be transmitted for each node remains the same, each node has to increase the transmission power to increase the data rate. In addition, with the increase of data arrival rate, the network lifetime reduces. For example, consider the case that sensors are scattered in the chemical reaction pool, the data arrival rate can be adjusted accordingly to sample more monitoring information of the process. This is due to the fact that with the same amount of sensor nodes in the network, each node is allocated a fixed time duration to access the wireless channel. Therefore, each node has to increase its transmission power to increase the data rate in order to meet the requirement of the network data arrival rate. Consequently, each node consumes more energy and causes the reduction of the network lifetime.

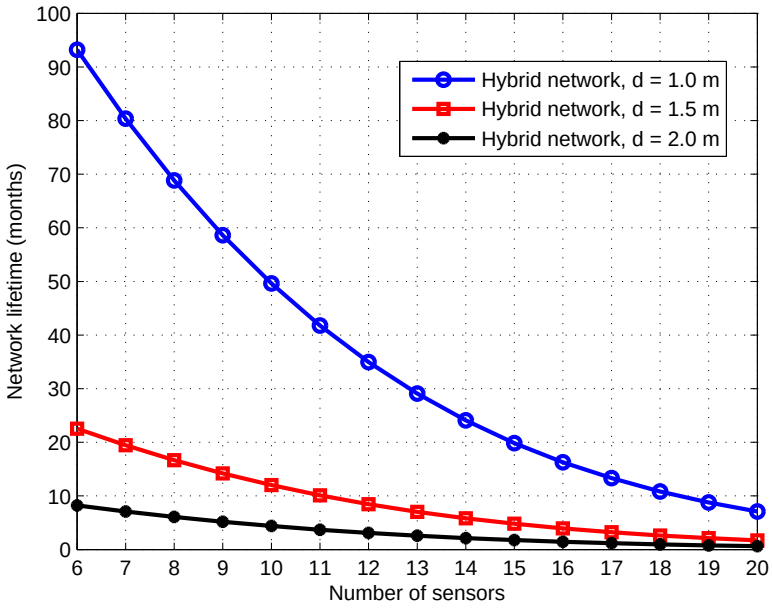

Figure 4.5: Network lifetime vs. the total number of sensor nodes in string topology under different separation distances (with 5 PL nodes for the hybrid network, the data arrival rate is fixed at 4 kbps)

The impact of total number of sensor nodes on network lifetime under different separation distances in the string topology is depicted in Fig. 4.5, where the data arrival rate is fixed at 4 kbps. It is obvious that when the separation between adjacent nodes in the the hybrid sensor network increases, the network lifetime reduces significantly under the same total number of sensor nodes. The reason is quite straight-forward. With the increase of the separation, each wireless link experiences poorer channel conditions and to compensate for the channel loss, each wireless link tends to use more transmission power. Nevertheless, with the increase of total number of sensors, each wireless link shares a decreased portion of the time to access the channel and thus leads to an increase on the transmission power, and hence a reduced network lifetime.

4.5.2 Linear Topology

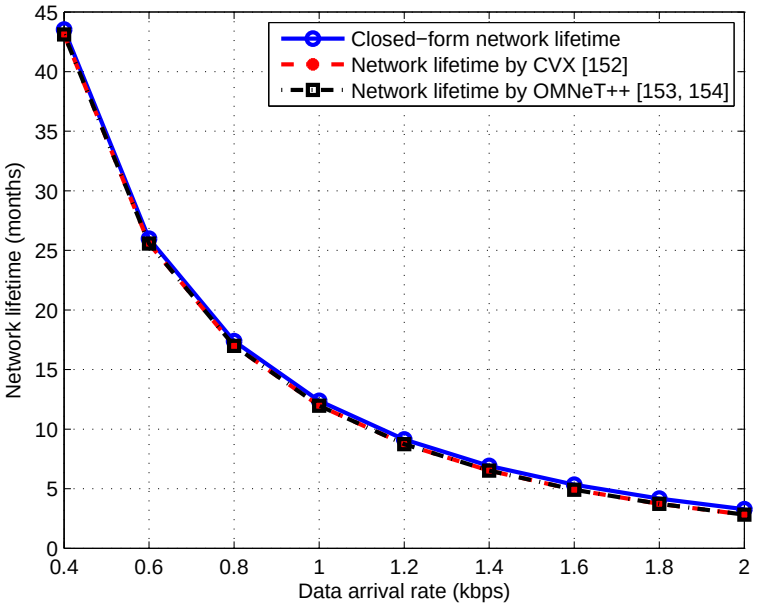

Figure 4.6: Comparison of network lifetime in linear topology with CVX [152] and OMNeT++ [153, 154]

To test the accuracy of the derived closed-form network lifetime expression, the separation between adjacent nodes is set to 1.5 m, and the total number of sensors is 10 with 5 PL nodes. Fig. 4.6 depicts the comparison of network lifetime obtained from the closed-form expression with the results obtained by CVX [152] and OMNeT++ [153, 154]. The results shown that the network lifetime obtained from the closed-form expression is slightly longer than the results obtained by the other two methods, especially when the data arrival rate is relatively larger. This is due to the fact that in deriving the closed-form network lifetime expression, the integer constraints on t_l are relaxed. Therefore, it provides an upper bound to the network lifetime. However, as shown in Fig. 4.6, this upper bound is very tight to the optimal solution when integer constraints are taken into account.

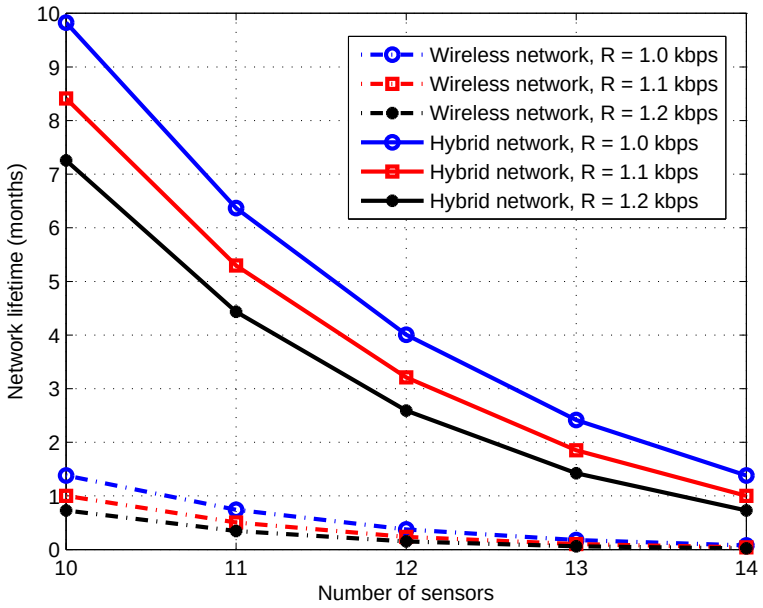

Figure 4.7: Network lifetime vs. the total number of sensor nodes in linear topology (with 5 PL sensors for the hybrid network)

In Fig. 4.7, the network lifetime of a hybrid sensor network is compared with a pure WSN (when $a = N$) with the same total number of sensors (including the Sink node). Under different data arrival rates, the number of PL nodes in the hybrid sensor network is fixed to 5 regardless of total number of nodes. The separation between adjacent nodes is set to 1.5 m. It is obvious that the lifetime of the hybrid sensor network is much longer than that of the WSN, especially when the network scale is relatively small and the data arrival rate is relatively low. For example, with a total of 12 sensors and a data arrival rate of 1 kbps, the hybrid network lifetime is enhanced by 8 times compared to a pure WSN with the same total number of sensors and with the same data arrival rate. This advantage is due to the fact that all the wireless nodes forward their data to the first PL node in the hybrid network, thus reduces transmission distances for wireless links. Also, since wireless links and PL links use two different mediums for transmission, each wireless node in hybrid network can access wireless channel for a longer time (the PL nodes use PL channel for transmission and does not interfere with the wireless channel), thus reduces the power requirement for each

wireless link. However, when the number of sensors is large, the lifetime of both networks drops rapidly due to lacking of enough energy.

Fig. 4.7 also shows that with the increase of total number of sensors, the lifetime of both networks decreases. This is mainly due to the fact that with an increase in the total number of sensors, the network scale increases and consequently the transmission distances of wireless nodes to the Sink (in WSN) and to the first PL node (in hybrid sensor network) increases, thus the wireless links suffer from poorer channel conditions. Also, since the time period T is fixed, each node is allocated less transmission time with the increase of total number of sensor. Therefore, with the same data arrival rate, each sensor node tend to use more power for transmission and causes a reduction in the network lifetime. Also, each sensor node will consume more energy for transmission with the increase of data arrival rate. This explains the reduction of the network lifetime with the increase of data arrival rate.

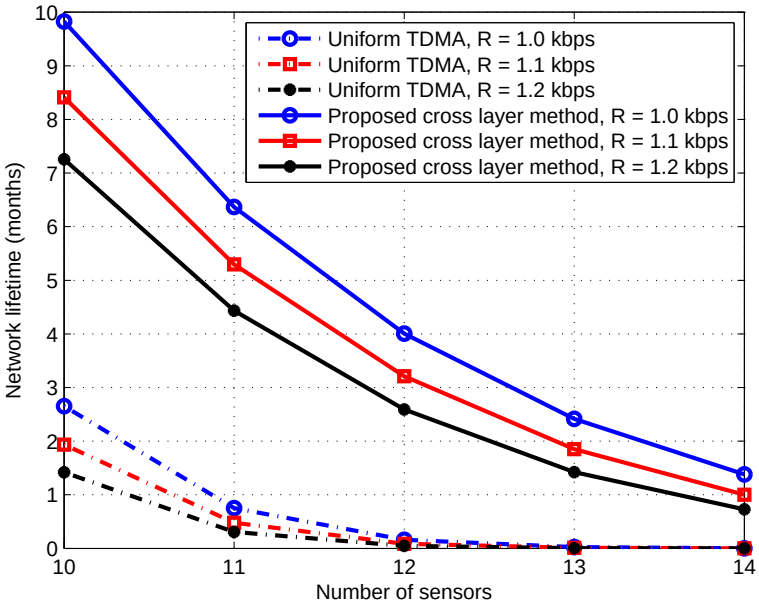

Figure 4.8: Network lifetime vs. the total number of sensor nodes in linear topology (with 5 PL sensors for the hybrid network)

In the case of string topology, the optimal solution for data transmission is such that each node transmits data in a single-hop fashion, and the duration

for transmission of each link is the same, which is exactly the uniform TDMA transmission mechanism. Therefore, the cross-layer optimization method and single-layer optimization method would provide exactly the same solution in the string topology. However, in the linear topology, the multi-hop transmission mechanism is used, and the joint cross-layer optimization results show that the optimal solution of time allocation on each link is not uniform TDMA. Therefore, it is necessary to compare the network lifetime of the hybrid sensor network using cross-layer optimization method and single-layer optimization method. Fig. 4.8 compares the network lifetime of a hybrid sensor network using the cross-layer optimization method and single-layer optimization method (where a uniform T-DMA mechanism is adopted for link time allocation, and the amount of data to be transmitted on each link is optimized, labelled as "Uniform TDMA" in Fig. 4.8) under different total number of sensor nodes and under different data arrival rates. The network setup is exactly the same as the network setup of the hybrid sensor network in Fig. 4.7. Fig. 4.8 depicts that the network lifetime of the hybrid sensor network adopting cross-layer optimization method is much longer than that of the single-layer optimization method, especially when the network scale is relatively small and the data arrival rate is relatively low. This proves the advantage of the cross-layer optimization method on the linear topology.

Since the linear network topology considered in this chapter can be viewed as a cluster in a sensor network for industrial automation system, the number of nodes in each cluster could be small, while the span of the network matters. Therefore, as shown in Fig. 4.9, the network lifetime performance of hybrid networks is compared under different sensor densities. The hybrid network with a total of 16 nodes including 5 PL nodes as in Fig. 4.7 is used as a reference for comparison. The total length of the network is 22.5 meters (15 segments multiplied by the separation of 1.5 meters). With a total of 16 nodes, the separation between two adjacent nodes is 1.5 meters, while the separation is 2.5 meters with 10 nodes. The rest simulation parameters are the same as in Table 4.2. From Fig. 4.9, the

hybrid network with lower sensor density outperforms the reference network in terms of the network lifetime, especially when the data arrival rate is low. This is due to the fact that although the distance between adjacent nodes are larger in the hybrid network with lower sensor density, the distance between each wireless node to the first PL node is reduced. Also, for a hybrid network with lower sensor density, each wireless node can access the wireless medium for a longer time, thus can reduce the transmission power.

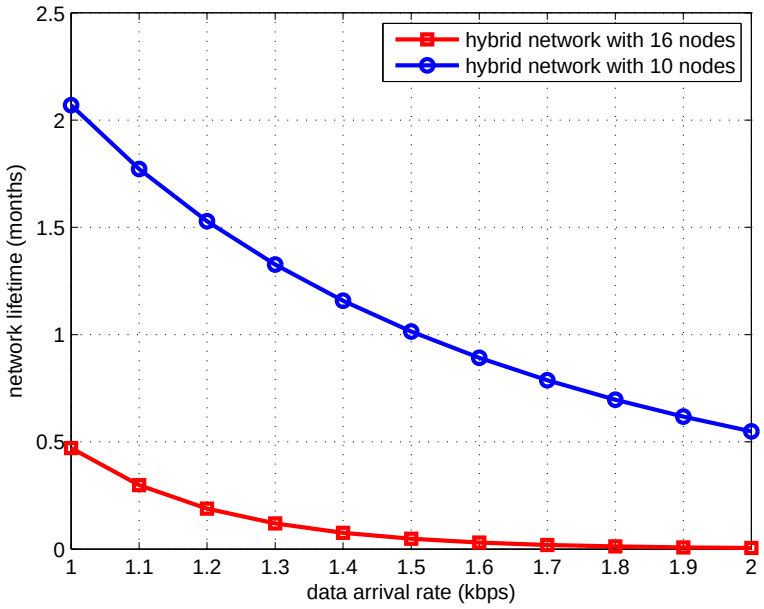

Figure 4.9: Impact of the data arrival rate on the network lifetime with a fixed total network range of 22.5 m

However, one may argue that the network lifetime is prolonged since the total amount of data forwarded to the Sink is decreased, which is true as with a same data arrival rate, 15 nodes will collect data in the reference network while only 9 nodes collect data in the hybrid network for comparison. It can be noticed from Fig. 4.9 that even with a same total amount of data collected, the hybrid network with a lower sensor density still exhibits a much longer lifetime than the reference one. For example, when the data arrival rate for the reference network is 1 kbps, the total amount of data collected in time period T is 15 kb, and

the corresponding lifetime is around 0.5 month. This means each node in the hybrid network with lower sensor density should collect data at a rate of 1.67 kbps to maintain a same amount of data collected. While at $R = 1.67$ kbps, the corresponding lifetime is around 0.8 month, which is still much longer than that of the reference network. Note that since a bandwidth of 10 kHz is considered, the data arrival rate in this chapter is generally low, which could be suitable for scalar information (such as temperature and humidity) collection.

Note that in Fig. 4.9, when the data rate is increased from 1 kbps to 2 kbps, the network lifetime of the hybrid network with 16 nodes drops significantly. This is due to the fact that only the power consumption of the active mode of the sensor network is considered. Also, for the ease of derivation of the closed-form expression, only the power consumption of transmission signal power and the power consumption of the power amplifier is considered as widely adopted in the literature [122, 124, 140]. More details on the power consumption of the sensor network is on p70 of this thesis. By considering the complete power consumption model would make the derivation very difficult and is left as a future work. In this case, another reason is that, since the hybrid network has 16 nodes, and each wireless node performs data collection. When the data arrival rate is increased from 1 kbps to 2 kbps, the overall amount of data collected by the sensor network becomes large and the sensor network may not be able to accommodate the required amount of traffic and hence results in a very low network lifetime.

Based on the above analysis, the hybrid sensor network has a significant improvement in prolonging the network lifetime compared to a pure WSN. Also, by limiting the data arrival rate of sensor nodes and the sensor density in a linear hybrid sensor network with given length and fixed PL nodes, the hybrid network lifetime can be maximized.

4.5.3 Transmission Strategies of PL Nodes

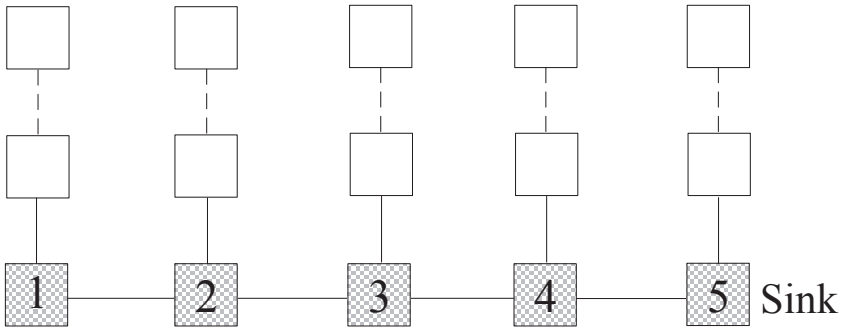

Figure 4.10: PL network topology (the greyed squares represent the PL nodes in the hybrid sensor network while the white squares denote the outlets with Bus or Star connection, detailed in Chapter 2)

In order to investigate the transmission strategies of PL nodes in the CENELEC band B (95-125 kHz) for a string/linear hybrid sensor network (*i.e.*, each PL node transmit data to the next PL node or to the Sink directly), the PL network topology is constructed as shown in Fig. 4.10 (the rightmost PL node is the Sink), where 5 PL nodes (labelled as node 1 to 5 in Fig. 4.10) are placed on the main span. These PL nodes are arranged such that they are evenly spaced at a separation of 1.5 m. The topology of the branches attached to each PL node is randomly generated according to the rules described as follows. Each branch attached to node 1 to 5 in Fig. 4.10 may have 5 to 10 outlets with Bus or Star connection and the distances between adjacent outlets (or between the outlets to the PL nodes) varies from 1 m to 5 m. Besides, it is assumed that each outlet is randomly connected with appliance that exhibit impedances of 5 Ω, 50 Ω, 150 Ω, 1000 Ω or frequency-selective impedances [155] with resistance at resonance equal to 394 Ω, 863 Ω or 1312 Ω. Please refer to [155] for the frequency-selective impedance model and the relative parameters. In addition, the impedance of PL nodes are assumed to be 100 Ω and transmission Cable type 1 in [155] is considered in this chapter. For the simulation, the impedance carry-back method and VRA in [86] (details are provided in Chapter 2) is utilised to determine the

channel frequency responses between each adjacent PL node pairs and between each PL node to the Sink. The frequency responses for an example PL network topology are shown in Fig. 4.11 and Fig. 4.12, respectively. Note that the PL node farthest to the Sink is denoted as the 1-st PL node.

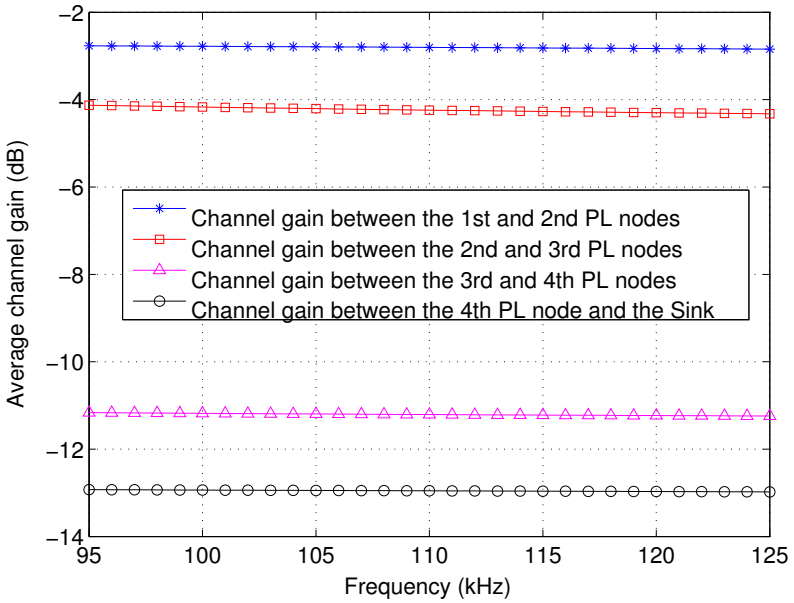

Figure 4.11: Average channel gain between two adjacent PL nodes

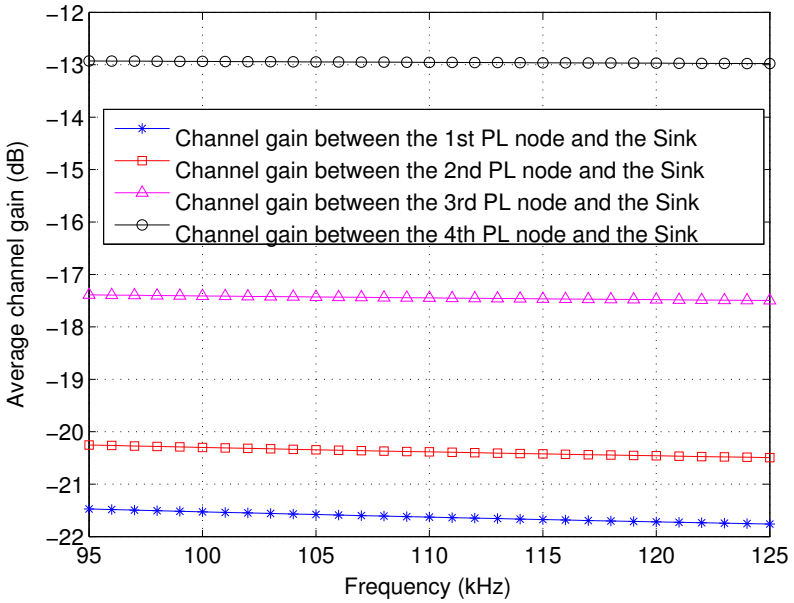

Figure 4.12: Average channel gain between each PL node and the Sink

Comparing Fig. 4.11 and Fig. 4.12, it can be noted that the PL channel between each PL node and the next PL node towards the Sink, in general, has a better channel performance than that between each PL node and the Sink node directly. This is mainly due to the fact that without intermediate PL nodes, the PL channel suffers from less path loss due to multi-path propagation effect and thus exhibits better channel performance. This is also valid when the PL nodes are placed at a larger distance (*e.g.,* 15 m) and thus provides larger network coverage. This fact supports the proposed transmission strategies that each PL node should relay their data to the PL node next to it. To simulate the achievable data rate for the PL links, the parameters shown in Table 4.2 is used. From extensive simulations, the maximum achievable data rate for the transmission of each PL node to the next PL node is between 100 kbps and 500 kbps depending on the channel conditions. Such a maximum achievable data rate is sufficient to support the data relaying for a small scale hybrid sensor network with low data arrival rate within given time period T.

4.6 Summary

In this chapter, a cross-layer design of a hybrid sensor network is proposed to maximize the network lifetime. The proposed system is suitable in situations where the wireless signal may not penetrate or in situations where wired communication infrastructure is a problem (*e.g.*, installing new communication systems in old facilities or the cost of installing wires for communication within refineries is very high due to safety requirements). Also, the optimal transmission scheme is obtained and the closed-form expression for the globally optimal solution for network lifetime maximization is derived for two network topologies. From the closed-form expressions, for both topologies, it is clear that the network lifetime of the hybrid network is only related to the initial battery capacity, the number of battery powered wireless nodes, and the data arrival rate. Further, in the string topology, the increase of the initial battery capacity will cause the network

lifetime to increase linearly, while the increase of the number of battery powered wireless nodes and the data arrival rate will result in the network lifetime to decrease exponentially. While the closed-form expression in the linear topology is complication, it facilities to sensor network system design by fast parameter fitting to investigate the relationship between the network lifetime and the related system parameters. It is also obvious that the optimal routing strategy in the string topology is single-path multihop routing and in the linear topology is multi-path multihop routing. Therefore, the proposed cross-layer optimization method may perform much better in the linear topology, since multi-path multihop routing in linear topology allows more design freedom.

The results show that the data arrival rate, the number of sensors, and the node separation distances have significant impact on the hybrid network in the string topology. In the linear topology, the hybrid sensor network enables a significant increase in the network lifetime over the pure WSN, especially with a relatively low data arrival rate. For example, in the linear topology, with 5 PL nodes in the hybrid network with a total of 12 sensors and a data arrival rate of 1 kbps, the network lifetime is prolonged by 8 times compared to a pure WSN with the same total number of sensors and with the same data arrival rate. Simulation results also validate the advantage of cross-layer optimization method over individual-layer optimization method on the linear topology. In addition, the simulation results reveal that the hybrid sensor network with a lower sensor node density exhibits a much longer network lifetime even when the same amount of data is collected in the linear topology. It can be concluded that closed-form expressions provide a useful guideline for the design of the sensor network. Also, the hybrid sensor network prolongs network lifetime mainly by increasing channel access time for each wireless link in the string topology while in the linear topology, it is achieved mainly by a combination of increasing channel access time and reducing transmission distance of the wireless link. By carefully setting the distance separation, data arrival rate and the sensor density in a hybrid network

with given number of PL nodes, the network lifetime can be maximized.

The network lifetime of the hybrid network in the linear topology is compared to a pure battery powered WSN with the same network configurations in this chapter, and the hybrid network has a much longer network lifetime. However, intuitively, in the pure wireless network, with the same number of total sensors as compared to the hybrid network, assuming that the wireless nodes that are placed at the same positions of the PL nodes in the corresponding hybrid network are mains powered. In this case, in the hybrid network, the transmission in the wireless link and in the PL link can occur concurrently. While in the wireless network, although the wireless nodes at the same positions of the PL nodes in the hybrid network are also mains powered, the transmission of these wireless nodes will interfere with the transmission of the wireless links of the battery powered wireless nodes. Since TDMA is considered in this chapter and concurrent transmission is not allowed in the same transmission medium, the transmission of the mains powered wireless nodes in the wireless network will have to share the transmission time frame with the battery powered wireless nodes. Therefore, each battery powered wireless node in the wireless network is allocated less transmission time as compared to the battery powered wireless node in the hybrid network, which consequently consumes more transmission power in order to achieve the required data arrival rate. While this is complicated to be analysed mathematically at the moment, or algorithms can be developed to solve the problem in this situation, this is left as a future work.

Chapter 5

Novel Hybrid Wireless-Power Line Video Sensor Networks with Distributed Cross-Layer Optimization

In Chapter 4, the optimality conditions (or KKT conditions) are used to derive the closed-form expression for the global optimal solutions for network lifetime maximization in the string topology and the linear topology. However, the hybrid sensor network proposed in Chapter 4 adopts the TDMA scheme to access the channel, which requires global synchronization. Therefore, when network scalability is considered, the hybrid sensor network proposed in Chapter 4 can only be in a small-scale. In addition, Chapter 4 mainly focuses on the general sensor network, where scalar information is collected. This has little requirement on the QoS and the data processing energy can often be neglected due to the low complexity of processing. In this chapter, a hybrid video sensor network (HVSN), which consists of both wireless nodes and PL nodes is proposed for network lifetime maximization through distributed solution by jointly considering video encoding rate, aggregate power consumption, channel access control, and link rate allocation. Nevertheless, it should be noted that network lifetime in chosen as a design criteria to demonstrate the performance improvement of the HVSN, and it can be readily modified to other design objectives.

Wireless video sensor networks (WVSNs), which are one of the high data

rate sensors (or multimedia sensor networks), are tasked to perform video capturing and processing and to deliver the processed video content to a remote control unit (or the sink node) via wireless channels for further information analysis and decision making [156]. Unlike standard mains powered WVSNs [157], battery-operated WVSNs may find widespread applications in fields such as impromptu surveillance installation and indoor elder care and home security due to the advantages of discreet and unobtrusive installation and removal. In addition, battery-operated WVSNs are immune to failure of the power distribution system. Several battery powered wireless cameras used for the purpose such as home security, baby monitoring and assisted living have been manufactured and marketed [158] [159].

In typical scenarios, battery-powered WVSNs are supposed to support high data rates and provide high-quality video, which necessitate a huge power consumption at the video sensor. Although battery replacement may be feasible in certain scenarios, replacing battery for a large number of video sensors regularly is cumbersome. Consequently, maintaining energy consumption at a low level is critical for WVSNs. This chapter therefore, focuses on improving the network lifetime through HVSN, which includes both hybrid wireless and PL video sensor nodes.

In [160], a distributed algorithm for maximizing the network lifetime of WVSNs is proposed based on the power-rate-distortion (P-R-D) model [161]. However, the channel capacity is assumed to be unlimited. The authors in [162] studied the optimization tradeoff between network lifetime and video distortion by jointly considering source/channel rate adaptation and network coding for an energy constrained WVSNs. A distributed algorithm is proposed in [163] to achieve optimal tradeoff between network lifetime and video distortion by joint design of coding and routing optimization in WVSNs with correlated sources. In [164], the authors studied the placement design of motion sensor and camera in order to maximize the network lifetime, in which the cameras are activated whenever

motion is detected.

Rate/channel adaptation has been proven as an effective means of enhancing the wireless network efficiency [165, 166]. In channel adaptation, the data being communicated are considered to be generic and, therefore, are generally encoded at the source with fixed rates [162]. However, it is difficult to fully utilize network resources with flexible channel adaptation together with predetermined source rate. When the instantaneous channel capacity fails to meet the predetermined source rate, network congestion would occur and could never be prevented by any rate adaptation scheme. On the contrary, the channel would be under-utilized. In [167], the authors investigated the nature of source data and proposed adaptive source encoding rates to satisfy the distortion constraints. However, the system they studied is a single-hop wireless system. In this work, a joint source/channel rate adaptation framework for multihop multipath video sensor network will be studied.

In this chapter, an HVSN that consists of both battery-powered wireless sensor nodes and PL sensor nodes to is proposed to maximize the network lifetime. This work is different in the following aspects. First, to the best of our knowledge, it is the first reported work to investigate video sensor networks with hybrid power sources and hybrid communication schemes. The proposed HVSN takes the advantage of the flexibility of wireless sensors while PL sensors are deployed to prolong the network lifetime. Second, the joint design of video encoding rate, aggregate power consumption, channel access control, along with link rate allocation is studied to maximize the hybrid network lifetime. The joint design achieves much better performance than separate optimization. Third, a distributed algorithm for the network lifetime maximization problem is proposed. The proposed distributed algorithm shares the computational burden among all nodes with much lower communication overhead. Fourth, the impact of dynamic network change and network scalability is studied.

The rest of this chapter is organized as follows. Section 5.1 describes the

system model. Section 5.2 formulates the optimization problem. In section 5.3, a distributed algorithm is proposed. Section 5.4 analyzes the numerical results. This chapter is summarised in section 5.5.

5.1 System Model

An HVSN that includes both wireless video sensor nodes and PL sensor nodes is studied, as depicted in Fig. 5.1. The wireless video sensor nodes are placed high above the room and perform video capturing, encoding, and routing. The PL sensor nodes simply perform as relay nodes to help to forward the video content collected by the wireless nodes to the sink node, which is the remote control unit acting as destinations of the HVSN. The PL nodes are assumed to be mounted with wireless receivers, such that they can receive wireless signals.

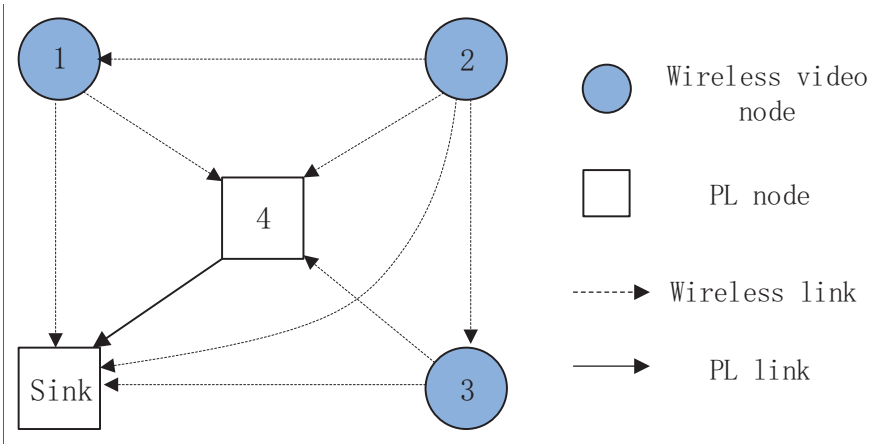

Figure 5.1: Topology of an example HVSN

Notations: The wireless nodes set is denoted by $\mathbb{W} = \{1, ..., |W|\}$ and the PL nodes set is indicated by $\mathbb{P} = \{1, ..., |P|\}$. S is used to denote the single sink node in the network. L_w is defined as the number of wireless links and L_p is the number of PL links. $\mathcal{L}_w$ and $\mathcal{L}_p$ are used to label all the wireless and PL links, such that $\mathcal{L}_w = \{1, ..., L_w\}$ and $\mathcal{L}_p = \{1, ..., L_p\}$. $l_w \in \mathcal{L}_w$ is the index used to denote the l-th wireless link and $l_p \in \mathcal{L}_p$ is used to represent the l-th PL link. $\mathcal{L} = \mathcal{L}_w \bigcup \mathcal{L}_p$ denotes all the links in the HVSN and $l \in \mathcal{L}$ indicates the l-th link,

which is from a transmitter node i to a receiver node j and is denoted by (i, j). Finally, $\mathcal{O}(i)$ and $\mathcal{I}(i)$ represent the set of outgoing and incoming links at node i, respectively.

5.1.1 Video Distortion Model

Unlike traditional WSNs, the video content captured by the video sensor network is first compressed locally before being injected into the channel for transmission. In video communication over lossy channels, the end-to-end distortion D is divided into two parts: 1) source coding distortion D_c caused by video compression and 2) transmission distortion D_t owing to channel errors. Since the encoding and transmission errors are generally uncorrelated [168], it follows that

$$D = D_c + D_t \tag{5.1}$$

in mean squared error (MSE). This model is widely used to estimate the end-to-end distortion in the literature [161, 162, 169]. For the distortion caused by video compression, an analytic P-R-D model is established in [161], which relates the encoding rate $R^{(i)}$, power consumption due to video encoding $P_c^{(i)}$, and the distortion caused by video compression $D_c^{(i)}$ for each wireless node i as

$$D_c^{(i)} = \sigma^2 e^{-\gamma \cdot R^{(i)} \cdot \left(P_c^{(i)}\right)^{2/3}} \tag{5.2}$$

where γ is a factor related to the encoding efficiency, and σ^2 represents the average input variance. Here, the distortion caused by video compression $D_c^{(i)}$ is defined as the distortion of the video quality by comparing the video content after compression to the original one, and is often measured by MSE.

Fig. 5.2 shows the encoding distortion D_c, measured in MSE, as a function of source rate after compression, R and encoding power P_c. Apparently, a target encoding distortion is achievable by adjusting either the encoding power or the source rate. If the encoding power P_c or the source rate after compression R is decreased, then the encoding distortion D_c increases for lacking enough power for compression. On the other hand, with the increase of encoding power P_c, the

transmission power will consequently decrease, which also results in the increase of the distortion D_c. Therefore, an allocation of R and P_c should be balanced to save the power consumption and adjust the video distortion.

Since the source rate shown in Fig. 5.2 is the source rate after compression. Assuming that the source rate of the original video content is 5 Mbps and the encoding distortion is fixed, in the first case, the video content is compressed to the source rate R of 2 Mbps, and in the second case, the video content is compressed to the source rate R of 1 Mbps. Apparently, compressing the original video content from 5 Mbps to 1 Mbps would consume more power as compared to the case that compressing the original video content from 5 Mbps to 2 Mbps. Therefore, less power consumption is needed for a higher source rate after compression.

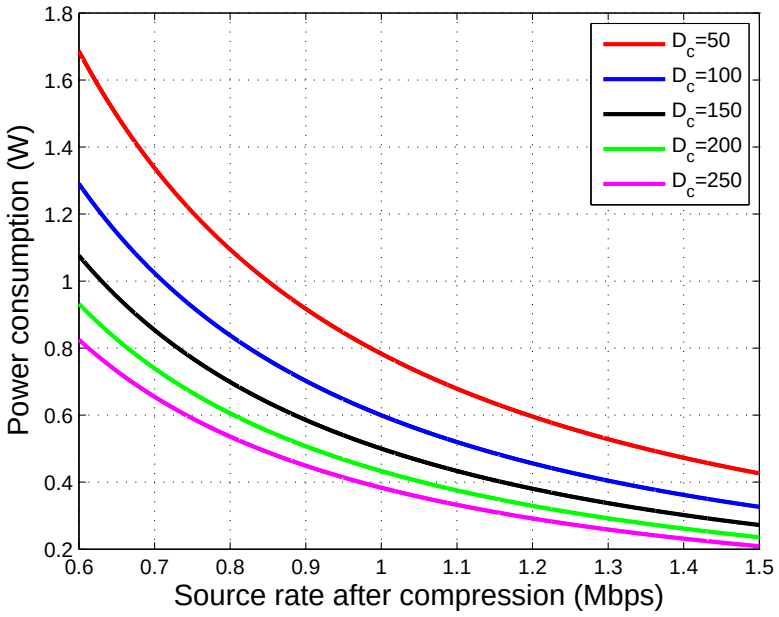

Figure 5.2: Relationship of video encoding power, compressed source rate, and distortion

On the other hand, for the distortion caused by transmission, it is shown in [170] that after a certain threshold of BER is achieved, the video quality would not increase significantly with further decrease in BER. Fig. 5.3 demonstrates that there is very little or no improvement on the structural similarity (SSIM) quality measurement [170] of the received video for BER up to 10^{-4} for H. 264

or for 10^{-3} for compressive video sensing (CVS). This indicates that, although channel conditions are rather variable, the distortion can be neglected with a proper target BER value.

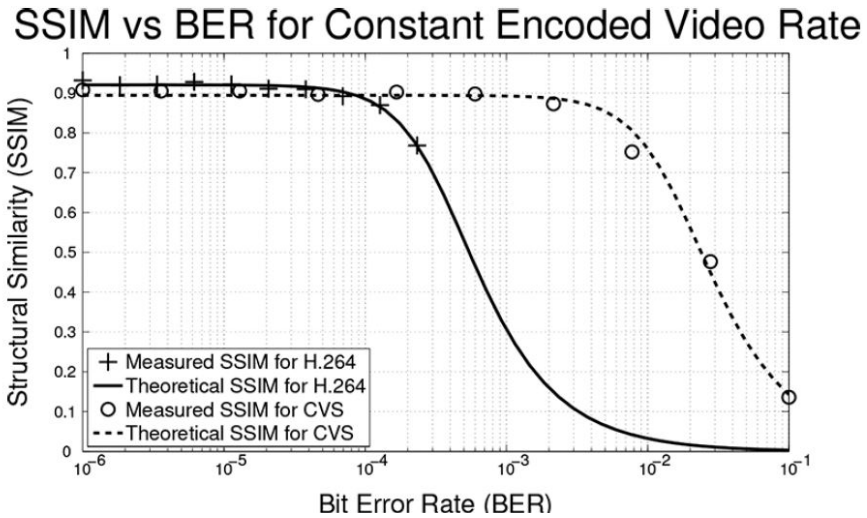

Figure 5.3: SSIM vs BER for H.264 and CVS encoders [170]

5.1.2 Channel Access Model

A widely adopted MAC protocol in sensor networks is the contention-based MAC protocol [171, 172]. In this chapter, the p-persistent contention based MAC protocol is used. In such a protocol [171, 172], each node i has a certain persistence probability P_i to compete for channel access. It is assumed that time is split into intervals and the transmission of the node begins at the start of each interval. If node i is ready for transmission, it picks a link $l \in \mathcal{O}(i)$ (*i.e.*, $(i,j) \in \mathcal{O}(i)$) out of all its outgoing wireless or PL links with probability q_l, and competes to access the channel with persistence probability P_i. Hence, link $l \in \mathcal{O}(i)$ has a transmission attempt probability $p_l = q_l \cdot P_i$, where $\sum_{l \in \mathcal{O}(i)} q_l = 1$. Therefore, the persistence probability is

$$P_i = \sum\nolimits_{l \in \mathcal{O}(i)} p_l \tag{5.3}$$

where $0 \leq p_l \leq 1, \forall l \in \mathcal{L}$, and $0 \leq P_i \leq 1, \forall i \in \mathbb{W} \bigcup \mathbb{P}$.

In continuous video acquiring applications, assuming the packet loss probability through link l is ε_l, the success probability for packet transmission can be

expressed as

$$\tau_l = (1 - \varepsilon_l) \cdot p_l \cdot \prod_{k \in N_l^I} (1 - P_k) \tag{5.4}$$

where N_l^I is the set of nodes whose transmissions introduces interferences to the end node of link l. For wireless links, it is assumed that any outgoing link of node m interferes with link (i, j) if $d_{(m,j)} < (1 + \Phi) \cdot d_{(i,j)}$, where $\Phi \geq 0$ represents the range of interference. The average throughput of link l can thus be defined as

$$c_l = C_l^0 \cdot \tau_l \tag{5.5}$$

where C_l^0 is the maximum rate support by the channel at link l. In addition, the information flow rate f_l on link l is limited by the link capacity, as

$$f_l \leq c_l, \forall l \in \mathcal{L} \tag{5.6}$$

In order to obtain the maximum transmission rate C_l^0, the ITU indoor path loss model [173] is used for the wireless links, as

$$G_l = 20 \cdot \log_{10}(f) + 10 \cdot n \cdot \log_{10}(d_l) + Lf(n) - 28dB \tag{5.7}$$

where f is the transmission frequency in MHz, n is the path loss exponent, d_l is the transmission range in m and $Lf(n) = 0$ for same floor transmission. For PL links, the random PLC channel generator [174] is used to determine the channel gain, G_l.

As in Chapter 4, MQAM is assumed in this chapter. Also, assuming the noise in both links is additive white Gaussian noise with power spectral density N_l. Then, with the corresponding transmission power $\overline{p}_l$ and transmission bandwidth B_l, the instantaneous transmission rate is determined as [74]

$$C_l^0 = B_l \cdot log_2(1 + \frac{K \cdot G_l \cdot \overline{p}_l}{N_l \cdot B_l}) \tag{5.8}$$

where $K = -1.5/\ln(5 \cdot BER)$ is the maximum possible coding gain given a target BER, BER, for modulation schemes such as MQAM [147].

5.1.3 Flow Conservation Constraint

In this chapter, each wireless node is tasked to capture and compress video that should be delivered to a single destination. Then the video traffic is generated with a source rate $R^{(i)}$ in each node i, which can be obtained from (5.2). Note that $R^{(i)} = 0$ for all PL nodes, that is, $\forall i \in \mathbb{P}$. Since the PL nodes perform as relay nodes. For the sink node, the source rate is defined as $R^{(S)} = -\sum_{i \in \mathbb{W}} R^{(i)}$. Therefore, for each node i, the following constraint holds,

$$\sum\nolimits_{l \in \mathcal{I}(i)} f_l + R^{(i)} = \sum\nolimits_{l \in \mathcal{O}(i)} f_l, \forall i \in \mathbb{W} \bigcup \mathbb{P} \tag{5.9}$$

where f_l is the information flow rate on link l. The flow conservation law simply states that for each node, the outgoing information flow rate should be equal to the incoming information flow rate plus the data rate generated locally.

5.1.4 Energy Consumption Model

In the HVSN, the energy consumption of the wireless nodes are of interest since the battery capacity of these nodes limits the network lifetime. In this chapter, the total power consumption of a wireless node is caused by video encoding, data transmission and reception.

The power consumption due to video compression can be calculated by the P-R-D model, as in (5.2). According to the power consumption model widely adopted in WVSNs [162, 163], the power consumption caused by transmission at wireless node i is expressed as

$$P_t^{(i)} = \sum\nolimits_{l \in \mathcal{O}(i)} (\alpha + \beta \cdot d_l^n) \cdot \frac{f_l}{\tau_l} \tag{5.10}$$

where f_l is the rate assigned on link l, τ_l is the probability for a successful packet transmission of link l, $\frac{f_l}{\tau_l}$ is the actual rate transmitted through link l. α denotes the energy cost of the transmit electronics, β represents a coefficient relating to the energy cost of the transmit amplifier, d_l is the transmission range of link l, and n is the path-loss exponent [74].

The data reception power consumption at node i is

$$P_r^{(i)} = c^r \cdot \sum\nolimits_{l \in \mathcal{I}(i)} \frac{f_l}{\tau_l} \tag{5.11}$$

where c^r is the energy consumption cost of the radio receiver and $\sum_{l \in \mathcal{I}(i)} \frac{f_l}{\tau_l}$ is the actual aggregate rate transmitted to node i.

Therefore, the overall power consumption at wireless node i can be expressed as

$$P^{(i)} = \left[\frac{1}{\gamma \cdot R^{(i)}} \cdot \ln \left(\frac{\sigma^2}{D_c^{(i)}} \right) \right]^{\frac{3}{2}} + P_t^{(i)} + P_r^{(i)} \tag{5.12}$$

5.1.5 Network Lifetime

The network lifetime is considered as the duration from the beginning of the network till the first wireless node running out of energy. In the HVSN, the battery capacity of each node $i \in \mathbb{W}$ is denoted as $E^{(i)}$. Therefore, the lifetime of each node i is

$$T_i = \frac{E^{(i)}}{P^{(i)}}, \forall i \in \mathbb{W} \tag{5.13}$$

Hence, the network lifetime is

$$T_{net} = \min_{i \in \mathbb{W}} \{T_i\} = \min_{i \in \mathbb{W}} \{\frac{E^{(i)}}{P^{(i)}}\} \tag{5.14}$$

5.2 Problem Formulation

The problem under study in this chapter can be described as follows: with a pre-determined static topology of a HVSN, the instantaneous transmission rate on each link and the battery capacity of each wireless node, to maximize the network lifetime by joint optimization of the video encoding rate, the encoding power, and the routing decision as well as the channel contention resolution on each link, subject to the pre-defined video quality should be satisfied. Mathematically, the problem can be formulated as:

$$\mathbf{P1}: \quad \max_{(\mathbf{f},\mathbf{R},\mathbf{p},\mathbf{T})} \quad [\min\nolimits_{i \in \mathbb{W}} \{T_i\}] \tag{5.15}$$

$$\text{s.t.} \quad \sigma^2 e^{-\gamma \cdot R^{(i)} \cdot \left(P_c^{(i)}\right)^{2/3}} \leq D_c^{(i)}, \quad \forall i \in \mathbb{W} \tag{5.16}$$

$$\frac{E^{(i)}}{T_i} = P_c^{(i)} + \sum\nolimits_{l \in \mathcal{O}(i)} (\alpha + \beta \cdot d_l^n) \cdot \frac{f_l}{\tau_l} + c^r \cdot \sum\nolimits_{l \in \mathcal{I}(i)} \frac{f_l}{\tau_l}, \quad \forall i \in \mathbb{W} \tag{5.17}$$

$$0 \leq p_l \leq 1, \quad \forall l \in \mathcal{L} \tag{5.18}$$

$$0 \leq P_i \leq 1, \quad \forall i \in \mathbb{W} \bigcup \mathbb{P} \tag{5.19}$$

$$f_l \geq 0, \quad \forall l \in \mathcal{L} \tag{5.20}$$

$$R^{(i)} \geq 0, \quad \forall i \in \mathbb{W} \tag{5.21}$$

along with (5.3) - (5.6) and (5.9). Constraint (5.16) represents that the encoding distortion should not exceed the corresponding upper bound on each wireless node. Constraint (5.17) reflects the power consumption of each wireless video sensor node. By observation, variables $P_c^{(i)}$, τ_l and P_i are dummy variables since these can be determined in expressions of other variables. Hence, the optimization variables in **P1** are $f_l, R^{(i)}$, p_l and T_i.

5.3 Optimization Approach and Distributed Algorithm

The problem in **P1** is not convex due to non-linearity in constraints (5.4) and (5.17). In order to convert the problem to a convex problem, constraint (5.4) can be reformulated by taking the logarithm on both sides. Also, variable $q_i = 1/T_i$ is introduced in (5.17) as node i's normalized power consumption regarding to its battery capacity $E^{(i)}$. Hence, the objective function becomes

$$\max(\min_{i \in \mathbb{W}}\{T_i\}) = \min(\max_{i \in \mathbb{W}}\{q_i\})$$

In addition, (5.16) is simplified by taking the logarithm on both sides. Further, $F_l = f_l/\tau_l$ is introduced as the total aggregated data flow rate on each link.

The objective function, $\max_{i \in \mathbb{W}}\{q_i\}$, however, is non-differentiable and needs all sensor nodes' information. Hence, it is difficult to develop a fully distributed algorithm to solve the problem. One solution is to introduce $q_i = q_j$ as the constraints, and the objective function is equivalent to $\sum_{i \in \mathbb{W}} q_i^2$.

Therefore, the optimization problem in **P1** becomes

$$\mathbf{P2}: \quad \min_{(\mathbf{F},\mathbf{R},\mathbf{p},\mathbf{q})} \quad \sum_{i\in\mathbb{W}} q_i^2 \tag{5.22}$$

$$\text{s.t.} \quad \sum\nolimits_{l\in\mathcal{O}(i)} F_l\cdot\tau_l - \sum\nolimits_{l\in\mathcal{I}(i)} F_l\cdot\tau_l = R^{(i)}, \forall i\in\mathbb{W}\bigcup\mathbb{P} \tag{5.23}$$

$$\frac{1}{\gamma\cdot\left(P_c^{(i)}\right)^{2/3}}\cdot\ln\left(\frac{\sigma^2}{D_c^{(i)}}\right)\le R^{(i)}, \quad \forall i\in\mathbb{W} \tag{5.24}$$

$$F_l\le C_l^0, \quad \forall l\in\mathcal{L} \tag{5.25}$$

$$E^{(i)}\cdot q_i = P_c^{(i)} + \sum\nolimits_{l\in\mathcal{O}(i)}(\alpha+\beta\cdot d_l^n)\cdot F_l + c^r\cdot\sum\nolimits_{l\in\mathcal{I}(i)} F_l, \quad \forall i\in\mathbb{W} \tag{5.26}$$

$$\ln\tau_l = \ln(1-\varepsilon_l)\cdot p_l + \sum\nolimits_{k\in N_l^I}\ln(1-P_k), \quad \forall l\in\mathcal{L} \tag{5.27}$$

$$P_i = \sum\nolimits_{l\in\mathcal{O}(i)} p_l, \quad \forall l\in\mathcal{L} \tag{5.28}$$

$$F_l\ge 0, \quad \forall l\in\mathcal{L} \tag{5.29}$$

$$0\le p_l\le 1, \quad \forall l\in\mathcal{L} \tag{5.30}$$

$$0\le P_i\le 1, \quad \forall i\in\mathbb{W}\bigcup\mathbb{P} \tag{5.31}$$

$$R^{(i)}\ge 0, \quad \forall i\in\mathbb{W} \tag{5.32}$$

$$q_i = q_j, \quad \forall i,j\in\mathbb{W} \tag{5.33}$$

The optimization variables are $F_l, R^{(i)}$, p_l and q_i. In **P2**, it can be proved that the objective function is strictly convex, the equality constraints are affine, and the inequality constraints are convex. Hence, **P2** is a convex optimization problem [114].

To develop a distributed algorithm for **P2**, the primal decomposition method [52] is used regarding the coupling variable F_l, which results in a two-level optimization problem. At the lower level, there is

$$\mathbf{P2-a}: \quad \min_{(\mathbf{R},\mathbf{p},\mathbf{q})} \quad \sum_{i\in\mathbb{W}} q_i^2 \tag{5.34}$$

$$s.t. \quad \sum\nolimits_{l\in\mathcal{O}(i)} F_l\cdot\tau_l - \sum\nolimits_{l\in\mathcal{I}(i)} F_l\cdot\tau_l = R^{(i)}, \quad \forall i\in\mathbb{W}\bigcup\mathbb{P} \tag{5.35}$$

$$\frac{1}{\gamma\cdot\left(P_c^{(i)}\right)^{2/3}}\cdot\ln\left(\frac{\sigma^2}{D_c^{(i)}}\right)\le R^{(i)}, \quad \forall i\in\mathbb{W} \tag{5.36}$$

$$E^{(i)} \cdot q_i = P_c^{(i)} + \sum\nolimits_{l \in \mathcal{O}(i)} (\alpha + \beta \cdot d_l^n) \cdot F_l + c^r \cdot \sum\nolimits_{l \in \mathcal{I}(i)} F_l \quad (5.37)$$

$$\ln \tau_l = \ln(1 - \varepsilon_l) \cdot p_l + \sum\nolimits_{k \in N_l^I} \ln(1 - P_k), \quad \forall l \in \mathcal{L} \quad (5.38)$$

$$P_i = \sum\nolimits_{l \in \mathcal{O}(i)} p_l, \quad \forall l \in \mathcal{L} \quad (5.39)$$

$$0 \leq p_l \leq 1, \quad \forall l \in \mathcal{L} \quad (5.40)$$

$$0 \leq P_i \leq 1, \quad \forall i \in \mathbb{W} \bigcup \mathbb{P} \quad (5.41)$$

$$R^{(i)} \geq 0, \quad \forall i \in \mathbb{W} \quad (5.42)$$

$$q_i = q_j, \quad \forall i, j \in \mathbb{W} \quad (5.43)$$

and at the higher level, it gives

$$\mathbf{P2-b}: \quad \min_{(\mathbf{F})} \quad U^*(\mathbf{F}) \quad (5.44)$$

$$s.t. \quad F_l \leq C_l^0, \quad \forall l \in \mathcal{L} \quad (5.45)$$

$$F_l \geq 0, \quad \forall l \in \mathcal{L} \quad (5.46)$$

$\mathbf{P2-a}$ performs a low-level optimization when the coupling variable $F_l = f_l/\tau_l$ is fixed, while $\mathbf{P2-b}$ performs a high-level optimization to update F_l. $U^*(F)$ is the optimal value of the objective function in $\mathbf{P2-a}$ for given variables, F_l. The output of the low-level optimization is locally optimal and provides an approximation to the global optimal solution using the result of the high-level optimization.

5.3.1 Low-Level Optimization

To solve the low-level optimization in problem $\mathbf{P2-a}$, the constraints (5.35), (5.36) and (5.43) in $\mathbf{P2-a}$ are relaxed, which yield the following Lagrangian [114]:

$$\begin{aligned}\mathbf{L}(\lambda, \theta, \nu, \mathbf{R}, \mathbf{p}, \mathbf{q}) =& \sum_{i \in \mathbb{W}} q_i^2 + \sum_{i \in \mathbb{W} \bigcup \mathbb{P}} \lambda_i \cdot (\sum\nolimits_{l \in \mathcal{O}(i)} F_l \cdot \tau_l - \sum\nolimits_{l \in \mathcal{I}(i)} F_l \cdot \tau_l - R^{(i)}) \\ &+ \sum_{i \in \mathbb{W}} \theta_i \cdot [\frac{1}{\gamma \cdot (P_c^{(i)})^{2/3}} \cdot \ln(\frac{\sigma^2}{D_c^{(i)}}) - R^{(i)}] \\ &+ \sum_{l \in \mathcal{L}_w} \nu_l \cdot (q_i - q_j)\end{aligned} \quad (5.47)$$

where λ, θ and ν are the Lagrange multipliers corresponding to constraints (5.35), (5.36) and (5.43), respectively. In addition, the corresponding Lagrange dual

function is

$$\begin{aligned} g(\lambda,\theta,\nu) &= \inf_{(\mathbf{R},\mathbf{p},\mathbf{q})} \mathbf{L}(\lambda,\theta,\nu,\mathbf{R},\mathbf{p},\mathbf{q}) \\ s.t. \quad &\text{Constraints (5.37) - (5.42) in} \quad \mathbf{P2-a} \end{aligned} \tag{5.48}$$

The Lagrange dual problem of $\mathbf{P2-a}$ is then defined as

$$\begin{aligned} \mathbf{P2-a-1}: \quad &\max \quad g(\lambda,\theta,\nu) \\ &s.t. \quad \theta_i \geq 0, \quad \forall i \in \mathbb{W} \end{aligned} \tag{5.49}$$

The corresponding Lagrange multipliers can be solved with the subgradient method as

$$\lambda_i(n_L+1) = \lambda_i(n_L) + \omega(n_L)\cdot(\sum\nolimits_{l\in\mathcal{O}(i)} F_l\cdot\tau_l - \sum\nolimits_{l\in\mathcal{I}(i)} F_l\cdot\tau_l - R^{(i)}) \tag{5.50}$$

$$\theta_i(n_L+1) = \{\theta_i(n_L) + \omega(n_L)\cdot[\frac{1}{\gamma\cdot\left(P_c^{(i)}\right)^{2/3}}\cdot\ln(\frac{\sigma^2}{D_c^{(i)}}) - R^{(i)}]\}^+ \tag{5.51}$$

$$\nu_l(n_L+1) = \nu_l(n_L) + \omega(n_L)\cdot(q_{\mathcal{O}^{-1}(l)} - q_{\mathcal{I}^{-1}(l)}) \tag{5.52}$$

where n_L represents the low-level iteration index, $\{\cdot\}^+$ denotes the projection onto the set of nonnegative real numbers, and $\omega(n_L)$ is a positive step size in low-level optimization problems. $\mathcal{I}^{-1}(l)$ denotes the node associated with the incoming link l, $\mathcal{O}^{-1}(l)$ denotes the node associated with the outgoing link l.

According to convex optimization theorem [52], if the original problem $\mathbf{P2-a}$ is convex, it is equivalent to its Lagrange dual problem in (5.49). Then, the low-level optimization problem $\mathbf{P2-a}$ can be further decomposed into a set of subproblems $\mathbf{P2-a-2}$ to $\mathbf{P2-a-4}$ that can be solved in a distributed manner,

$$\begin{aligned} \mathbf{P2-a-2}: \quad &\min \quad \sum_{i\in\mathbb{W}} q_i^2 + \sum_{i\in\mathbb{W}} \theta_i\cdot[\frac{1}{\gamma\cdot\left(P_c^{(i)}\right)^{2/3}}\cdot\ln(\frac{\sigma^2}{D_c^{(i)}})] + \sum_{l\in\mathcal{L}_w}\nu_l\cdot(q_i-q_j) \\ &s.t. \quad (5.37) \end{aligned}$$

$$\begin{aligned} \mathbf{P2-a-3}: \quad &\min \quad -\sum_{i\in\mathbb{W}} \lambda_i\cdot R^{(i)} - \sum_{i\in\mathbb{W}} \theta_i\cdot R^{(i)} \\ &s.t. \quad (5.42) \end{aligned}$$

$$\mathbf{P2-a-4}: \quad \min \sum_{i\in\mathbb{W}\bigcup\mathbb{P}} \lambda_i \cdot (\sum\nolimits_{l\in\mathcal{O}(i)} F_l \cdot \tau_l - \sum\nolimits_{l\in\mathcal{I}(i)} F_l \cdot \tau_l)$$
$$s.t. \quad (5.38)-(5.41)$$

Subproblem $\mathbf{P2-a-2}$ is the energy conservation in wireless sensor nodes taking into account impacts both from the MAC layer and the network layer. Subproblem $\mathbf{P2-a-3}$ is the source rate control problem at the application layer. Subproblem $\mathbf{P2-a-4}$ is the channel contention resolution problem at the MAC layer. These three problems are solved separately and coordinated by Lagrange multipliers λ, θ and ν.

Energy conservation problem (application layer): The variable q_i in $\mathbf{P2-a-2}$ can be solved using the subgradient algorithm as

$$\begin{aligned} q_i(n_L+1) &= \{q_i(n_L) - \omega(n_L)\cdot \frac{\partial \mathbf{L}(\lambda,\theta,\nu,\mathbf{R},\mathbf{p},\mathbf{q})}{\partial q_i}\}^+ \\ &= \{q_i(n_L) - \omega(n_L)\cdot [2\cdot q_i - \frac{2}{3}\cdot\theta_i\cdot\frac{\ln(\frac{\sigma^2}{D_c^{(i)}})}{\gamma}\cdot (P_c^{(i)})^{-5/3}\cdot E^{(i)} \\ &\quad + (\sum\nolimits_{l\in\mathcal{O}(i)}\nu_l - \sum\nolimits_{l\in\mathcal{I}(i)}\nu_l)]\}^+ \end{aligned} \tag{5.53}$$

where $P_c^{(i)}$ can be obtained as

$$P_c^{(i)} = E^{(i)}\cdot q_i - \sum\nolimits_{l\in\mathcal{O}(i)}(\alpha+\beta\cdot d_l^n)\cdot F_l - c^r\cdot\sum\nolimits_{l\in\mathcal{I}(i)} F_l \tag{5.54}$$

The energy conservation at each wireless node i is achieved by adjusting the value of F_l and q_i, with θ_i working as the energy consumption price, and ν_l as the energy balancing price.

Source rate control problem (application layer): The variable $R^{(i)}$ can be updated using the subgradient algorithm as

$$\begin{aligned} R_i(n_L+1) &= \{R_i(n_L) - \omega(n_L)\cdot\frac{\partial \mathbf{L}(\lambda,\theta,\nu,\mathbf{R},\mathbf{p},\mathbf{q})}{\partial R_i}\}^+ \\ &= \{R_i(n_L) - \omega(n_L)\cdot(-\lambda_i-\theta_i)\}^+ \end{aligned} \tag{5.55}$$

Channel contention resolution problem (MAC layer): The channel contention resolution problem aims to find the optimal transmission persistence probabilities of the links under given variable F_l and price λ_i. Its problem formulation is similar to that in [171]. Hence, the same algorithm can be used in

which defining

$$\mu_i = \sum\nolimits_{l\in\mathcal{O}(i)} F_l \cdot (\lambda_{\mathcal{I}^{-1}(l)} - \lambda_{\mathcal{O}^{-1}(l)}) + \sum\nolimits_{k\in L^{\mathcal{I}}(i)} F_k \cdot (\lambda_{\mathcal{I}^{-1}(k)} - \lambda_{\mathcal{O}^{-1}(k)}) \quad (5.56)$$

where $L^{\mathcal{I}}(i)$ represents the set of links whose transmission get interfered from the transmission of node i, excluding outgoing links from node i. Then the transmission attempt probability of the link l is

$$p_l = \begin{cases} \frac{F_l\cdot(\lambda_{\mathcal{I}^{-1}(l)} - \lambda_{\mathcal{O}^{-1}(l)})}{\mu_i} & , \quad \mu_i \neq 0 \\ \frac{1}{|\mathcal{O}(i)|+|L^{\mathcal{I}}(i)|} & , \quad \mu_i = 0 \end{cases} \quad (5.57)$$

5.3.2 High-Level Optimization

The high-level optimization problem aims to find the routing and link rate allocation, which is in the network layer. Suppose $\hat{\tau}_l$, $\hat{\lambda}_{O^{-1}(l)}$ and $\hat{\lambda}_{I^{-1}(l)}$ are the optimal variable and Lagrange price corresponding to (5.35) in problem $\mathbf{P2-a}$. The optimization approach proceeds as taking a dual decomposition with respect to (5.45) in problem $\mathbf{P2-b}$ and thus formulating the Lagrangian as

$$\mathbf{L}'(\varphi, \mathbf{F}) = U^*(\mathbf{F}) + \sum_{l\in\mathcal{L}} \varphi_l (F_l - C_l^0) \quad (5.58)$$

where φ is the Lagrangian multiplier. The optimal value of F_l can be found by the subgradient algorithm

$$\begin{aligned} F_l(n_H+1) &= \{F_l(n_H) - \varpi(n_H)\cdot \frac{\partial \mathbf{L}'(\varphi,\mathbf{F})}{\partial F_l}\}^+ \\ &= \{F_l(n_H) - \varpi(n_H)\cdot(\hat{\tau}_l\cdot(\hat{\lambda}_{\mathcal{O}^{-1}(l)} - \hat{\lambda}_{\mathcal{I}^{-1}(l)}) + \varphi_l)\}^+ \end{aligned} \quad (5.59)$$

and the corresponding Lagrangian dual variable is updated as

$$\varphi_l(n_H+1) = \{\varphi_l(n_H) + \varpi(n_H)\cdot(F_l - C_l^0)\}^+ \quad (5.60)$$

where n_H denotes the high level iteration index, and $\varpi(n_H)$ is the positive step size of the high level optimization problem.

5.3.3 Summary of the Distributed Algorithm

The distributed implementation of the proposed two-level iterative algorithm is summarized in Algorithm 1. In Algorithm 1, each link $l = (i, j)$ is delegated to its

Algorithm 1 Distributed two-level optimization algorithm

Initialization

• Set $n_L = 1$ and $n_H = 1$

• Initialize optimization variables q_i, $R^{(i)}$, θ_i, $\forall i \in \mathbb{W}$, and λ_i, $\forall i \in \mathbb{W} \bigcup \mathbb{P}$, ν_i, $\forall i \in \mathbb{W}$ and p_l, F_l, φ_l, $\forall l \in \mathcal{L}$ with, e.g., zeros.

repeat

I. **Low-level implementation**

a) Update at each wireless node, $\forall i \in \mathbb{W}$

1) Update $\theta_i(n_L)$, $\nu_l(n_L)$, $q_i(n_L)$ and $R^{(i)}(n_L)$ according to (5.51), (5.52), (5.53) and (5.55), respectively.

2) Communicate the updated dual variable $\nu_i(n_L+1)$ to the end nodes of incoming links $l \in \mathcal{I}(i)$.

b) Update at each wireless and PL node, $\forall i \in \mathbb{W} \bigcup \mathbb{P}$

1) Update $\lambda_i(n_L)$ according to (5.50).

2) Communicate the updated dual variable $\lambda_i(n_L+1)$ to the end nodes of incoming links $l \in \mathcal{I}(i)$.

c) Update at each wireless and PL link, $\forall l \in \mathcal{L}$

1) Update $p_l(n_L)$ according to (5.57).

II. **High-level implementation**

a) Update at each wireless and PL link, $\forall l \in \mathcal{L}$

1) Update $F_l(n_H)$ and $\varphi_l(n_H)$ according to (5.59) and (5.60), respectively.

2) Communicate the updated actual transmission rate $F_l(n_H + 1)$ to the corresponding end nodes of outgoing links $l \in \mathcal{O}(i)$.

until All variables converge to the optimums.

sender node i, and all computations related to that link will be executed on node i. It can be seen that the communication overhead at each iteration consists of conveying $\lambda_i(n_L+1)$, $\nu_i(n_L+1)$ and $F_l(n_H+1)$ to the corresponding nodes. Thus compared to the main stream of video transmission traffic, the communication overhead introduced by such information exchange is quite small.

The proposed distributed algorithm needs to be implemented whenever the initial network starts monitoring or the dynamic change of network condition suddenly happens, to catch up with the optimal network lifetime for the network.

5.4 Numerical Results

Table 5.1: Configuration of Model Parameters in the HVSN

Parameter	Description	Value
σ^2	Average input variance of the video in MSE	3500
γ	Encoding efficiency coefficient	5 $W^{3/2}/Mb/s$
α	Energy cost of the transmit electronics	0.2 J/Mb
β	Coefficient term of the transmit amplifier	1.3×10^{-8} $J/Mb/m^4$
c^r	Energy consumption cost of the radio receiver	0.1 J/Mb
$E^{(i)}$	The initial energy at wireless node i	2 MJ
f_w	Radio frequency	900 MHz
$\overline{p}_{l_w}$	Transmission power of wireless link	0.5 W
$\overline{B}_{l_w}$	Transmission bandwidth of wireless link	1 MHz
N_{l_w}	Noise PSD level of wireless link	-131 dBm/Hz
BER	Target BER	10^{-4}
n	Wireless path loss exponent	4
ε_l	Packet loss rate at link l	0.1

In this section, the overall performance of the proposed distributed algorithm will be evaluated. The topology used for the HVSN is a square area of 20 m $\times$ 20 m where 8 nodes are randomly placed (including the sink node, as shown in Fig. 5.4). Without lose of generality, the node located at position (0, 0) is considered to be the sink node. For performance comparison, two WVSN topologies are considered: a) same as HVSN except that all nodes are wireless nodes, b) same

as the topology in a) except that PL nodes are removed. In the following, the topologies in a) and b) are referred to as 8-node and 6-node WVSNs, respectively. Numerically, the values of all the related model parameters are listed in Table 5.1. Also, the upper bound of the encoding distortion $D_c^{(i)}$ in MSE is set to 100 if not specified otherwise. For PL links, the random PLC channel generator [174] is used to determine the channel gain. BB PLC with a total bandwidth of 26 MHz consisting 917 subcarriers is considered. Each PL node is allocated with 5 subcarriers. The transmission power of PL link is -50 dBm/Hz and the noise PSD level is -120 dBm/Hz. A fixed step-size of 0.01 is used.

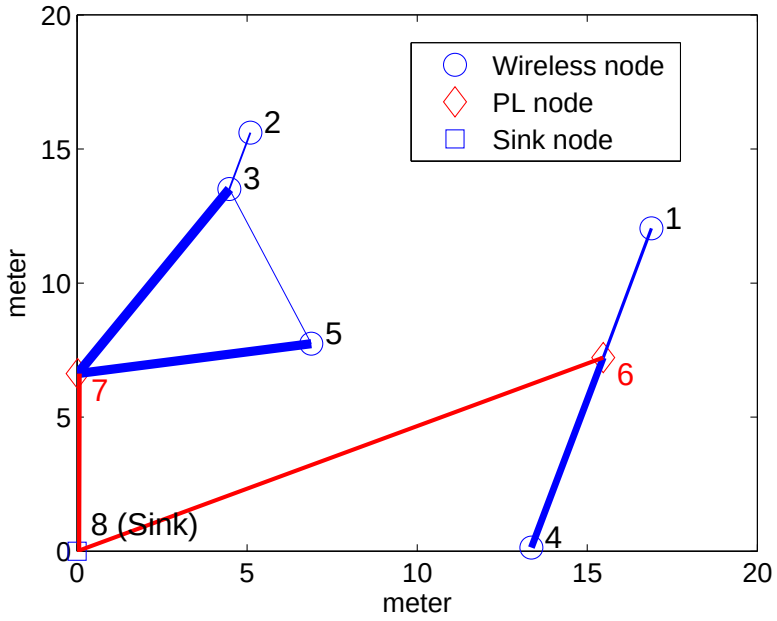

Figure 5.4: Randomly generated topology of HVSN with illustration of aggregate link rates (blue line indicates a wireless link, red line represents a PL link, the thickness of the line is proportional to the aggregate link rate)

Fig. 5.5, Fig. 5.6 and Fig. 5.7 show the convergence behaviour of the proposed distributed algorithm with the illustrations of iterations of node lifetime, source rate and link transmission attempt probabilities, respectively based on the topology shown in Fig. 5.4. It can be observed that these variables converge to the optimum value within 220 iterations. Therefore, the proposed algorithm can converge to the steady state in a relatively short period of time. Also, Fig. 5.5

depicts that the node lifetime of each node in the network can achieve a common node lifetime in the steady state. The proposed distributed algorithm allows each node to exchange its local information about node lifetime with its neighbouring nodes and thus can effectively balance the energy consumption among all nodes.

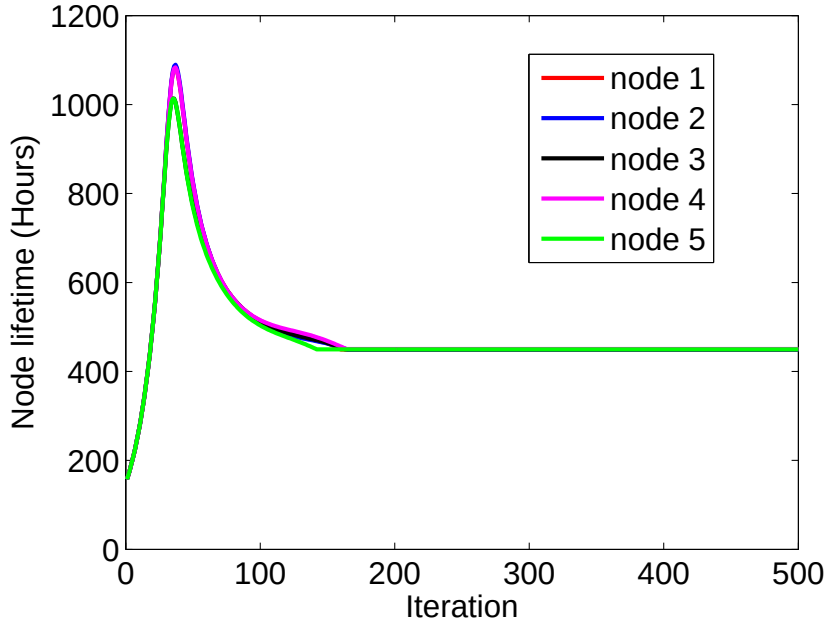

Figure 5.5: Iterations of node lifetime

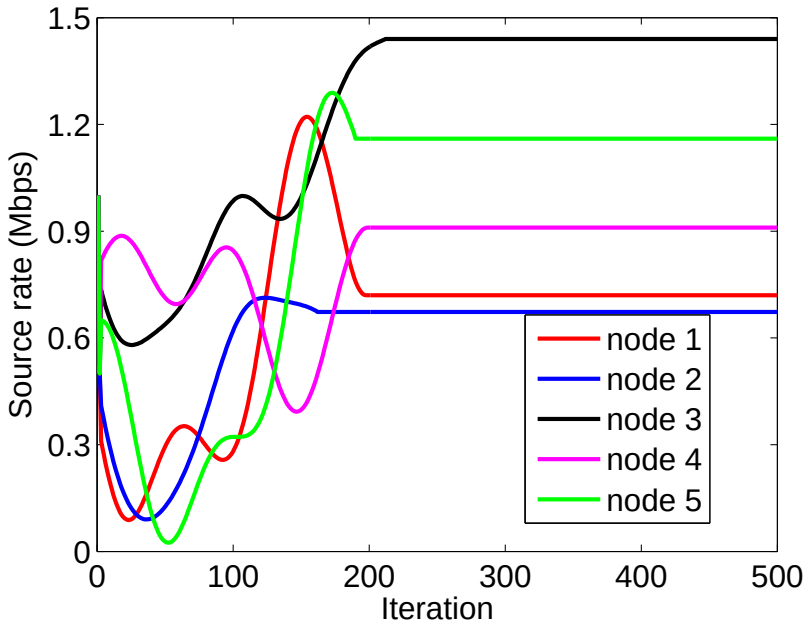

Figure 5.6: Iterations of source rate

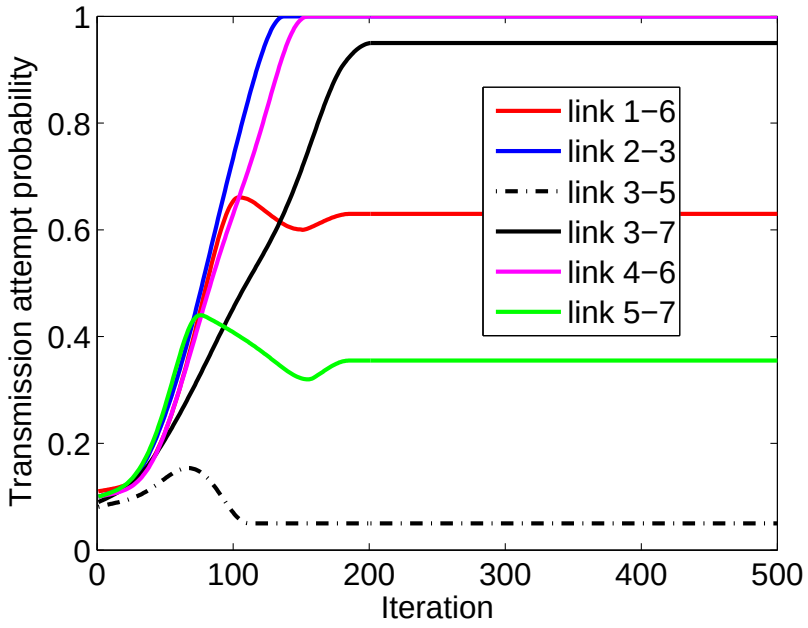

Figure 5.7: Iterations of link transmission attempt probability

Fig. 5.4 shows the aggregate link rates, where the thickness of the line is proportional to the aggregate link rate. Combining Fig. 5.4 and Fig. 5.6, it is found that the nodes have heavy duty in relaying the data tend to encode the video with a lower encoding power (and hence larger source rate), thus saves the power for data transmission and reception. For example, node 3 relays the traffic originating from node 2, therefore node 3 consumes much less energy for video encoding (consequently, node 3 has a much larger source rate than node 2), which saves energy for data transmission and reception. While for node 2, since it depends on other nodes to transmit its data to the sink node, it consumes much energy for video encoding (node 2 has a much lower source rate), this saves the transmission and reception energy for the relay nodes.

Another example of the randomly generated topology is shown in Fig. 5.8, where the topology is a square area of 40 m $\times$ 40 m where 12 nodes (including the sink node), which includes 8 wireless nodes are randomly placed.

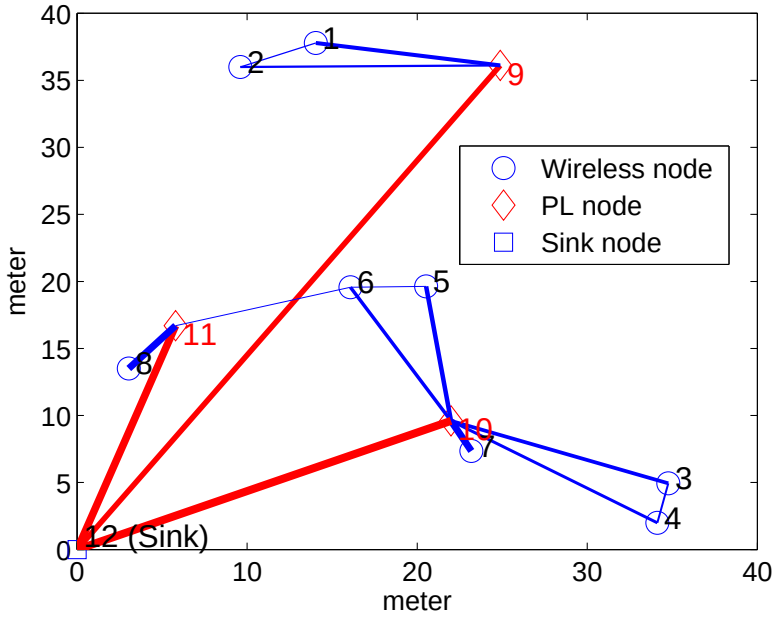

Figure 5.8: Randomly generated topology of HVSN with illustration of aggregate link rates (blue line indicates a wireless link, red line represents a PL link, the thickness of the line is proportional to the aggregate link rate)

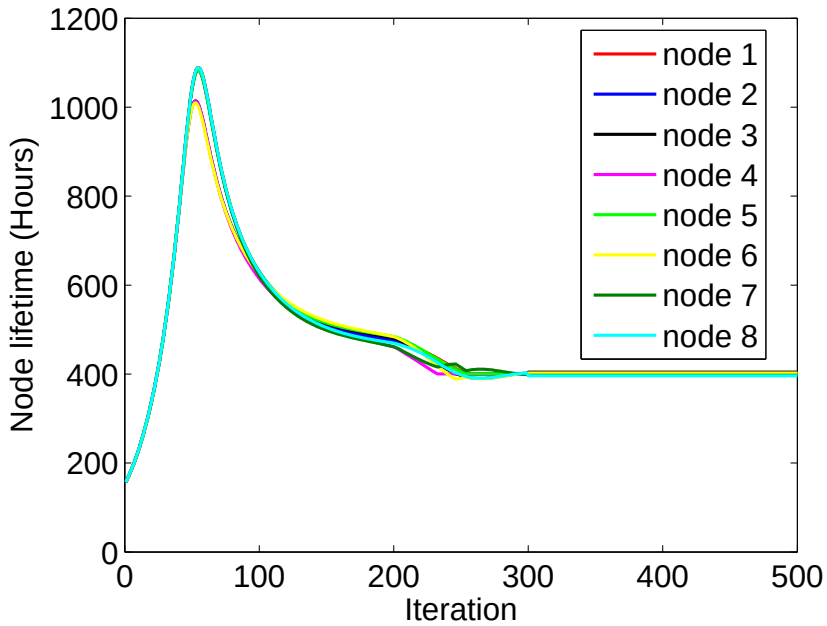

Figure 5.9: Iterations of node lifetime

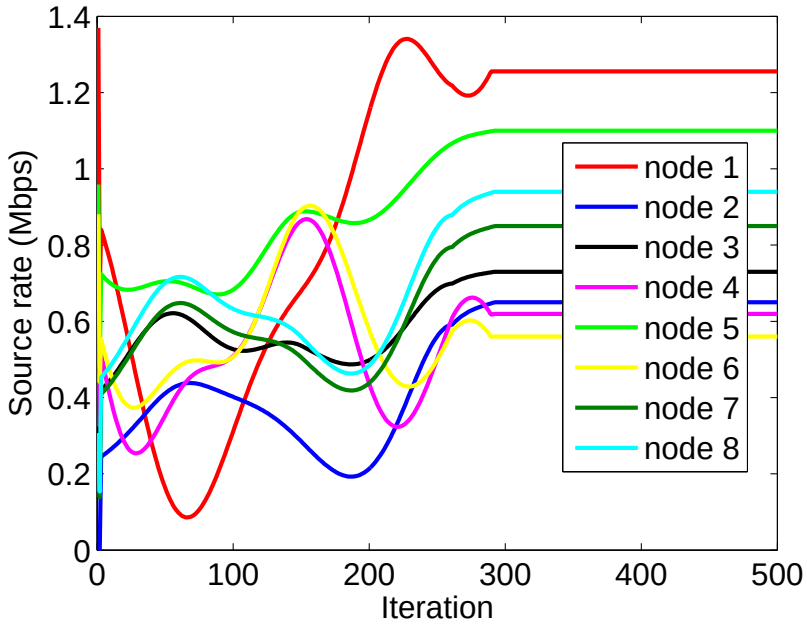

Figure 5.10: Iterations of source rate

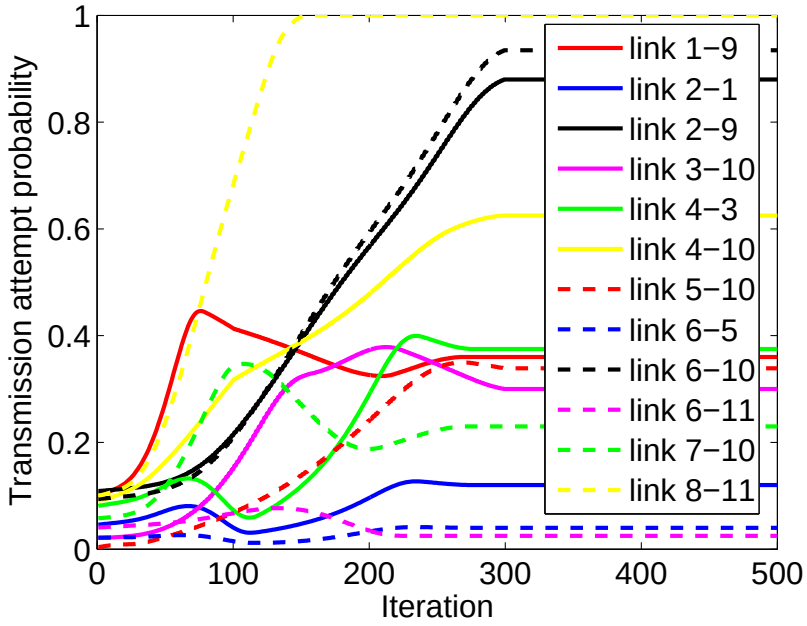

Figure 5.11: Iterations of link transmission attempt probability

Fig. 5.9, Fig. 5.10 and Fig. 5.11 show the convergence behaviour of the proposed distributed algorithm with the illustrations of iterations of node lifetime, source rate and link transmission attempt probabilities, respectively based on the

topology shown in Fig. 5.8. It can be observed that these variables converge to the optimum value within 300 iterations. Therefore, the proposed algorithm can converge to the steady state in a relatively short period of time. Compared to the convergence speed of the algorithm on the network topology shown in Fig. 5.4, it is clear that more iterations are required for a more complex network topology. Also, Fig. 5.9 depicts that the node lifetime of each node in the network can achieve a common node lifetime in the steady state.

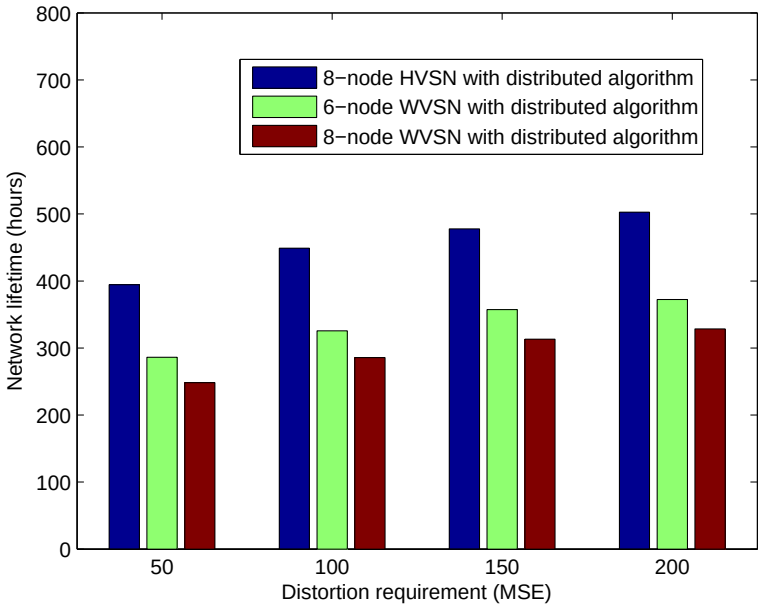

Figure 5.12: Comparison of the network lifetime under different distortion requirements

Fig. 5.12 depicts the network lifetime of the proposed HVSN (shown in Fig. 5.4), the 6-node WVSN and the 8-node WVSN under different distortion requirements. With a smaller distortion requirement, the network lifetime of the networks decreases. In this case, each node either consumes more power for video encoding, or encodes the video content with a larger source rate, which increases the transmission and reception power consumption of each node. By comparing the network lifetime of the proposed 8-node HVSN with the pure WVSN, *i.e.*, the 6-node WVSN and the 8-node WVSN, it can be deduced that the network

lifetime is increased by around 37.5% and 58.1%, respectively, under different distortion requirements. The deployment of PL nodes reduces the channel access contention for the wireless links. This is also the reason that 6-node WVSN has a longer network lifetime than the 8-node WVSN, as with the increase of wireless nodes, each wireless link has a lower transmission attempt probability, and thus consumes more power for data transmission.

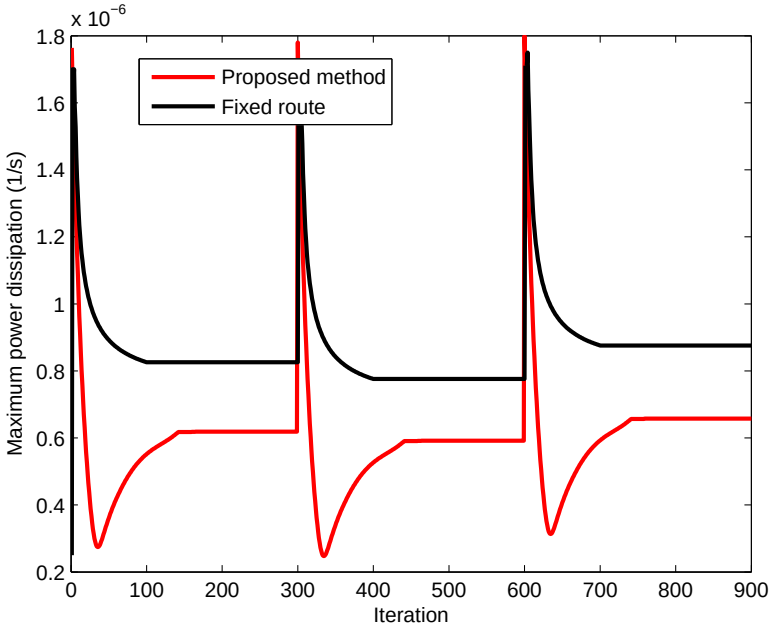

Figure 5.13: Convergence behaviour of the proposed algorithms with dynamic changes of the video content

The convergence behaviour of the proposed distributed algorithm under dynamic changes of the video content for the HVSN illustrated in Fig. 5.4 is shown in Fig. 5.13. The video content is characterized through the average input variance σ^2. At the startup of the distributed algorithm, the average input variance is set to be 3500. After it reaches the steady state, at iteration 300, the average input variance is changed to 2500. It can be observed that the maximum power dissipation among all nodes adapt themselves to this change and reaches another steady state in around 140 iterations. It can be observed that the steady state maximum power dissipation when the average input variance is changed to 2500

has a smaller value than that when the average input variance is 3500. Then at iteration 600, the average input variance is changed from 2500 to 5500. Again, the algorithm quickly adapts itself to converge to a new steady state in around 140 iterations. It can be observed that the steady state maximum power dissipation when the average input variance is changed to 5500 has a larger value than that when the average input variance is 3500.

In order to the compare the convergence speed and performance of the proposed algorithm, it is compared to the algorithm that each node has a selection of pre-defined paths to the sink node, which is generated by existing routing algorithms such as the Dijkstra's algorithm, denoted as "fixed route" in Fig. 5.13. Other optimization parameters are the same as in the proposed algorithm. It can be observed that the algorithm with fixed route converges faster (within 100 iterations) than the proposed algorithm with respect to the change of the average input variance. While, since a selection of pre-defined paths to the sink node is used for each node, this may result in some battery powered wireless nodes being the "hot spot" where other nodes may relay data to. Consequently, these nodes will be drained out of energy very rapidly, and hence the algorithm with fixed routes has a much shorter network lifetime.

Fig. 5.14 shows the convergence behaviour of the proposed distributed algorithm under dynamic changes of the the network topology for the HVSN shown in Fig. 5.4. Initially, the HVSN with 8 nodes reaches a steady state. At iteration 300, node 5 (shown in Fig. 5.4) is turned off. The algorithm detects the topology change, and adapts itself to the change by reaching a new steady state in around 140 iterations. This actually causes the network lifetime to increase significantly since with the remove of node 5, other wireless nodes can access the wireless channel for a longer time. Later at iteration 600, node 5 is turned back on. The algorithm automatically adapts to the topology change and converges to a new steady state in around 140 iterations.

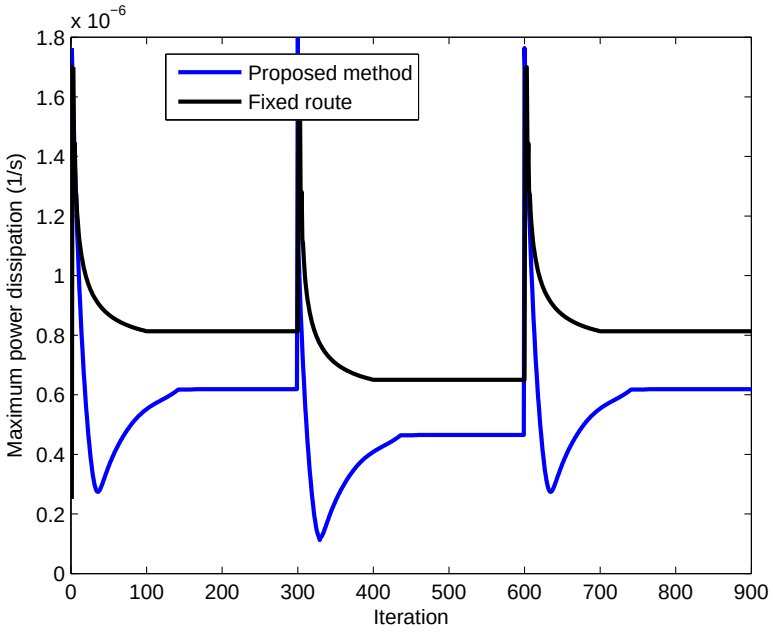

Figure 5.14: Convergence behaviour of the proposed algorithms with dynamic changes of the network topology

Again, in Fig. 5.14, the convergence speed and performance of the proposed algorithm is compared to the algorithm that each node has a selection of pre-defined paths to the sink node, which is generated by existing routing algorithms such as the Dijkstra's algorithm, denoted as "fixed route" in Fig. 5.14. It can be observed that the algorithm with fixed route generally converges within 100 iterations, as compared to 140 iterations by the proposed algorithm with respect to the removal and addition of node 5. Again, since a selection of pre-defined paths to the sink node is used for each node, the routing decision for each node is not optimized. Therefore, this may result in some battery powered wireless nodes being the "hot spot" where other nodes may relay data to, or the node may send data directly to the sink node other than the PL nodes. Consequently, these nodes will be drained out of energy very rapidly, and hence the algorithm with fixed routes has a much shorter network lifetime.

From the analysis of Fig. 5.13 and Fig. 5.14, it demonstrates that the proposed distributed algorithm can fast adapt itself under dynamic changes of the video content or network topology. This indicates that the proposed algorithm is

suitable for the application where frequent sensor node re-positioning is required. In addition, by comparing the proposed algorithm with the algorithm with fixed routes for each node, it demonstrates the effectiveness of the proposed cross-layer optimization method.

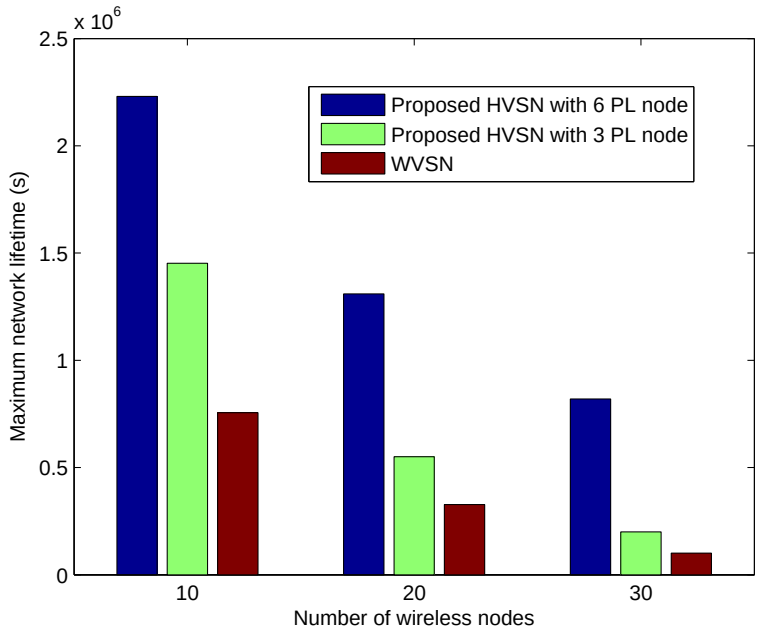

Figure 5.15: Comparison of network lifetime under different network scales

In order to assess the impact of network scale on the performance of the proposed HVSN, three larger network topologies are considered. In the first case, 10 nodes are randomly scattered in an area of 40 m $\times$ 40 m. In the second case, 20 nodes are randomly deployed in an area of 60 m $\times$ 60 m. In the third case, 30 nodes are placed in an area of 80 m $\times$ 80 m in a random fashion. The results are averaged over 50 random realizations in each case for fair comparison. For the topology setup of the HVSN, 3 PL nodes and 6 PL nodes are randomly placed on the network in each case. Fig. 5.15 shows that with the increase of network scale, the network lifetime of the 6-node HVSN, 3-node HVSN and pure WVSN decreases rapidly. This is due to the fact that with more wireless nodes in the network, more video content is generated that needs to be forwarded to the sink node. Therefore, it increases the power dissipation at each node. Also, with the

increase of the number of wireless links, each link has a lower transmission attempt probability, which further increases the power consumption. By comparing the network lifetime of HVSN and WVSN, it is clear that the HVSN can improve network lifetime significantly, especially when the number of PL nodes is large in the network. However, as in the case of network with 30 nodes, the 3-node HVSN improves the network lifetime by a small amount. This is due to the fact that the throughput of PL links can not support the amount of data generated in the network.

5.5 Summary

In this chapter, a distributed algorithm for network lifetime maximization in HVSN is proposed by joint design of video encoding rate, aggregate power consumption, channel access control, along with link rate allocation. Each node solves the optimization problem locally and only requires information exchange with its neighbouring nodes. Through numerical simulations, the performance of the proposed algorithm is evaluated. It is shown that the proposed HVSN can improve the network lifetime of a pure WVSN significantly (by around 37.5% and 58.1%, with 8-node HVSN compared with the 6-node WVSN and 8-node WVSN). Also, the proposed algorithm adapts rapidly with dynamic changes of video content and network topology. By comparing the proposed algorithm with the algorithm with fixed routes for each node, it is observed that the proposed algorithm has a longer convergence time (140 iterations compared to 100 iterations) while can achieve a much longer network lifetime. This proves the effectiveness of the proposed cross-layer algorithm.

Chapter 6

Conclusions and Future Work

6.1 Conclusions

In this thesis, the performance improvement in the hybrid wireless-PL sensor networks for in-door applications have been investigated through cross-layer design with a particular focus on the network lifetime maximization.

In chapter 4, a cross-layer design of a hybrid sensor network was proposed to maximize the network lifetime. The proposed system is suitable in situations where the wireless signal may not penetrate or in situations where wired communication infrastructure is a problem (*e.g.*, installing new communication systems in old facilities or the cost of installing wires for communication within refineries is very high due to safety requirements). Also, the optimal transmission scheme is obtained and the closed-form expression for the globally optimal solution for network lifetime maximization is derived for two network topologies. From the closed-form expressions, for both topologies, it is clear that the network lifetime of the hybrid network is only related to the initial battery capacity, the number of battery powered wireless nodes, and the data arrival rate. The closed-form expression facilities to sensor network system design by fast parameter fitting to investigate the relationship between the network lifetime and the related system parameters. It is also obvious that the optimal routing strategy in the string topology is single-path multihop routing and in the linear topology is multi-path multihop routing. Therefore, the proposed cross-layer optimization method may

perform much better in the linear topology, since multi-path multihop routing in linear topology allows more design freedom. Simulation results validated the accuracy of the derived closed-form expression and demonstrated that in the linear topology, the hybrid sensor network enables a significant increase in the network lifetime over the pure WSN. It can be concluded that closed-form expressions provide a useful guideline for the design of the sensor network.

In chapter 5, a distributed algorithm for network lifetime maximization in HVSN was proposed by joint design of video encoding rate, aggregate power consumption, channel access control, along with link rate allocation. The proposed algorithm only requires information exchange with its neighbouring nodes with very little communication overhead. The performance of the proposed distributed algorithm was evaluated through extensive simulations. The HVSN can improve a significant amount of network lifetime as compared to the traditional WVSN. The proposed distributed algorithm can response to video content or network topology change rapidly. Therefore, it is suitable for the application where frequent node re-positioning is required. By comparing the proposed algorithm with the algorithm with fixed routes for each node, it is observed that the proposed algorithm has a longer convergence time while can achieve a much longer network lifetime. This proves the effectiveness of the proposed cross-layer algorithm.

As a conclusion, the proposed hybrid sensor network can achieve a much longer network lifetime as compared to a pure WSN. Also, it is demonstrated that the proposed cross-layer algorithm performs better in terms of the network lifetime as compared to the algorithm with pre-defined route for each node. This validates the effectiveness of the cross-layer approach in this work.

6.2 Future Work

Future directions of this thesis are:

1. In chapter 4, in order to derive the closed form expression of the network lifetime, only the power consumption in the active mode and only the power

consumption of transmission signal power and the power consumption of the power amplifier is considered. While this is widely adopted in the literature, it is not quite realistic. Future work can be devoted to consider the complete power consumption model and develop efficient algorithms to solve the network lifetime maximization problem.

2. In chapter 4, the network lifetime of the hybrid network in the linear topology is compared to a pure battery powered WSN with the same network configurations. However, intuitively, in the pure wireless network, with the same number of total sensors as compared to the hybrid network, assuming that the wireless nodes that are placed at the same positions of the PL nodes in the corresponding hybrid network are mains powered. In this case, in the hybrid network, the transmission in the wireless link and in the PL link can occur concurrently. While in the wireless network, although the wireless nodes at the same positions of the PL nodes in the hybrid network are also mains powered, the transmission of these wireless nodes will interfere with the transmission of the wireless links of the battery powered wireless nodes. Since TDMA is considered in this chapter and concurrent transmission is not allowed in the same transmission medium, the transmission of the mains powered wireless nodes in the wireless network will have to share the transmission time frame with the battery powered wireless nodes. Therefore, each battery powered wireless node in the wireless network is allocated less transmission time as compared to the battery powered wireless node in the hybrid network, which consequently consumes more transmission power in order to achieve the required data arrival rate. Future work can be devoted to develop algorithms to solve the problem in this scenario.

3. Other technologies such as energy harvesting and simultaneous information and power transfer can be integrated into the hybrid sensor network to further extend the network lifetime.

Bibliography

[1] L. Atzori, A. Iera, and G. Morabito, "The internet of things: A survey," *Computer networks*, vol. 54, no. 15, pp. 2787–2805, 2010.

[2] A. Zanella, N. Bui, A. Castellani, L. Vangelista, and M. Zorzi, "Internet of things for smart cities," *IEEE Internet of Things journal*, vol. 1, no. 1, pp. 22–32, 2014.

[3] I. Yaqoob, E. Ahmed, I. A. T. Hashem, A. I. A. Ahmed, A. Gani, M. Imran, and M. Guizani, "Internet of things architecture: Recent advances, taxonomy, requirements, and open challenges," *IEEE wireless communications*, vol. 24, no. 3, pp. 10–16, 2017.

[4] E. Fadel, V. C. Gungor, L. Nassef, N. Akkari, M. A. Malik, S. Almasri, and I. F. Akyildiz, "A survey on wireless sensor networks for smart grid," *Computer Communications*, vol. 71, pp. 22–33, 2015.

[5] P. Bellavista, G. Cardone, A. Corradi, and L. Foschini, "Convergence of manet and wsn in iot urban scenarios," *IEEE Sensors Journal*, vol. 13, no. 10, pp. 3558–3567, 2013.

[6] L. Hu, M. Qiu, J. Song, M. S. Hossain, and A. Ghoneim, "Software defined healthcare networks," *IEEE Wireless Communications*, vol. 22, no. 6, pp. 67–75, 2015.

[7] A. Samanta, S. Bera, and S. Misra, "Link-quality-aware resource allocation with load balance in wireless body area networks," *IEEE Systems Journal*, 2015.

[8] J. Pan, R. Jain, S. Paul, T. Vu, A. Saifullah, and M. Sha, "An internet of things framework for smart energy in buildings: designs, prototype, and experiments," *IEEE Internet of Things Journal*, vol. 2, no. 6, pp. 527–537, 2015.

[9] S. Bera, S. Misra, and J. J. Rodrigues, "Cloud computing applications for smart grid: A survey," *IEEE Transactions on Parallel and Distributed Systems*, vol. 26, no. 5, pp. 1477–1494, 2015.

[10] S. S. Iyengar and R. R. Brooks, *Distributed sensor networks: sensor networking and applications*. CRC press, 2016.

[11] A. Al-Fuqaha, M. Guizani, M. Mohammadi, M. Aledhari, and M. Ayyash, "Internet of things: A survey on enabling technologies, protocols, and applications," *IEEE Communications Surveys & Tutorials*, vol. 17, no. 4, pp. 2347–2376, 2015.

[12] I. F. Akyildiz, W. Su, Y. Sankarasubramaniam, and E. Cayirci, "Wireless sensor networks: a survey," *Computer networks*, vol. 38, no. 4, pp. 393–422, 2002.

[13] F. Alduraibi, N. Lasla, and M. Younis, "Coverage-based node placement optimization in wireless sensor network with linear topology," in *Proc. IEEE International Conference on Communications (ICC)*, Kuala Lumpur, Malaysia, May 2016, pp. 1–6.

[14] G. Sharma and R. R. Mazumdar, "A case for hybrid sensor networks," *IEEE/ACM Transactions on Networking*, vol. 16, no. 5, pp. 1121–1132, 2008.

[15] H.-Y. Chen and C.-h. Lee, "A spatial study of mixed wireless and wireline heterogeneous networks," in *Proc. IEEE International Symposium on Personal Indoor and Mobile Radio Communications (PIMRC)*, Toronto, Canada, 2011, pp. 258–262.

[16] F. Salvadori, C. Gehrke, A. De Oliveira, M. De Campos, and P. S. Sausen, "Smart grid infrastructure using a hybrid network architecture," *IEEE Transactions on Smart Grid*, vol. 4, no. 3, pp. 1630–1639, 2013.

[17] T. Qiu, D. Luo, F. Xia, N. Deonauth, W. Si, and A. Tolba, "A greedy model with small world for improving the robustness of heterogeneous internet of things," *Computer Networks*, vol. 101, pp. 127–143, 2016.

[18] A. Helmy, "Small worlds in wireless networks," *IEEE Communications Letters*, vol. 7, no. 10, pp. 490–492, 2003.

[19] G. Sharma and R. Mazumdar, "Hybrid sensor networks: a small world," in *Proc. ACM international symposium on Mobile ad hoc networking and computing*, Chicago, IL, USA, 2005, pp. 366–377.

[20] W. Dongyang, W. Muqing, L. Bo, and W. Jingrong, "A small world-based energy-efficient mechanism in wireless ad hoc networks," in *Proc. IEEE International Conference on Communications (ICC)*, Budapest, Hungary, 2013, pp. 447–451.

[21] L. Bo, W. Muqing, W. Jingrong, and W. Dongyang, "Small worlds in multi-channel wireless networks: An analytical approach," in *Proc. IEEE International Conference on Communications (ICC)*, Budapest, Hungary, 2013, pp. 1527–1531.

[22] D. L. Guidoni, R. A. Mini, and A. A. Loureiro, "Applying the small world concepts in the design of heterogeneous wireless sensor networks," *IEEE Communications Letters*, vol. 16, no. 7, pp. 953–955, 2012.

[23] N. Tadayon, A. E. Zonouz, S. Aïssa, and L. Xing, "Cost-effective design and evaluation of wireless sensor networks using topology-planning methods in small-world context," *IET Wireless Sensor Systems*, vol. 4, no. 2, pp. 43–53, 2014.

[24] H. Ferreira, L. Lampe, J. Newbury, and T. Swart, *Power Line Communications: Theory and Applications for Narrowband and Broadband Communications over Power Lines*. Wiley Online Library, 2010.

[25] S. Galli and O. Logvinov, "Recent developments in the standardization of power line communications within the ieee," *IEEE Communications Magazine*, vol. 46, no. 7, 2008.

[26] N. Pavlidou, A. H. Vinck, J. Yazdani, and B. Honary, "Power line communications: state of the art and future trends," *IEEE Communications magazine*, vol. 41, no. 4, pp. 34–40, 2003.

[27] C.-K. Lin, H.-W. Chu, S.-C. Yeh, M.-T. Lu, J. Yao, and H. Chen, "Robust video streaming over power lines," in *Proc. IEEE International Symposium on Power Line Communications and Its Applications (ISPLC)*, Orlando, Florida, USA, 2006, pp. 196–201.

[28] A. Gnazzo, A. Bergaglio, M. Palma, F. Pittoni, M. Giunta, and F. Ballesio, "Powerline technology over coaxial cables for in-home multimedia applications: Performances and emc issues," in *Proc. IEEE International Symposium on Power Line Communications and Its Applications (ISPLC)*, Udine, Italy, 2011, pp. 130–134.

[29] L. Lampe, *Power Line Communications: Principles, Standards and Applications from Multimedia to Smart Grid*. John Wiley & Sons, 2016.

[30] S. Galli and T. C. Banwell, "A deterministic frequency-domain model for the indoor power line transfer function," *IEEE Journal on Selected Areas in Communications*, vol. 24, no. 7, pp. 1304–1316, 2006.

[31] G. Held, *Understanding broadband over power line*. CRC Press, 2016.

[32] C. Cano, A. Pittolo, D. Malone, L. Lampe, A. M. Tonello, and A. G. Dabak, "State of the art in power line communications: From the applications to

the medium," *IEEE Journal on Selected Areas in Communications*, vol. 34, no. 7, pp. 1935–1952, 2016.

[33] S. Galli, A. Scaglione, and Z. Wang, "Power line communications and the smart grid," in *Proc. IEEE International Conference on Smart Grid Communications (SmartGridComm)*, Maryland, USA, 2010, pp. 303–308.

[34] M. Li and H.-J. Lin, "Design and implementation of smart home control systems based on wireless sensor networks and power line communications," *IEEE Transactions on Industrial Electronics*, vol. 62, no. 7, pp. 4430–4442, 2015.

[35] B. A. A. Nunes, M. Mendonca, X.-N. Nguyen, K. Obraczka, and T. Turletti, "A survey of software-defined networking: Past, present, and future of programmable networks," *IEEE Communications Surveys & Tutorials*, vol. 16, no. 3, pp. 1617–1634, 2014.

[36] D. F. Macedo, D. Guedes, L. F. Vieira, M. A. Vieira, and M. Nogueira, "Programmable networksfrom software-defined radio to software-defined networking," *IEEE communications surveys & tutorials*, vol. 17, no. 2, pp. 1102–1125, 2015.

[37] S. Bera, S. Misra, and A. V. Vasilakos, "Software-defined networking for internet of things: A survey," *IEEE Internet of Things Journal*, vol. 4, no. 6, pp. 1994–2008, 2017.

[38] J.-H. Lee and Y.-H. Kim, "Diversity relaying for parallel use of power-line and wireless communication networks," *IEEE Transactions on Power Delivery*, vol. 29, no. 3, pp. 1301–1310, 2014.

[39] S. W. Lai and G. G. Messier, "Using the wireless and plc channels for diversity," *IEEE Transactions on Communications*, vol. 60, no. 12, pp. 3865–3875, 2012.

[40] S. W. Lai, N. Shabehpour, G. G. Messier, and L. Lampe, "Performance of wireless/power line media diversity in the office environment," in *Proc. IEEE Global Communications Conference (GLOBECOM)*, Austin, USA, 2014, pp. 2972–2976.

[41] M. Sayed, T. A. Tsiftsis, and N. Al-Dhahir, "On the diversity of hybrid narrowband-plc/wireless communications for smart grids," *IEEE Transactions on Wireless Communications*, vol. 16, no. 7, pp. 4344–4360, 2017.

[42] G. Sebaali and B. L. Evans, "Design tradeoffs in joint powerline and wireless transmission for smart grid communications," in *Proc. IEEE International Symposium on Power Line Communications and its Applications (ISPLC)*, Austin, USA, 2015, pp. 83–88.

[43] M. Sayed, G. Sebaali, B. L. Evans, and N. Al-Dhahir, "Efficient diversity technique for hybrid narrowband-powerline/wireless smart grid communications," in *Proc. IEEE International Conference on Smart Grid Communications (SmartGridComm)*, Miami, FL, USA, 2015, pp. 1–6.

[44] L. de MBA Dib, V. Fernandes, M. d. L. Filomeno, and M. V. Ribeiro, "Hybrid plc/wireless communication for smart grids and internet of things applications," *to appear on IEEE Internet of Things Journal*, 2017.

[45] M. Mokhtar, W. U. Bajwa, and N. Al-Dhahir, "Sparsity-aware joint narrowband interference and impulse noise mitigation for hybrid powerline-wireless transmission," in *Proc. IEEE Wireless Communications and Networking Conference (WCNC)*, New Orleans, LA, USA, 2015, pp. 615–620.

[46] A. Mathur, M. R. Bhatnagar, and B. K. Panigrahi, "Performance of a dual-hop wireless-powerline mixed cooperative system," in *Proc. IEEE International Conference on Advanced Technologies for Communications (ATC)*, Hanoi, Vietnam, 2016, pp. 401–406.

[47] M. Kuhn, S. Berger, I. Hammerstrom, and A. Wittneben, "Power line enhanced cooperative wireless communications," *IEEE Journal on Selected Areas in Communications*, vol. 24, no. 7, pp. 1401–1410, 2006.

[48] T. Oliveira, F. Andrade, A. Picorone, H. Latchman, S. Netto, and M. Ribeiro, "Characterization of hybrid communication channel in indoor scenario," *Journal of Communication and Information Systems*, vol. 31, no. 1, 2016.

[49] M. Chiang, S. H. Low, A. R. Calderbank, and J. C. Doyle, "Layering as optimization decomposition: A mathematical theory of network architectures," *Proceedings of the IEEE*, vol. 95, no. 1, pp. 255–312, 2007.

[50] F. P. Kelly, A. K. Maulloo, and D. K. Tan, "Rate control for communication networks: shadow prices, proportional fairness and stability," *Journal of the Operational Research society*, vol. 49, no. 3, pp. 237–252, 1998.

[51] R. Rockafellar, "Network flows and monotropic programming," *J. Wiley, NY*, 1984.

[52] D. P. Palomar and M. Chiang, "A tutorial on decomposition methods for network utility maximization," *IEEE Journal on Selected Areas in Communications*, vol. 24, no. 8, pp. 1439–1451, 2006.

[53] M. Chiang, "Balancing transport and physical layers in wireless multihop networks: Jointly optimal congestion control and power control," *IEEE Journal on Selected Areas in Communications*, vol. 23, no. 1, pp. 104–116, 2005.

[54] X. Lin, N. B. Shroff, and R. Srikant, "A tutorial on cross-layer optimization in wireless networks," *IEEE Journal on Selected areas in Communications*, vol. 24, no. 8, pp. 1452–1463, 2006.

[55] D. P. Palomar and M. Chiang, "Alternative distributed algorithms for network utility maximization: Framework and applications," *IEEE Transactions on Automatic Control*, vol. 52, no. 12, pp. 2254–2269, 2007.

[56] P. Gaj, J. Jasperneite, and M. Felser, "Computer communication within industrial distributed environmenta survey," *IEEE Transactions on Industrial Informatics*, vol. 9, no. 1, pp. 182–189, 2013.

[57] S. Zoppi, A. Van Bemten, H. M. Gürsu, M. Vilgelm, J. Guck, and W. Kellerer, "Achieving hybrid wired/wireless industrial networks with wdetserv: Reliability-based scheduling for delay guarantees," *IEEE Transactions on Industrial Informatics*, vol. 14, no. 5, pp. 2307–2319, 2018.

[58] K. Ovsthus, L. M. Kristensen *et al.*, "An industrial perspective on wireless sensor networksa survey of requirements, protocols, and challenges," *IEEE communications surveys & tutorials*, vol. 16, no. 3, pp. 1391–1412, 2014.

[59] J. N. Al-Karaki and A. E. Kamal, "Routing techniques in wireless sensor networks: a survey," *IEEE wireless communications*, vol. 11, no. 6, pp. 6–28, 2004.

[60] I. F. Akyildiz, W. Su, Y. Sankarasubramaniam, and E. Cayirci, "A survey on sensor networks," *IEEE Communications magazine*, vol. 40, no. 8, pp. 102–114, 2002.

[61] G. Anastasi, M. Conti, M. Di Francesco, and A. Passarella, "Energy conservation in wireless sensor networks: A survey," *Ad hoc networks*, vol. 7, no. 3, pp. 537–568, 2009.

[62] E. J. Duarte-Melo and M. Liu, "Analysis of energy consumption and lifetime of heterogeneous wireless sensor networks," in *Proc. IEEE Global Communications Conference (GLOBECOM)*, vol. 1, Taipei, Taiwan, Nov. 2002, pp. 21–25.

[63] W. R. Heinzelman, A. Chandrakasan, and H. Balakrishnan, "Energy-efficient communication protocol for wireless microsensor networks," in *Proc. IEEE annual Hawaii international conference on System sciences*, Hawaii, USA, Jan. 2000, pp. 10–pp.

[64] S. R. Cui, "Cross-layer optimization in energy constrained networks," Ph.D. dissertation, stanford university, 2005.

[65] K. Chintalapudi, T. Fu, J. Paek, N. Kothari, S. Rangwala, J. Caffrey, R. Govindan, E. Johnson, and S. Masri, "Monitoring civil structures with a wireless sensor network," *IEEE Internet Computing*, vol. 10, no. 2, pp. 26–34, 2006.

[66] T. Harms, S. Sedigh, and F. Bastianini, "Structural health monitoring of bridges using wireless sensor networks," *IEEE Instrumentation & Measurement Magazine*, vol. 13, no. 6, 2010.

[67] F. Wang, D. Wang, and J. Liu, "High-rise structure monitoring with elevator-assisted wireless sensor networking: design, optimization, and case study," *Wireless Networks*, pp. 1–19, 2017.

[68] G. Hackmann, W. Guo, G. Yan, Z. Sun, C. Lu, and S. Dyke, "Cyber-physical codesign of distributed structural health monitoring with wireless sensor networks," *IEEE Transactions on Parallel and Distributed Systems*, vol. 25, no. 1, pp. 63–72, 2014.

[69] S. Kim, S. Pakzad, D. Culler, J. Demmel, G. Fenves, S. Glaser, and M. Turon, "Health monitoring of civil infrastructures using wireless sensor networks," in *Proc. ACM international conference on Information processing in sensor networks*, Cambridge, Massachusetts, USA, 2007, pp. 254–263.

[70] I. F. Akyildiz, T. Melodia, and K. R. Chowdury, "Wireless multimedia sensor networks: A survey," *IEEE Wireless Communications*, vol. 14, no. 6, 2007.

[71] K. Lin, J. J. Rodrigues, H. Ge, N. Xiong, and X. Liang, "Energy efficiency qos assurance routing in wireless multimedia sensor networks," *IEEE Systems Journal*, vol. 5, no. 4, pp. 495–505, 2011.

[72] K. B. Lee and M. E. Reichardt, "Open standards for homeland security sensor networks," *IEEE Instrumentation & Measurement Magazine*, vol. 8, no. 5, pp. 14–21, 2005.

[73] M. Patel and J. Wang, "Applications, challenges, and prospective in emerging body area networking technologies," *IEEE Wireless communications*, vol. 17, no. 1, 2010.

[74] A. Goldsmith, *Wireless communications*. Cambridge university press, 2005.

[75] J. C. Maxwell, "A dynamical theory of the electromagnetic field," *Philosophical transactions of the Royal Society of London*, vol. 155, pp. 459–512, 1865.

[76] A. F. Molisch, *Wireless communications*. John Wiley & Sons, 2012.

[77] T. S. Rappaport, *Wireless communications: principles and practice*. Prentice Hall PTR, 2002.

[78] C. E. Shannon, "A mathematical theory of communication," *Bell System Technical Journal*, vol. 27, pp. 623–656, 1948.

[79] P. Brown, "Power line communications-past, present, and future," in *Proc. IEEE International Symposium on Power-line Communications and its Applications (ISPLC)*, Lancaster, UK, 1999, pp. 1–8.

[80] M. Schwartz, "Carrier-wave telephony over power lines: Early history [history of communications]," *IEEE Communications Magazine*, vol. 47, no. 1, pp. 14–18, 2009.

[81] C. Xavier, "Power line communications in practice," *ArtechHouse*, 2006.

[82] S. Galli, A. Scaglione, and Z. Wang, "For the grid and through the grid: The role of power line communications in the smart grid," *Proceedings of the IEEE*, vol. 99, no. 6, pp. 998–1027, 2011.

[83] K. Y. See, P. L. So, A. Kamarul, and E. Gunawan, "Radio-frequency common-mode noise propagation model for power-line cable," *IEEE Transactions on power Delivery*, vol. 20, no. 4, pp. 2443–2449, 2005.

[84] S. Galli, M. Koch, H. Latchman, S. Lee, V. Oksman, H. Ferreira, L. Lampe, J. Newbury, and T. Swart, "Industrial and international standards on plc base networking technologies," *Power Line Communications*, p. 377, 2010.

[85] M. Nassar, J. Lin, Y. Mortazavi, A. Dabak, I. H. Kim, and B. L. Evans, "Local utility power line communications in the 3–500 khz band: channel impairments, noise, and standards," *IEEE signal processing magazine*, vol. 29, no. 5, pp. 116–127, 2012.

[86] A. M. Tonello and F. Versolatto, "Bottom-up statistical plc channel modelingpart i: Random topology model and efficient transfer function computation," *IEEE Transactions on Power Delivery*, vol. 26, no. 2, pp. 891–898, 2011.

[87] F. J. Canete, J. A. Cortes, L. Diez, and J. T. Entrambasaguas, "A channel model proposal for indoor power line communications," *IEEE Communications Magazine*, vol. 49, no. 12, pp. 166–174, 2011.

[88] T. Banwell and S. Galli, "A novel approach to the modeling of the indoor power line channel part i: circuit analysis and companion model," *IEEE Transactions on Power Delivery*, vol. 20, no. 2, pp. 655–663, 2005.

[89] M. Zimmermann and K. Dostert, "A multipath model for the powerline

channel," *IEEE Transactions on communications*, vol. 50, no. 4, pp. 553–559, 2002.

[90] S. Guzelgoz, H. B. Çelebi, and H. Arslan, "Statistical characterization of the paths in multipath plc channels," *IEEE Transactions on Power Delivery*, vol. 26, no. 1, pp. 181–187, 2011.

[91] A. M. Tonello, F. Versolatto, B. Bejar, and S. Zazo, "A fitting algorithm for random modeling the plc channel," *IEEE Transactions on Power Delivery*, vol. 27, no. 3, pp. 1477–1484, 2012.

[92] C. R. Paul, *Analysis of multiconductor transmission lines*. John Wiley & Sons, 2008.

[93] S. Galli and T. Banwell, "A novel approach to the modeling of the indoor power line channel-part ii: Transfer function and its properties," *IEEE Transactions on Power Delivery*, vol. 20, no. 3, pp. 1869–1878, 2005.

[94] M. Babic, M. Hagenau, K. Dostert, and J. Bausch, "Theoretical postulation of plc channel model," *Open PLC European Research Alliance (OPERA)*, 2005.

[95] M. Tlich, A. Zeddam, F. Moulin, and F. Gauthier, "Indoor power-line communications channel characterization up to 100 mhzpart ii: Time-frequency analysis," *IEEE transactions on power delivery*, vol. 23, no. 3, pp. 1402–1409, 2008.

[96] L. Di Bert, P. Caldera, D. Schwingshackl, and A. M. Tonello, "On noise modeling for power line communications," in *Proc. IEEE International Symposium on Power Line Communications and Its Applications (ISPLC)*, Udine, Italy, 2011, pp. 283–288.

[97] T. Esmailian, F. R. Kschischang, and P. Glenn Gulak, "In-building power lines as high-speed communication channels: channel characterization and a

test channel ensemble," *International Journal of Communication Systems*, vol. 16, no. 5, pp. 381–400, 2003.

[98] D. Middleton, "Statistical-physical models of electromagnetic interference," *IEEE Transactions on Electromagnetic Compatibility*, no. 3, pp. 106–127, 1977.

[99] M. Katayama, T. Yamazato, and H. Okada, "A mathematical model of noise in narrowband power line communication systems," *IEEE Journal on Selected areas in Communications*, vol. 24, no. 7, pp. 1267–1276, 2006.

[100] M. Zimmermann and K. Dostert, "Analysis and modeling of impulsive noise in broad-band powerline communications," *IEEE transactions on Electromagnetic compatibility*, vol. 44, no. 1, pp. 249–258, 2002.

[101] M. O. Ahmed and L. Lampe, "Power line network topology inference using frequency domain reflectometry," in *Proc. IEEE International Conference on Communications (ICC)*, Ottawa, Canada, 2012, pp. 3419–3423.

[102] ——, "Parametric and nonparametric methods for power line network topology inference," in *Proc. IEEE International Symposium on Power Line Communications and Its Applications (ISPLC)*, Beijing, China, 2012, pp. 274–279.

[103] C. Zhang, X. Zhu, Y. Huang, and G. Liu, "High-resolution and low-complexity dynamic topology estimation for plc networks assisted by impulsive noise source detection," *IET Communications*, vol. 10, no. 4, pp. 443–451, 2016.

[104] F. Passerini and A. M. Tonello, "Power line network topology identification using admittance measurements and total least squares estimation," in *Proc. IEEE International Conference on Communications (ICC)*, Paris, France, 2017, pp. 1–6.

[105] A. M. Tonello, S. D'Alessandro, and L. Lampe, "Cyclic prefix design and allocation in bit-loaded ofdm over power line communication channels," *IEEE Transactions on Communications*, vol. 58, no. 11, pp. 3265–3276, 2010.

[106] S. DAlessandro, A. M. Tonello, and L. Lampe, "Adaptive pulse-shaped ofdm with application to in-home power line communications," *Telecommunication Systems*, vol. 51, no. 1, pp. 3–13, 2012.

[107] T. N. Vo, K. Amis, T. Chonavel, and P. Siohan, "Achievable throughput optimization in ofdm systems in the presence of interference and its application to power line networks," *IEEE transactions on communications*, vol. 62, no. 5, pp. 1704–1715, 2014.

[108] L. Lampe, "Bursty impulse noise detection by compressed sensing," in *Proc. IEEE International Symposium on Power Line Communications and Its Applications (ISPLC)*, Udine, Italy, 2011, pp. 29–34.

[109] F. H. Juwono, Q. Guo, D. Huang, and K. P. Wong, "Deep clipping for impulsive noise mitigation in ofdm-based power-line communications," *IEEE Transactions on Power Delivery*, vol. 29, no. 3, pp. 1335–1343, 2014.

[110] Y.-R. Chien, "Iterative channel estimation and impulsive noise mitigation algorithm for ofdm-based receivers with application to power-line communications," *IEEE Transactions on Power Delivery*, vol. 30, no. 6, pp. 2435–2442, 2015.

[111] D. P. Bertsekas, R. G. Gallager, and P. Humblet, *Data networks*. Prentice-hall Englewood Cliffs, NJ, 1987, vol. 2.

[112] A. J. Goldsmith and S. B. Wicker, "Design challenges for energy-constrained ad hoc wireless networks," *IEEE wireless communications*, vol. 9, no. 4, pp. 8–27, 2002.

[113] I. F. Akyildiz, T. Melodia, and K. R. Chowdhury, "A survey on wireless multimedia sensor networks," *Computer networks*, vol. 51, no. 4, pp. 921–960, 2007.

[114] S. Boyd and L. Vandenberghe, *Convex optimization*. Cambridge university press, 2004.

[115] D. P. Bertsekas and J. N. Tsitsiklis, *Parallel and distributed computation: numerical methods*. Prentice hall Englewood Cliffs, NJ, 1989, vol. 23.

[116] D. P. Bertsekas, A. Nedi, A. E. Ozdaglar *et al.*, "Convex analysis and optimization," 2003.

[117] D. P. Bertsekas, *Nonlinear programming*. Athena scientific Belmont, 1999.

[118] M. J. Herrmann and G. G. Messier, "Cross-layer lifetime optimization for practical industrial wireless networks: A petroleum refinery case study," *IEEE Transactions on Industrial Informatics*, vol. 14, no. 8, pp. 3559–3566, 2018.

[119] I. Johnstone, J. Nicholson, B. Shehzad, and J. Slipp, "Experiences from a wireless sensor network deployment in a petroleum environment," in *Proceedings of the 2007 international conference on Wireless communications and mobile computing*, Honolulu, Hawaii, USA, 2007, pp. 382–387.

[120] S. C. Pereira, A. S. Caporali, and I. R. Casella, "Power line communication technology in industrial networks," in *2015 IEEE International Symposium on Power Line Communications and Its Applications (ISPLC)*, Austin, TX, USA, 2015, pp. 216–221.

[121] J. W. Jung and M. A. Weitnauer, "On using cooperative routing for lifetime optimization of multi-hop wireless sensor networks: analysis and guidelines," *IEEE Transactions on Communications*, vol. 61, no. 8, pp. 3413–3423, 2013.

[122] H. Yetgin, K. T. K. Cheung, M. El-Hajjar, and L. Hanzo, "Cross-layer network lifetime maximization in interference-limited wsns," *IEEE Transactions on Vehicular Technology*, vol. 64, no. 8, pp. 3795–3803, 2015.

[123] C. G. Cassandras, T. Wang, and S. Pourazarm, "Optimal routing and energy allocation for lifetime maximization of wireless sensor networks with nonideal batteries," *IEEE Transactions on Control of Network Systems*, vol. 1, no. 1, pp. 86–98, 2014.

[124] H. Yetgin, K. T. K. Cheung, M. El-Hajjar, and L. Hanzo, "Network-lifetime maximization of wireless sensor networks," *IEEE Access*, vol. 3, pp. 2191–2226, 2015.

[125] H. Zhang and J. C. Hou, "On the upper bound of α-lifetime for large sensor networks," *ACM Transactions on Sensor Networks (TOSN)*, vol. 1, no. 2, pp. 272–300, 2005.

[126] K. Wu, Y. Gao, F. Li, and Y. Xiao, "Lightweight deployment-aware scheduling for wireless sensor networks," *Mobile Networks and applications*, vol. 10, no. 6, pp. 837–852, 2005.

[127] E. B. Hamida and G. Chelius, "Strategies for data dissemination to mobile sinks in wireless sensor networks," *IEEE Wireless Communications*, vol. 15, no. 6, pp. 31–37, 2008.

[128] H. Yetgin, K. T. K. Cheung, M. El-Hajjar, and L. H. Hanzo, "A survey of network lifetime maximization techniques in wireless sensor networks," *IEEE Communications Surveys & Tutorials*, vol. 19, no. 2, pp. 828–854, 2017.

[129] C.-Y. Chang, J.-P. Sheu, Y.-C. Chen, and S.-W. Chang, "An obstacle-free and power-efficient deployment algorithm for wireless sensor networks," *IEEE Transactions on Systems, Man, and Cybernetics-Part A: Systems and Humans*, vol. 39, no. 4, pp. 795–806, 2009.

[130] F. Marcelloni and M. Vecchio, "A simple algorithm for data compression in wireless sensor networks," *IEEE communications letters*, vol. 12, no. 6, 2008.

[131] S. Yang, H. Cheng, and F. Wang, "Genetic algorithms with immigrants and memory schemes for dynamic shortest path routing problems in mobile ad hoc networks," *IEEE Transactions on Systems, Man, and Cybernetics, Part C (Applications and Reviews)*, vol. 40, no. 1, pp. 52–63, 2010.

[132] S. Okdem and D. Karaboga, "Routing in wireless sensor networks using an ant colony optimization (aco) router chip," *Sensors*, vol. 9, no. 2, pp. 909–921, 2009.

[133] Y. Liang, J. Cao, L. Zhang, R. Wang, and Q. Pan, "A biologically inspired sensor wakeup control method for wireless sensor networks," *IEEE Transactions on Systems, Man, and Cybernetics, Part C (Applications and Reviews)*, vol. 40, no. 5, pp. 525–538, 2010.

[134] T. R. Park, K.-J. Park, and M. J. Lee, "Design and analysis of asynchronous wakeup for wireless sensor networks," *IEEE Transactions on Wireless Communications*, vol. 8, no. 11, 2009.

[135] X.-M. Hu, J. Zhang, Y. Yu, H. S.-H. Chung, Y.-L. Li, Y.-H. Shi, and X.-N. Luo, "Hybrid genetic algorithm using a forward encoding scheme for lifetime maximization of wireless sensor networks," *IEEE transactions on evolutionary computation*, vol. 14, no. 5, pp. 766–781, 2010.

[136] Y. Lin, J. Zhang, H. S.-H. Chung, W. H. Ip, Y. Li, and Y.-H. Shi, "An ant colony optimization approach for maximizing the lifetime of heterogeneous wireless sensor networks," *IEEE Transactions on Systems, Man, and Cybernetics, Part C (Applications and Reviews)*, vol. 42, no. 3, pp. 408–420, 2012.

[137] L. D. Mendes and J. J. Rodrigues, "A survey on cross-layer solutions for wireless sensor networks," *Journal of Network and Computer Applications*, vol. 34, no. 2, pp. 523–534, 2011.

[138] S. Cui, R. Madan, A. J. Goldsmith, and S. Lall, "Cross-layer energy and delay optimization in small-scale sensor networks," *IEEE Transactions on Wireless Communications*, vol. 6, no. 10, 2007.

[139] L. Shi and A. O. Fapojuwo, "Tdma scheduling with optimized energy efficiency and minimum delay in clustered wireless sensor networks," *IEEE Transactions on Mobile Computing*, vol. 9, no. 7, pp. 927–940, 2010.

[140] R. Madan, S. Cui, S. Lall, and N. A. Goldsmith, "Cross-layer design for lifetime maximization in interference-limited wireless sensor networks," *IEEE Transactions on Wireless Communications*, vol. 5, no. 11, 2006.

[141] H. Kwon, T. H. Kim, S. Choi, and B. G. Lee, "A cross-layer strategy for energy-efficient reliable delivery in wireless sensor networks," *IEEE Transactions on Wireless Communications*, vol. 5, no. 12, 2006.

[142] S. Ehsan, B. Hamdaoui, and M. Guizani, "Radio and medium access contention aware routing for lifetime maximization in multichannel sensor networks," *IEEE Transactions on Wireless Communications*, vol. 11, no. 9, pp. 3058–3067, 2012.

[143] J.-H. Jeon, H.-J. Byun, and J.-T. Lim, "Joint contention and sleep control for lifetime maximization in wireless sensor networks," *IEEE Communications Letters*, vol. 17, no. 2, pp. 269–272, 2013.

[144] Y. Sun, S. Bhadra, S.-H. Choi, M. Fu, and X. Lu, "Achieving robust sensor networks through close coordination between narrow-band power line and low-power wireless communications," in *Proc. ACM Conference on Embedded Networked Sensor Systems*, Seattle, WA, U.S.A, 2011, pp. 373–374.

[145] A. M. Tonello, S. D'Alessandro, F. Versolatto, and C. Tornelli, "Comparison of narrow-band ofdm plc solutions and i-uwb modulation over distribution grids," in *Proc. IEEE International Conference on Smart Grid Communications (SmartGridComm)*, Brussels, Belgium, 2011, pp. 149–154.

[146] H. Gassara, F. Rouissi, and A. Ghazel, "Statistical characterization of the indoor low-voltage narrowband power line communication channel," *IEEE Transactions on Electromagnetic Compatibility*, vol. 56, no. 1, pp. 123–131, 2014.

[147] A. J. Goldsmith and S.-G. Chua, "Variable-rate variable-power mqam for fading channels," *IEEE transactions on communications*, vol. 45, no. 10, pp. 1218–1230, 1997.

[148] M. K. Kazimierczuk, *RF power amplifier*. John Wiley & Sons, 2014.

[149] S. Cui, A. J. Goldsmith, A. Bahai *et al.*, "Energy-constrained modulation optimization," *IEEE transactions on wireless communications*, vol. 4, no. 5, pp. 2349–2360, 2005.

[150] I. . W. Group *et al.*, "Ieee standard for information technology-local and metropolitan area networks-specific requirements-part 11: Wireless lan, medium access control (mac) and physical layer (phy) specifications amendment 6: Wireless access in vehicular environments; ieee 802.11 p," *IEEE Standards Association: Piscataway, NJ, USA*, 2010.

[151] H. Yetgin, K. T. K. Cheung, M. El-Hajjar, and L. Hanzo, "Cross-layer network lifetime optimisation considering transmit and signal processing power in wireless sensor networks," *IET Wireless Sensor Systems*, vol. 4, no. 4, pp. 176–182, 2014.

[152] M. Grant, S. Boyd, and Y. Ye, "Cvx: Matlab software for disciplined convex programming," 2008.

[153] A. Varga, "Omnet++," *Modeling and Tools for Network Simulation*, pp. 35–59, 2010.

[154] H. Kellerbauer and H. Hirsch, "Simulation of powerline communication with omnet++ and inet-framework," in *Proc. IEEE International Symposium on Power Line Communications and Its Applications (ISPLC)*, Udine, Italy, 2011, pp. 213–217.

[155] G. Marrocco, D. Statovci, and S. Trautmann, "A plc broadband channel simulator for indoor communications," in *Proc. IEEE International Symposium on Power Line Communications and Its Applications (ISPLC)*, Johannesburg, South Africa, 2013, pp. 321–326.

[156] Y. He, L. Guan, and W. Zhu, *Optimal Resource Allocation for Distributed Video Communication*. CRC Press, 2013.

[157] L. Gasparini, R. Manduchi, M. Gottardi, and D. Petri, "An ultralow-power wireless camera node: Development and performance analysis," *IEEE Transactions on Instrumentation and Measurement*, vol. 60, no. 12, pp. 3824–3832, 2011.

[158] https://www.arlo.com/.

[159] http://www.logitech.com/en-gb/product/circle/.

[160] Y. He, I. Lee, and L. Guan, "Distributed algorithms for network lifetime maximization in wireless visual sensor networks," *IEEE Transactions on Circuits and Systems for Video Technology*, vol. 19, no. 5, pp. 704–718, 2009.

[161] Z. He and D. Wu, "Resource allocation and performance analysis of wireless video sensors," *IEEE transactions on circuits and systems for video technology*, vol. 16, no. 5, pp. 590–599, 2006.

[162] J. Zou, H. Xiong, C. Li, R. Zhang, and Z. He, "Lifetime and distortion optimization with joint source/channel rate adaptation and network coding-based error control in wireless video sensor networks," *IEEE Transactions on Vehicular Technology*, vol. 60, no. 3, pp. 1182–1194, 2011.

[163] C. Li, J. Zou, H. Xiong, and C. W. Chen, "Joint coding/routing optimization for distributed video sources in wireless visual sensor networks," *IEEE Transactions on Circuits and Systems for Video Technology*, vol. 21, no. 2, pp. 141–155, 2011.

[164] N. Yang, I. Demirkol, and W. Heinzelman, "Motion sensor and camera placement design for in-home wireless video monitoring systems," in *Proc. IEEE Global Telecommunications Conference (GLOBECOM 2011)*, Houston, Texas, USA, 2011, pp. 1–5.

[165] S. T. Chung and A. J. Goldsmith, "Degrees of freedom in adaptive modulation: a unified view," *IEEE Transactions on Communications*, vol. 49, no. 9, pp. 1561–1571, 2001.

[166] D. V. Djonin, A. K. Karmokar, and V. K. Bhargava, "Joint rate and power adaptation for type-i hybrid arq systems over correlated fading channels under different buffer-cost constraints," *IEEE Transactions on Vehicular Technology*, vol. 57, no. 1, pp. 421–435, 2008.

[167] J. C. Li, S. Dey, and J. Evans, "Maximal lifetime power and rate allocation for wireless sensor systems with data distortion constraints," *IEEE Transactions on Signal Processing*, vol. 56, no. 5, pp. 2076–2090, 2008.

[168] K. Stuhlmuller, N. Farber, M. Link, and B. Girod, "Analysis of video transmission over lossy channels," *IEEE Journal on selected areas in communications*, vol. 18, no. 6, pp. 1012–1032, 2000.

[169] X. Zhu, E. Setton, and B. Girod, "Congestion–distortion optimized video

transmission over ad hoc networks," *Signal Processing: Image Communication*, vol. 20, no. 8, pp. 773–783, 2005.

[170] S. Pudlewski, N. Cen, Z. Guan, and T. Melodia, "Video transmission over lossy wireless networks: A cross-layer perspective," *IEEE Journal of Selected Topics in Signal Processing*, vol. 9, no. 1, pp. 6–21, 2015.

[171] J.-W. Lee, M. Chiang, and R. Calderbank, "Optimal mac design based on utility maximization: Reverse and forward engineering," in *Proc. IEEE International Conference on Computer Communications (INFOCOM)*, Barcelona, Spain, 2006, pp. 1–13.

[172] J. Zhu, S. Chen, B. Bensaou, and K.-L. Hung, "Tradeoff between lifetime and rate allocation in wireless sensor networks: A cross layer approach," in *Proc. IEEE International Conference on Computer Communications (INFOCOM)*, Anchorage, Alaska, USA, 2007, pp. 267–275.

[173] J. S. Seybold, *Introduction to RF propagation*. John Wiley & Sons, 2005.

[174] http://www.plc.uma.es/channels.htm/.